إقـــــرار

أنا الموقع أدناه مقدم الرسالة التي تحمل العنوان:

Optical Sensors Based on Photonic Crystal

أقر بأن ما اشتملت عليه هذه الرسالة إنما هو نتاج جهدي الخاص، باستثناء ما تمت الإشارة إليه حيثما ورد، وإن هذه الرسالة ككل أو أي جزء منها لم يقدم من قبل لنيل درجة أو لقب علمي أو بحثي لدى أي مؤسسة تعليمية أو بحثية أخرى.

DECLARATION

The work provided in this thesis, unless otherwise referenced, is the researcher's own work, and has not been submitted elsewhere for any other degree or qualification

Student's name:	اسم الطالب/ة: سمية علي عبدالله شاهين
Signature:	التوقيع:
Date:	التاريخ: 29 / 03 / 2016

Islamic University of Gaza
Deanery of Higher Studies
Faculty of Science
Department of Physics

Optical Sensors Based on Photonic Crystal

Somaia Ali Shaheen

B.Sc. in Physics, Islamic University of Gaza

Supervisor

Dr. Sofyan A. Taya
Associate Professor of Physics

Submitted to the Faculty of Science as a Partial Fulfillment of the Master Degree of Science (M. Sc.) in Physics

1437 – 2016

بسم الله الرحمن الرحيم

الجامعة الإسلامية – غزة
The Islamic University - Gaza
مكتب نائب الرئيس للبحث العلمي والدراسات العليا هاتف داخلي 1150

الرقم ج.س.غ/35/..... Ref

التاريخ 02/06/2016 Date

نتيجة الحكم على أطروحة ماجستير

بناءً على موافقة شئون البحث العلمي والدراسات العليا بالجامعة الإسلامية بغزة على تشكيل لجنة الحكم على أطروحة الباحثة/ سمية علي عبدالله شاهين لنيل درجة الماجستير في كلية العلوم قسم الفيزياء وموضوعها:

المجسات الضوئية المعتمدة على البلورة الضوئية

Optical Sensors Based on Photonic Crystal

وبعد المناقشة العلنية التي تمت اليوم السبت 23 ربيع الآخر 1437هـ، الموافق 2016/02/06م الساعة العاشرة صباحاً بمبني طيبة، اجتمعت لجنة الحكم على الأطروحة والمكونة من:

د. سفيان عبد الرحمن تايه	مشرفاً و رئيساً	.....
د. ختام يوسف الوصيفي	مناقشاً داخلياً	.....
د. هناء محمد موسى	مناقشاً خارجياً	.....

وبعد المداولة أوصت اللجنة بمنح الباحثة درجة الماجستير في كلية العلوم/ قسم الفيزياء.

واللجنة إذ تمنحها هذه الدرجة فإنها توصيها بتقوى الله ولزوم طاعته وأن تسخر علمها في خدمة دينها ووطنها.

والله ولي التوفيق،،،

نائب الرئيس لشئون البحث العلمي والدراسات العليا

أ.د. عبدالرؤوف علي المناعمة

P.O. Box 108, Rimal, Gaza, Palestine fax: +970 (8) 286 0800 فاكس Tel: +970 (8) 286 0700 هاتف ص.ب. 108 الرمال، غزة، فلسطين
public@iugaza.edu.ps www.iugaza.edu.ps

DEDICATION

I dedicate my thesis to:

My loving parents who deserve my great love and respect for her long encouragement at every stage,

My beloved husband for his continous assistance,

My aunt and uncle for their support,

My dear brother and sisters for their encouragement,

To every one who helped me to finish the thesis.

Somaia A. Shaheen

ACKNOWLEDGMENT

All praise to the Almighty Allah, the one to whome all dignity, honor and glory are due to. Peace and blessing of Allah be upon all the prophets and messengers. As prophet Mohamed peace of Allah be upon him, said " who does not thank people, will not thank Allah".

I would like to express my deep thanks, gratitude and appreciation to Professor Dr. Sofyan Taya for his extensive help, kind supervision and the continuous encouragement throughout the course of this work.

I would like to thank the staff members in Physics department at IUG for their continued support. I would like to express my special thanks to my family who helped me pursue my thesis.

ABSTRACT

In recent years, photonic crystals have achieved a lot of research significance due to their applications in many fields. Many photonic ccrystal sensors have been proposed based on their novel structure and unique physical properties such as reflectance/transmittance.

In this thesis, two layers one dimensional photonic crystal slab waveguide was assumed in which the first layer was considered to be the analyte layer and the second layer was considered to be LHM, dielectric or metal for transverse electric (TE) and transverse magnetic (TM) waves.

The dispersion relation of the proposed structure was derived and solved numerically and the sensitivity was also calculated. The condition required for the sensor to have its maximum sensitivity were presented. The dependence of the sensitivity on some different parameters of the structure was plotted and studied. It was found that the highest sensitivity was achieved by using the LHM materials in the photonic crystal rather than using metal and dielectric materials in photonic crystal. Our results show that it is possible for LHM photonic structure to achieve a sensitivity improvement of 412% for TE mode and 1056% for TM mode when compared to conventional slab waveguide sensor.

Moreover, one dimensional ternary photonic crystals were investigated as refractometric sensors for sensing very small refractive index change of an analyte material. The principle of operation of photonic crystal as a refractometric sensors in reflection mode was explained. The transmission of an incident wave were studied in details using Fresnel reflection coefficients. The transmission coefficient was plotted with the angle of incidence and wavelength of incident light for air and water as analyte materials. It was observed that a slight refractive index change in analyte layer of the ternary structure causes a sufficiently large transmission peak shift.

الملخص

لقد حقق موضوع البلورات الضوئية أهمية بحثية كبيرة نتيجة لاستخداماتها الواسعة في العديد من المجالات، حيث اقترح استخدام البلورات الضوئية كمجسات نتيجة تركيبها و خصائصها الفيزيائية التي تملكها مثل الانعكاسية و النفاذية بالإضافة الى قدرتها على الحساسية العالية في الكشف.

تم في هذه الأطروحة دراسة البلورات الضوئية والتى تتكون من طبقتين حيث الطبقة الأولى هى المادة التي يراد فحصها و الطبقة الثانية هي مادة يسارية أو عازلة أو موصلة حيث اقتصرت الدراسة على حالتين من حالات استقطاب المجال الكهرومغناطيسي هما المجال الكهربي المستعرض و المجال المغناطيسي المستعرض.

كما تم اشتقاق علاقة التشتت لكل حالة من الحالات السابقة و معادلة الحساسية للمجس و الحصول على الشرط الذي يعطي أكبر حساسية للمجس. و كذلك أيضا تم دراسة اعتماد حساسية المجس على بعض المتغيرات.

لقد وجد أن الحساسية تكون أعلى ما يمكن في حالة استخدام المواد اليسارية في البلورات الضوئية أكثر من المواد الموصلة و العازلة حيث أوضحت النتائج ان الحساسية تصل إلى 412 % في حالة المجال الكهربي المستعرض و1056% في حالة المجال المغناطيسي المستعرض عند المقارنة مع النموذج التقليدي لمجسات الموجهات الموجية.

علاوة على ذلك تم تقديم البلورات الضوئية كمجس تستشعر التغيرات البسيطة في معامل الانكسار للمادة المراد فحصها بالاعتماد على خاصية انعكاس الموجات الكهرومغناطيسية حيث وضح مبدأ العمل بالإضافة إلى دراسة ورسم معامل النفاذية مع زاوية السقوط للضوء الساقط و الطول الموجي، و أوضحت النتائج أن أي تغير في معامل الانكسار للمادة (ماء أو هواء) يقابله إزاحة مناسبة في منحنى معامل النفاذية.

CONTENTS

LIST OF FIGURES

CHAPTER ONE

CHAPTER TWO

CHAPTER THREE

CHAPTER FOUR

CHAPTER FIVE

Chapter One

Basic Waveguide Equations

This chapter is intended to establish the fundamental concepts and basic background of electromagnetic and waveguide theories. The basic equations needed to analyze slab waveguide structures are presented. A brief review of Maxwell's equation, homogenous wave equation, refractive index, phase and group velocities, boundary conditions, total internal reflection, and power considerations are given. Moreover, transverse electric and magnetic polarizations are presented.

1.1. Introduction

In the year 1864, James Clerk Maxwell (1831-1879) proposed his "Dynamical Theory of the Electromagnetic Field", in which he observed theoretically that an electromagnetic wave travels in free space with the velocity of light. He conjectured from his famous equations that light is a transverse electromagnetic wave. Herinrich Hertz (1857-1894) discovered experimentally electromagnetic waves around the year 1888. The results of Hertz experiments and his related theoretical work confirmed Maxwell's predictions. Maxwell's ideas and equations were expanded, modified, and made understandable after his death, mainly by the efforts of Heinrich Hertz, George Francis Fitz Gerald (1854-1901), Oliver Lodge (1851-1940) and Oliver Heaviside (1850-1925) [1].

1.2. Propagation of electromagnetic waves

1.2.1. Maxwell's equations

Maxwell's equations that governing the electromagnetic fields can be expressed in the following form [2,3]

$$\nabla . \boldsymbol{D} = \rho, \tag{1.1}$$

$$\nabla . \boldsymbol{B} = 0, \tag{1.2}$$

$$\nabla \times \boldsymbol{E} = -\frac{\partial \boldsymbol{B}}{\partial t}, \tag{1.3}$$

$$\nabla \times \boldsymbol{H} = \boldsymbol{J} + \frac{\partial \boldsymbol{D}}{\partial t}, \tag{1.4}$$

where $\boldsymbol{D}$, $\boldsymbol{B}$, $\boldsymbol{E}$, $\boldsymbol{H}$, $\boldsymbol{J}$ and ρ are the electric flux density**,** magnetic flux density, electric field, magnetic field, current density and free charge density, respectively.

Consider a linear, isoropic, homogeneous medium, the constitutive relations can be written as:

$$\boldsymbol{D}=\varepsilon\boldsymbol{E}, \tag{1.5}$$

$$\boldsymbol{B}=\mu\boldsymbol{H}, \tag{1.6}$$

where the permittivity ε and the permeability μ are defined as

$$\varepsilon=\varepsilon_o\varepsilon_r, \tag{1.7}$$

$$\mu=\mu_o\mu_r, \tag{1.8}$$

where ε_o and μ_o are the permittivity and permeability of vacuum, and ε_r and μ_r are the relative permittivity and permeability of the material.

For a charge-free, linear isotropic medium Maxwell's equations become

$$\nabla.\boldsymbol{E}=0, \tag{1.9}$$

$$\nabla.\boldsymbol{H}=0, \tag{1.10}$$

$$\nabla\times\boldsymbol{E}=-\mu\frac{\partial\boldsymbol{H}}{\partial t}, \tag{1.11}$$

$$\nabla\times\boldsymbol{H}=\varepsilon\frac{\partial\boldsymbol{E}}{\partial t}. \tag{1.12}$$

1.2.2. Homogenous wave equation

The solution of the wave equation describes the propogation of energy in the free charge medium. To derive the wave equation , we first take the curl of Eq. (1.11)

$$\nabla\times\nabla\times\boldsymbol{E}=-\mu\frac{\partial(\nabla\times\boldsymbol{H})}{\partial t} \tag{1.13}$$

Using Eq. (1.12) into Eq. (1.13)

$$\nabla\times\nabla\times\boldsymbol{E}=-\mu\varepsilon\frac{\partial^2\boldsymbol{E}}{\partial t^2} \tag{1.14}$$

Using the following vector identity

$$\nabla\times\nabla\times\boldsymbol{E}=\nabla(\nabla.\boldsymbol{E})-\nabla^2\boldsymbol{E} \tag{1.15}$$

Substituting Eq. (1.14) into Eq. (1.15) and using Eq. (1.9) yield

$$\nabla^2\boldsymbol{E}-\mu\varepsilon\frac{\partial^2\boldsymbol{E}}{\partial t^2}=0 \tag{1.16}$$

Differentiation in the time domain is the equivalent to multiplication by $i\omega$ in the frequency domain, Eq. (1.16) becomes

$\nabla^2 \boldsymbol{E} + \omega^2 \mu\varepsilon \mathbf{E} = 0$ (1.17)

Similarily, the homogenous wave equation for **H** is

$\nabla^2 \boldsymbol{H} + \omega^2 \mu\varepsilon \mathbf{H} = 0$ (1.18)

In a lossless medium in which $\sigma = 0$, the wavenumber k is defined by $k^2 = \omega^2 \mu\varepsilon$. Then Eq. (1.17) and Eq. (1.18) can be written as

$\nabla^2 \boldsymbol{E} + k^2 \boldsymbol{E} = 0$ (1.19)

$\nabla^2 \boldsymbol{H} + k^2 \boldsymbol{H} = 0$ (1.20)

1.3. Geometric optics

When light strikes an object, it may be transmitted, absorbed and converted into heat, and/or reflected off. The reflection and refraction will be investigated in this section.

1.3.1. Reflection of light

When a ray of light is reflected at an interface between two different media, the reflected beam remains within the plane of incidence, and the angle of reflection equals that of incidence. The plane of incidence includes the incident ray and the normal to the interface at point of incidence as shown in Fig. 1.1 [4].

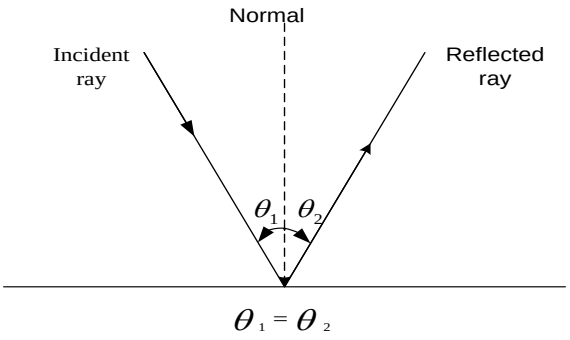

Fig. 1.1. Reflection of light at an interface

1.3.2. Refraction of light

When rays of light strike a differing medium in the refractive index obliquely, or at an angle θ_1, they are refracted or bent, at the interface between the two media as shown in Fig. 1.2 [5]. The angle of refraction θ_2 depends on the properties of the two media and on the angle of incidence through the relationship

$$\frac{\sin\theta_2}{\sin\theta_1} = \frac{v_2}{v_1} = constant, \tag{1.21}$$

where υ_1 is the speed of light in the first medium and υ_2 is the speed of light in the second medium.

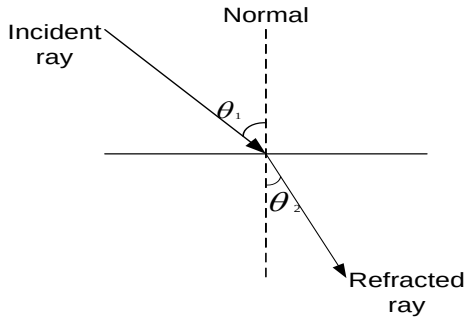

Fig. 1.2. Refraction of light at an interface between two media

1.3.3. Refractive index

Experiments showed that the index of refraction of a medium is inversely proportional to the speed of light in that medium. Since $\boldsymbol{c}$ is defined as the speed of light in vacuum, and n=1 is defined as the index of refraction of vacuum [6], we have

$$n = \frac{speed\ of\ light\ in\ vacuum}{speed\ of\ light\ in\ a\ medium} = \frac{c}{v}. \tag{1.22}$$

Therefore, because the relationship $\upsilon=f\lambda$ must be valid in both media and because $f_1=f_2=f$, where f and λ are the wave frequency and wavelength respectively, then

$\upsilon_1=f\lambda_1$ $\upsilon_2=f\lambda_2$

$$\frac{\lambda_1}{\lambda_2} = \frac{v_1}{v_2} = \frac{c/n_1}{c/n_2} = \frac{n_2}{n_1} \tag{1.23}$$

replacing the v_2/v_1term in Eq. (1.21) with n_1/n_2 , Snell's law of refraction is obtained

$$n_1 \sin\theta_1 = n_2 \sin\theta_2 \tag{1.24}$$

1.3.4. Total internal reflection

When light travels from a medium with high index of refraction into another one with smaller index of refraction, Snell's law shows that as θ_1 increases, it will reach a finite

value at which θ_2=90°. For angles of incidence less than θ_c, some of light is reflected and some is transmitted (refracted) as shown in Fig. 1.3(a). However, for an angle of incidence $\theta_1 \geq \theta_c$, all of the light is reflected back into medium 1 as shown in Fig. 1.3(b). This total internal reflection requires $n_\iota \sin\theta_c = n_2 \sin 90^\circ$, so the critical angle θ_c is determined by [7]

$$\sin\theta_c = \frac{n_2}{n_1} \tag{1.25}$$

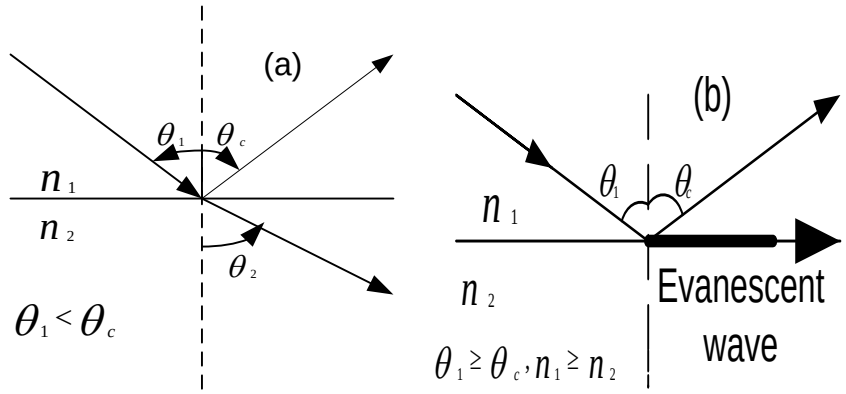

Fig. 1.3. Light reflection at a) $\theta_1<\theta_c$ and b) $\theta_1 \geq \theta_c$. θ_1 and θ_c represent the incidence and critical angles, respectively.

Total internal reflection is a very important phenomenon as it is the basic principle of operation of waveguides of all kinds.

An important result of total internal reflection is the propagation of an evanescent wave across the interface. Essentially, even though the entire incident wave is reflected back into the first medium, there is some penetration into the second medium at the boundary as shown in Fig. 1.3(b).

1.4. **Phase and group velocities**

The solution of the wave equation

$$\frac{\partial^2\Psi}{\partial t^2} = c^2\frac{\partial^2\Psi}{\partial x^2} \tag{1.26}$$

is given by

$$\Psi(x,t)=Ae^{i(kx-wt)} \tag{1.27}$$

Plugging Eq. (1.27) into Eq. (1.26) we get

$$w^2 = c^2k^2 \tag{1.28}$$

Then, the velocity of the wave is $\frac{\omega}{k} = c$, which is dependent of w and k. This phenomenon is called dispersion [8].

Consider the case where the wave group consists of two waves that have the same amplitude A but differ by a small amount Δw in angular frequency and a small amount Δk in wave number [9].

$$y_1 = A\cos(\omega t - kx) \tag{1.29}$$

$$y_2 = A\cos\big((\omega + \Delta\omega)t - (k + \Delta k)x\big) \tag{1.30}$$

Adding y_1 and y_2, we get

$$y = 2A\cos\tfrac{1}{2}(\Delta\omega t - \Delta kx)\cos\tfrac{1}{2}\big((2\omega + \Delta\omega)t - (2k + \Delta k)\big) \tag{1.31}$$

Since Δω<<ω and Δk<<k, Eq. (1.31) reduces to

$$y = 2A\cos\tfrac{1}{2}(\Delta\omega\Delta t - \Delta kx)\cos(\omega t - kx) \tag{1.32}$$

The above equation represents a wave of angular frequency ω and wave number k whose amplitude is modulated by an angular frequency $\frac{\Delta\omega}{2}$ and wave number $\frac{\Delta k}{2}$.

The effect of the modulation is to produce successive wave group. The phase velocity is $v_p = \frac{\omega}{k}$ and the velocity of the successive wave group is $v_g = \frac{\Delta\omega}{\Delta k}$

When ω and k have continous spreads, then the group velocity is $v_g = \frac{d\omega}{dk}$

1.5. **Boundary conditions**

Various relations between electric field **E**, magnetic field **H**, electric flux density **D** and magnetic flux density **B** in terms of Maxwell's equations are only valid for a point in the continuous medium. Consider an interface separating medium 1 and medium 2, the following boundary conditions hold [10]

1. Boundary condition '1':

$$E_{tan'1'} = E_{tan'2'} \tag{1.33}$$

It means that the tangential component of an electric field at the boundary of medium '1' is the same as the tangential component of electric field at the boundary of medium '2'. Thus, at a point of discontinuity, the tangential component of an electric field is continuous.

2. Boundary condition '2':

$$H_{tan\,'1'} - H_{tan\,'2'} = J_s \tag{1.34}$$

It means that the tangential component of magnetic field at the surface of a perfect conductor is discontinuous. This discontinuity is equal to J_s. Other than a perfect conductor, the tangential component of magnetic field is continuous across the surface.

3. Boundary condition '3':

$$B_{n\,'1'} = B_{n\,'2'} \tag{1.35}$$

It means that at the boundary surface (point of discontinuity), the normal component of magnetic flux density B_n is continuous.

4. Boundary condition '4':

$$D_{n\,'1'} - D_{n\,'2'} = \rho_s \tag{1.36}$$

It means that the normal component of electric flux density D_n is discontinuous for that surface, where surface charge density exists. Discontinuity is equal to ρ_s. For those surfaces, where the surface charge density is zero, the normal component of electric flux density D_n is continuous.

1.6. Planar optical waveguide

1.6.1. Introduction

There are many engineering applications in which it is necessary to use devices to confine the propogation of electromagnetic waves in order to transmit electromagnetic energy from one point to another with a minimum of interference, radiation and heat losses. In general, any device used to transmit confined electromagnetic waves can be considered a waveguide [11]. A waveguide is a dispersive structure that confines and directs a wave. In other words, it conveys a wave between its ends. An optical waveguide is used to guide waves in the optical spectrum.

1.6.2. Waveguide structure

Fig. 1.4 shows the structure of the basic step-index planar slab waveguide which consists of three layers. A thin dielectric film of refractive index n_f is deposited on a dielectric substrate of index of refraction n_s. Above the film is a dielectic cover or cladding of index of refraction n_c such as air as shown in Fig. 1.4. To achieve propogation by total internal

reflection within the film, the refractive indices must satisfy $n_f > n_s \geq n_c$. The case of symmetric dielectric waveguide slab is obtained when $n_c = n_s$. Otherwise, the structure is called asymmetric. Furthermore, the film thickness *d* should be comparable to the operating wavelength λ. In contrary, the substrate and cover (cladding) layers are much thicker than λ.

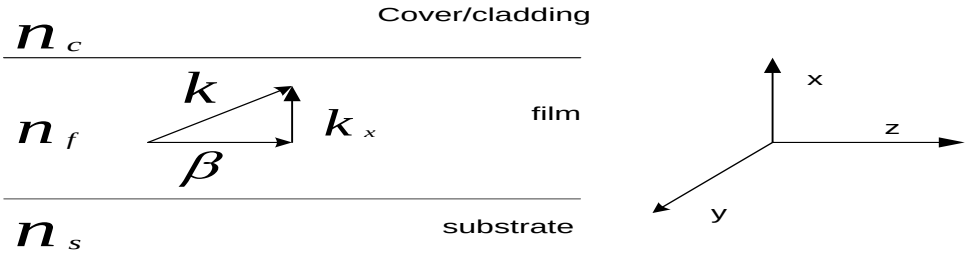

Fig. 1.4. Basic structure of the dielectric planar waveguide

As mentioned above, light is confined in the core of a planar waveguide by total internal reflection at both film/cover and film/substrate interfaces as shown in Fig. 1.5. This occurs when the refractive index of the film is greater than those of cover and substrate. Consequently, light will be reflected back and forth between the two interfaces till it is transmitted.

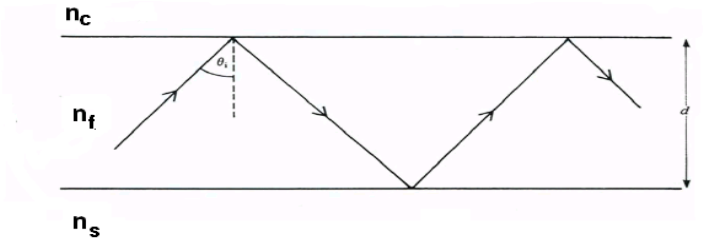

Fig. 1.5. Light confinement in a planar waveguide by Total Internal Reflection

1.6.3. Basic equations

In a waveguiding system, Maxwell's equations are solved for electromagnetic waves that are propogating along the guiding direction (say z direction) and are confined in the guiding structure. Thus, the magnetic and electric fields are assumed to have the forms [12]

$$\boldsymbol{E}(x,y,z,t) = \boldsymbol{E}(x,y)e^{j\omega t - j\beta z}, \tag{1.37}$$

$$\boldsymbol{H}(x,y,z,t) = \boldsymbol{H}(x,y)e^{j\omega t - j\beta z}, \tag{1.38}$$

where β is the propogation wavenumber along the guiding direction as shown in the Fig.1.4.

Using Maxwell's equation in the form

$$\nabla \times \boldsymbol{H} = j\omega\varepsilon\boldsymbol{E} \tag{1.39}$$

$$\nabla \times \boldsymbol{E} = -j\omega\mu\boldsymbol{H} \tag{1.40}$$

Expanding these equations, we get

$$\nabla \times \boldsymbol{H} = \begin{vmatrix} \mathbf{a}_x & \mathbf{a}_y & \mathbf{a}_z \\ \frac{\partial}{\partial x} & \frac{\partial}{\partial y} & \frac{\partial}{\partial z} \\ H_x & H_y & H_z \end{vmatrix} = \mathbf{a}_x\left[\frac{\partial H_z}{\partial y} - \frac{\partial H_y}{\partial z}\right] + \mathbf{a}_y\left[\frac{\partial H_x}{\partial z} - \frac{\partial H_z}{\partial x}\right] + \mathbf{a}_z\left[\frac{\partial H_y}{\partial x} - \frac{\partial H_x}{\partial y}\right]$$

$$= \mathrm{j}\omega\varepsilon E_x\mathbf{a}_x + \mathrm{j}\omega\varepsilon E_y\mathbf{a}_y + \mathrm{j}\omega\varepsilon E_z\,\mathbf{a}_z \tag{1.41}$$

Equating the respective components, we get

$$\frac{\partial H_z}{\partial y} - \frac{\partial H_y}{\partial z} = \mathrm{j}\omega\varepsilon E_x \tag{1.42}$$

$$\frac{\partial H_x}{\partial z} - \frac{\partial H_z}{\partial x} = \mathrm{j}\omega\varepsilon E_y \tag{1.43}$$

$$\frac{\partial H_y}{\partial x} - \frac{\partial H_x}{\partial y} = \mathrm{j}\omega\varepsilon E_z \tag{1.44}$$

$$\nabla \times \boldsymbol{E} = \begin{vmatrix} \mathbf{a}_x & \mathbf{a}_y & \mathbf{a}_z \\ \frac{\partial}{\partial x} & \frac{\partial}{\partial y} & \frac{\partial}{\partial z} \\ E_x & E_y & E_z \end{vmatrix} = \mathbf{a}_x\left[\frac{\partial E_z}{\partial y} - \frac{\partial E_y}{\partial z}\right] + \mathbf{a}_y\left[\frac{\partial E_x}{\partial z} - \frac{\partial E_z}{\partial x}\right] + \mathbf{a}_z\left[\frac{\partial E_y}{\partial x} - \frac{\partial E_x}{\partial y}\right]$$

$$= -\mathrm{j}\omega\mu H_x\mathbf{a}_x - \mathrm{j}\omega\mu H_y\mathbf{a}_y - \mathrm{j}\omega\mu H_z\,\mathbf{a}_z \tag{1.45}$$

Equating the respective components, we get

$$\frac{\partial E_z}{\partial y} - \frac{\partial E_y}{\partial z} = -\mathrm{j}\omega\mu H_x \tag{1.46}$$

$$\frac{\partial E_x}{\partial z} - \frac{\partial E_z}{\partial x} = -\mathrm{j}\omega\mu H_y \tag{1.47}$$

$$\frac{\partial E_y}{\partial x} - \frac{\partial E_x}{\partial y} = -\mathrm{j}\omega\mu H_Z \quad (1.48)$$

As fields are assumed to be varying in the form of $e^{-j\beta z}$, Eqs.(1.42)-(1.44) can be written as

$$\frac{\partial H_z}{\partial y} + j\beta H_y = \mathrm{j}\omega\varepsilon E_x \quad (1.49)$$

$$j\beta H_x + \frac{\partial H_z}{\partial x} = -\mathrm{j}\omega\varepsilon E_y \quad (1.50)$$

$$\frac{\partial H_y}{\partial x} - \frac{\partial H_x}{\partial y} = \mathrm{j}\omega\varepsilon E_z \quad (1.51)$$

and Eqs. (1.46) - (1.48) can be written as

$$\frac{\partial E_z}{\partial y} + j\beta E_y = -\mathrm{j}\omega\mu H_x \quad (1.52)$$

$$j\beta E_x + \frac{\partial E_z}{\partial x} = \mathrm{j}\omega\mu H_y \quad (1.53)$$

$$\frac{\partial E_y}{\partial x} - \frac{\partial E_x}{\partial y} = -\mathrm{j}\omega\mu H_Z \quad (1.54)$$

For nonmagnetic materials μ_r=1, then $\mu=\mu_\circ$and $n^2=\varepsilon_r$, then $\varepsilon=\varepsilon_\circ n^2$

The waveguide is assumed to be infinitly in y-direction. Then there is no variation in the waveguide in the y-direction, $\frac{\partial}{\partial y} = 0$

Then Eqs. (1.49)-(1.51) become

$$j\beta H_y = \mathrm{j}\omega\varepsilon_\circ n^2 E_x \quad (1.55)$$

$$j\beta H_x + \frac{dH_z}{dx} = -\mathrm{j}\omega\varepsilon_\circ n^2 E_y \quad (1.56)$$

$$\frac{dH_y}{dx} = \mathrm{j}\omega\varepsilon_\circ n^2 E_z \quad (1.57)$$

and Eqs. (1.52) - (1.54) can be written as

$$j\beta E_y = -\mathrm{j}\omega\mu_\circ H_x \quad (1.58)$$

$$j\beta E_x + \frac{\partial E_z}{\partial x} = \mathrm{j}\omega\mu_\circ H_y \quad (1.59)$$

$$\frac{\partial E_y}{\partial x} = -\mathrm{j}\omega\mu_\circ H_Z \quad (1.60)$$

Two commonly used light polarizations are transverse electric (TE) and transverse magnetic (TM) polatrizations

I. Transverse electric mode (TE mode)

TE polarization is in which the electric field vector of the incident wave is parallel to the interface between the layers. In our model there's a non-zero y-component of the electric field, while the magnetic field has non-zero x and z-components. In other words, $E_x = E_z = H_y = 0$. Using Eqs. (1.58) and (1.60), H_x and H_z can be written in terms of E_y as

$$H_x = -\frac{\beta}{\omega\mu_\circ} E_y \tag{1.61}$$

$$H_z = \frac{j}{\omega\mu_\circ}\frac{dE_y}{dx} \tag{1.62}$$

Substituting from Eq. (1.61) and Eq. (1.62) into Eq. (1.56) gives the wave equation which is called Helmholtz equation

$$\frac{d^2E_y}{dx^2} + (k^2n^2 - \beta^2)E_y = 0 \tag{1.63}$$

II. Transverse magnetic mode (TM mode)

TM polarization is in which the magnetic field vector of the incident wave is parallel to the interface between the layers. So there's a non-zero y-component of the magnetic field, while there are non-zero x and z-components of the electric field. In other words, $H_x = H_z = E_y = 0$.

$$E_x = \frac{\beta}{\omega\varepsilon_\circ n^2} H_y, \tag{1.64}$$

$$E_z = \frac{1}{j\omega\varepsilon_\circ n^2}\frac{dH_y}{dx} \tag{1.65}$$

Substituting from Eq. (1.64) and Eq. (1.65) into Eq. (1.59) gives the Helmholtz equation for TM modes

$$\frac{d^2H_y}{dx^2} + (k^2n^2 - \beta^2)H_y = 0 \tag{1.66}$$

1.6.4. Power consideration

Electromagnetic waves carry energy through the space. At any point in the space, the flow of energy can be described by a power density vector **P**, which specifies both the power density in watts per square meter and the direction of flow. The vector **P** is called the pointing vector, and is defined as

$\mathbf{P}=\mathbf{E}\times\mathbf{H}$ (1.67)

The total power passing through a surface S is obtained by integration over the S,i.e.

$W=\int \mathbf{p}.\, d\mathbf{S}$ watts (1.68)

For an electromagnetic wave that oscillates at a single angular frequency ω, the time-average Poynting vector is calculated as follows [2]

$\langle \mathbf{P} \rangle = \langle \mathbf{E} \times \mathbf{H} \rangle$ (1.69)

$= \langle Re\{\boldsymbol{E}(r)exp(j\omega t)\} \times Re\{\boldsymbol{H}(r)exp(j\omega t)\}\rangle$

$=\left\langle \frac{(\mathbf{E}\exp(j\omega t)+\boldsymbol{E}^{*}\exp(-j\omega t))}{2} \times \frac{(\boldsymbol{H}\exp(j\omega t)+\mathbf{H}^{*}\exp(-j\omega t))}{2} \right\rangle$

$= \frac{1}{4}\langle(\mathbf{E}\times\mathbf{H}^{*}+\mathbf{E}^{*}\times\mathbf{H}+\mathbf{E}\times\mathbf{H}exp(2j\omega t)+\mathbf{E}^{*}\times\mathbf{H}^{*}\exp(-2j\omega t))\rangle$

$\langle \mathbf{P} \rangle = \frac{1}{2}\, Re[\langle \mathbf{E}\times\mathbf{H}^{*}\rangle]$ (1.70)

For a multilayer waveguide, the power flowing through the structure can be evaluated using

$P_{total} = \frac{\beta}{2\omega}\int_{-\infty}^{+\infty}\frac{|E_{y(x)}|}{\mu(x)}\, dx$; for TE mode (1.71)

and

$P_{total} = \frac{\beta}{2\omega}\int_{-\infty}^{+\infty}\frac{|H_{y(x)}|}{\varepsilon(x)}\, dx$; for TM mode (1.72)

Chapter Two

Optical Sensing and Photonic Crystal

In this chapter, an overview of optical waveguide sensing is presented. Photonic crystal and materials with negative electric permittivity and negative magnetic permeability are also discussed.

2.1. Optical sensing

In the past few years, extensive research and development activites have been devoted to evanescent- field- based optical waveguide sensors, which are now playing important roles in a variety of sensing applications. By means of measuring small changes in optical phase or intensity of the guided light, these sensors present an excellent properties such as high sensitivity, fast response, immunity to electromagnetic fields, and safety in the detection of combustible and explosive materials [13].

2.1.1. Principle of operation

An optical sensor is a device in which light interacts with the substance to be detected (measurand) and converts light affected by the measurand substance into electrical signal which gives information about the analyte (substance to be detected). As mentioned before, light is confined within the guiding layer, but there is a small part of the guided mode called the evanescent field that extends to the surrounding media as shown in Fig. 2.1. The evanescent field detects any refractive index variation of the covering medium in homogeneous sensing. The interaction of the evanescent field with the measurand causes a change in the effective refractive index of the guided mode. The change in the effective refractive index due to the change in the analyte index is the sensing criteria. The effective refractive index of the propogating mode depends on the structure parameters such as the guiding layer thickness and dielectric permitivity and magnetic permeability of the media constituting the waveguide. Therefore, it undergoes a change when the index of any layer changes.

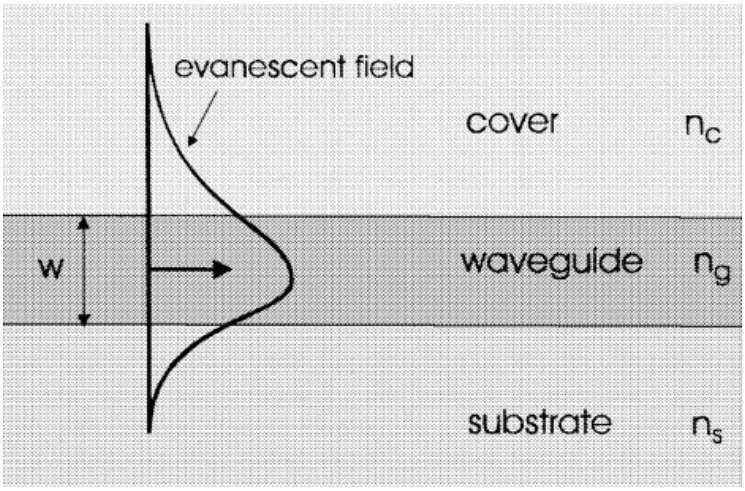

Fig. 2.1. Schematic illustrating of an evanescent field penetrating the cover and substrate layers [14].

2.1.2. Homogenous sensing

If the measurand substance is homogenously distributed in the cover layer, then the process of detecting changes of these substances is called homogenous sensing. It's assumed that the cover medium is a liquid or a gas, which implies that the contact zone between the cover and the waveguide surface is of zero thickness and does not exhibit an air film as shown in Fig 2.1. In this case, the sensitivity is defined as the change in the effective refractive index per any change in the index of the cover medium [14,15] , $S = \frac{\partial N}{\partial n_c}$.

2.1.3. Surface sensing

If there is an ultra thin film of biological molecules at the waveguide – cover interface, then the process is called surface sensing as shown in Fig. 2.2 and the sensitivity is defined as the change of the effective refractive index with respect to change in the adlayer width d_A or the refractive index of the adlayer n_A, such as [16]

$$S_{d_A} = \frac{\partial N}{\partial d_A} \qquad S_{n_A} = \frac{\partial N}{\partial n_A}$$

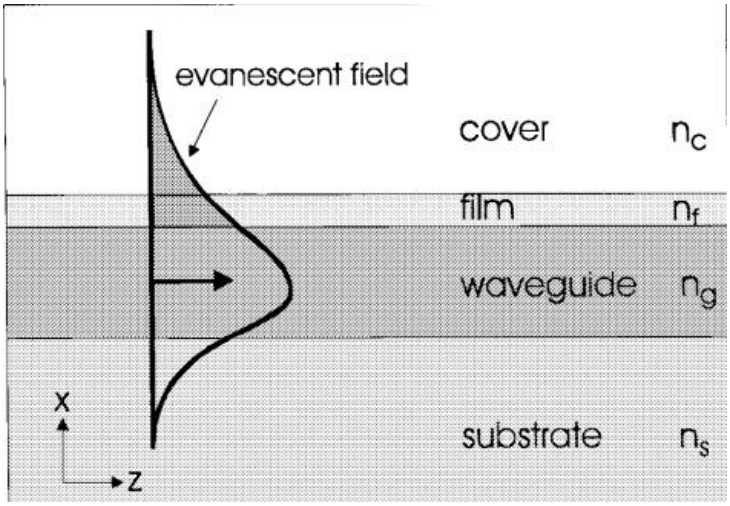

Fig. 2.2. Schematic representation of a surface sensor [14].

2.1.4. Uses and application

Optical sensors have many applications in biomedical which can be categorized into three main types: physical, chemical and biological sensors. Physical sensors measure a variety of physiological parameters, like body temperature, blood pressure and radiation dose. Chemical sensors have been utilized for the measutement of PH, glucose level and blood oxygen. They detect specific chemical species for diagnostic purposes, as well as monitor the body's chemical reactions and activity. Biological sensors tend to be more complex and rely on biologic recognition reactions—such as enzyme-substrate, antigen-antibody, or ligand-receptor—to identify and quantify specific biochemical molecules of interest [17].

2.1.5. Previous work

In 1983, Teifenthelar and Lukosz, who are the fathers of slab waveguide sensors, proved the applicability of a dielectric slab waveguide as an optical sensor [18]. They were studying a waveguide with grating coupler and discovered changes in coupling angles due to variations of humidity.

Recently, various attempts at improving the sensitivity have been presented. Two types of operation for metal-clad waveguides have been analyzed: peak-type and dip-type

operation were presented in details [19]. The newly discovered peak-type operation was obtained by using thin claddings (few nanometers) between the substrate and the film that consist of metals with a large imaginary permittivity, whereas dip-type operation was obtained by use of thicker claddings (some tens of nanometers) of metals with small imaginary permittivity. Skivesen et al. [20] analyzed metal-clad waveguides for sensor applications to achieve high sensitivity for adlayer and refractive index measurements. Their optimization showed that it is possible for metal-clad waveguides to achieve a sensitivity improvement up to 6 times compared to surface-plasmon-resonance sensors. Parruiax et al. deduced analytically the conditions for maximum sensitivity for both transverse electric (TE) and transverse magnetic (TM) evanescent- wave step index waveguide sensors [15].

H. Mukundan et al. [21] described the basic principles, advantages and disadvantages of planar optical waveguide based biodetection technologies. This discussion included already commercialized technologies and new technologies that are under research and development. Moreover, they discussed reverse-symmetry waveguides, resonant waveguide grating sensors and metal-clad leaky waveguides as alternative signal transducers in optical biosensing.

The recent progress in optical biosensors that use the label-free detection protocol, in which biomolecules are unlabeled, was reviewed [22]. The paper focused on the optical biosensors that utilize the refractive index change as the sensing transduction signal. Various optical label-free biosensing platforms were introduced, including surface plasmon resonance, interferometers, waveguides, fiber gratings, ring resonators, and photonic crystals. Taya et al. [23-24] proposed optical waveguide sensors in which one or both of the surrounding media have an intensity dependent refractive index.The results were compared with those of the well known linear evanescent waveguide sensors. It is found that utilizing nonlinear media can enhance the sensitivity of slab waveguide sensors.

Taya et al. have investigated the variation of the sensitivity of optical slab waveguide sensors with the wavelength of guided wave [25]. They found that an optimum wavelength exists for each guiding layer thickness and this optimum value increases linearly with the thickness of the guiding layer. Left-handed materials (LHMs) of

simultaneously negative dielectric permittivity ε and magnetic permeability μ have been studied in the field of optical waveguide sensors [26,27]. It was verified that LHMs can amplify evanescent waves. Therefore, slab waveguide structures comprising LHMs are expected to improve the sensitivity of waveguide sensors. The sensitivity of an optical waveguide sensor was shown to be dramatically enhanced by using a LHM layer between the guiding layer and the covering medium [26]. In 2011, four layer slab waveguide structure was studied with one of these layers made of a LHM [28]. Using the Fresnel reflection coefficients, the reflectance of the structure was studied in details. Also the sensitivity of the effective index to variation in the refractive index of a measured homogenously distributed in the cladding layer was presented. A LHM layer embedded between a semi- infinite linear substrate and a semi-infinte nonlinear cladding with an intensity – dependent refractive index of Kerr type was studied as an optical sensor [29].
The sensitivity of the three – layer waveguide sensor consisting of thin left-handed material core layer was investigated [30]. It was found that the sensitivity of the proposed sensor is improved compared to that of convevtional three- layer slab waveguide sensor. Also they found that the sensitivity of the proposed structure is negative and critically dependent on the dispersive permittivity and permeability of the core layer.
Transverse magnetic waves in a four – layer slab waveguide structure were studied for optical sensing application [31]. The stucture consists of a semi-infinite substrate , a thin metal layer, a medium with negative permittivity and permeability as a guiding layer, and a semi-infinte layer as a cover. The proposed sensor was operated in reflection mode in which the angular position of the reflectance peaks is used to detect small changes in the refractive index of the cover medium. The results revealed that for aluminum metal layer, a thickness of about 9 nm represents the optimum metal thickness. Also, the thickness, negative permittivity, and negative permeability of the guiding layer were found to have great impacts on the performance of the proposed optical waveguide sensor. The possibility of using photonic crystals for sensing purpose was also studied [32]. The optical properties of photonic crystals allow to realize sensing devices characterized by a high degree of compactness and a good resolution of the quantity to detect. A particular attention is devoted to force/pressure sensors and the design of a

photonic crystal microcavity pressure sensor was reported. D.El.Amassi [33] investigated a multilayer slab waveguide optical sensor consisting of one- dimensional left- handed photonic crystal. A mathematical and numerical analysis for propogation of electromagnetic waves in the structure have been carried out. Dispersion equation has been derived theoretically. Moreover, the multilayer slab waveguide sensor has been studied for TE- and TM- modes. Also, sensitivity and power flowing within each layer for various physical parameters of the structure have been studied.

2.2. Left-handed material

2.2.1. Concept of left- handed material

In 1968, Veselago theoretically investigated materials with simultaneously negative permeability and permittivity. Such materials are usually termed as metamaterials or left-handed materials (LHMs) [34]. The word 'meta' derives from the Greek word that means 'beyond'. While conventional materials provide their intended physical propreties in terms of design on the atomic or molecular level, metamaterials realize their specified physical properties through the design of an artificial structure. Veselago showed that such materials exhibit a number of unusual properties which can be summarized as follows [34]:

- Negative refraction index since $\varepsilon < 0$ and $\mu < 0$, then physical and mathematical considerations lead to choosing the negative square root $n = -\sqrt{\mu\varepsilon}$.
- Reversal of Snell's law as shown in Fig. 2.3.

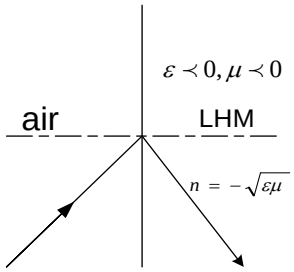

Fig. 2.3. Reversal of Snell's law in LHM

- The Doppler shift is reversed, that is a light source moving toward on observer appears to reduce its frequency.
- Electric field, magnetic field and wavevector of an electromagnetic wave in a LHM form a left-handed set as shown in Fig 2.4.

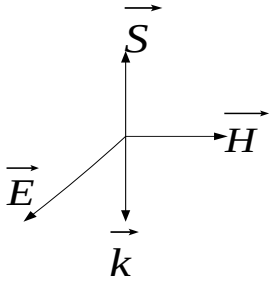

Fig. 2.4. Electric field, Magnetic field, wave vector form a Left-Handed set

2.2.2. Design of left-handed materials

LHMs are not found in nature. They were artificially constructed in 2000. LHMs realize their specified physical properties through the design of an artificial structure that can be regarded as a quasi-uniform medium in a macroscopic view [35]. LHM is an assembly of two kinds of cell elements. Split ring resonators (SRRs) produce negative μ and a wire array produces negative ε [36] as shown in Fig. 2.5. The wire array media can be described by the effective dielectric function [37]

$$\varepsilon_{eff}(\omega) = 1 - \frac{\omega_p^2}{\omega^2 + i\gamma\omega} \quad (2.1)$$

with the plasma frequency ω_p related to the geometry of the wire array. The SRR medium can be described by an effective frequency-dependent permeability having the form

$$\mu_{eff}(\omega) = 1 - \frac{F\omega_\circ^2}{\omega^2 - \omega_\circ^2 - i\omega\gamma} \quad (2.2)$$

where $\omega_\circ$ is the resonance frequency, γ is the electron scattering rate and F is the fractional area occupied by the split ring.

Fig. 2.5. Metamaterial proposed by D.R. Smith [36]

2.2.3. Applications of left-handed materials:

LHMs have been proposed for a set of potential applications due to their unusual properties such as metamaterial antenna, superlenss and optical sensors.

Metamaterial antenna

Metamaterial antenna is a class of antennas which uses metamaterials to enhance or increase the performance of the system. The metamaterials could enhance the radiated power of an antenna. Materials which can attain negative permeability could possibly allow for properties such as an electrically small antenna size, high directivity and tunable operational frequency [38].

Superlens

A superlens uses LHM to achieve resolution beyond the diffraction limit. The diffraction limit is inherent in conventional optical devices or lenses [39].

Cloaking devices

LHM are basis for attempting to build a practical cloaking devices. The cloak deflects microwave beam so they flow around a ‘hidden’ object inside with little distortion, making it appear almost as if nothing were there at all [38].

Sensors

LHMs can be used to provide more sensitive guided mode sensors. It is found that LHMs can enhance the intensity of the evanescent waves in the cladding without alternating the propogation constant of the waveguide for both TE and TM modes.

2.3. Photonic crystal

2.3.1. Definition of a photonic crystal

Photonic crystal or photonic band gap materials are periodic dielectric structures that are designed to form the energy band structure for photons, which either allows or forbids the propagation of electromagnetic waves of certain frequency ranges in the same manner as the periodic potential does for electron crystal [40]. The analogy between electromagnetism and solid state physics has led to the study of band structures of periodic materials and further to the possibility of occurrence of localized modes in the band gap when a defect is introduced in the lattice. These defect-enhanced structures are called doped photonic crystals. When light propagates inside the periodic structures, it obeys some selection rules. In particular, depending on the geometrical symmetries of the materials, some modes are allowed or not created by a defect inside the photonic crystal. The defect mode can be excited by a source with appropriate frequency and polarization [41]. The control of the propagation of the light by these materials is linked to the control of localized modes and has been extended to the study of propagation in waveguides.

2.3.2. History of photonic crystal

Although photonic crystals have been studied in one form or another in 1887, the term 'photonic crystal' was first used over 100 years later, after Eli Yabonovitch and Saier John published two papers on photonic crystal in 1987. Lord Rayleigh started research in 1887 on 1-D photonic crystal in the form of periodic multi-layer dielectric stacks, and found 1-D band gap [42]. By 1991, Eli Yablonovitch had demonsrated the first 3-D photonic band- gap in the microwave region. In 1996, [43], Thomas Krauss made first demonstration of 2-D photonic crystal at optical wavelength. Photonic crystal fiber were

first developed by Philib Russell in 1998. In 1996-2015, many research have been studied. Photonic crystal slabs are used in integrated computer chips.

2.3.3. Applications of photonic crystal

Many applications have been proposed for photonic crystals. They can be used as waveguides. Inside of a photonic crystal with a complete band-gap, a zero loss waveguide can be created by introducing a line defect into a perfect structures. These photons with energies inside the band-gap will be guided through the photonic by the defect while being unable to escape the waveguide [44]. Other applications include omni-directional mirror, where photons at any incident angle are reflected for energies within the band-gap.

Chapter Three

Photonic crystal sensor: TE mode

In this chapter, two-layer slab photonic crystal is investigated for sensing applications. The dispersion relation, sensitivity, and power flow relations are derived, plotted and analyzed for TE mode.

3.1. Structure analysis

The geometry of two-layer slab photonic crystal structure is shown in Fig. 3.1. It consists of two different layers in periodic arrangement which have refractive indices n_1 and n_2 and thicknesses d_1 and d_2, respectively.

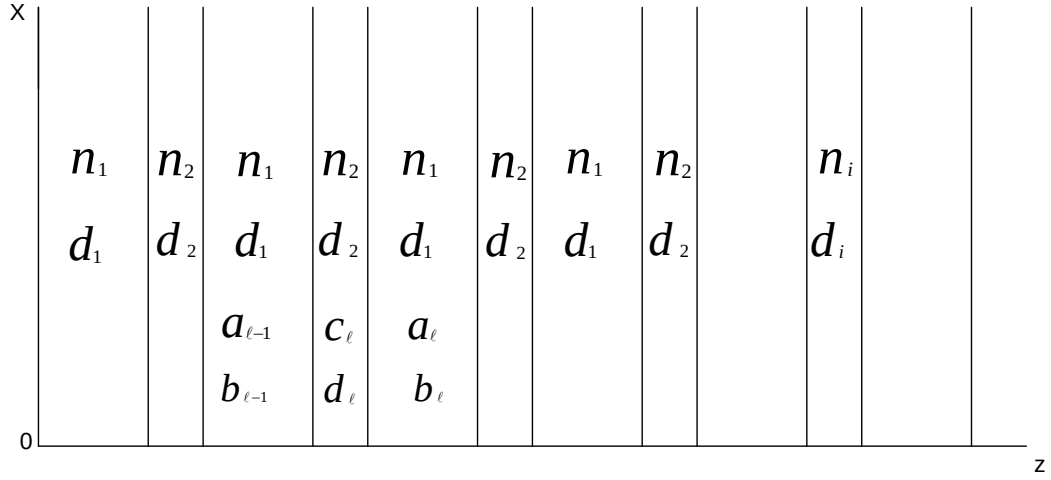

Fig. 3.1. 1 D multilayer photonic crystal consisting of two different layers in periodic arrangement.

The refractive index profile of the structure is written as

$$n(z) = \begin{cases} n_1 & 0 < z < d_1 \\ n_2 & d_1 < z < d \end{cases} \tag{3.1}$$

where $n(z) = n(z + d)$ and $d = d_1 + d_2$.

3.2. **Basic equations**

3.2.1. Dispersion relation

Consider TE polarization in which the waves are travelling along the x-axis and the electric field is polarized along the y- axis, then there's a non-zero y-component of the electric field, while there are non-zero x and z-components of the magnetic field as mentioned before.

Helmholtz equation for TE mode can be written as

$$\frac{\partial^2 E_y}{\partial x^2} + \frac{\partial^2 E_y}{\partial z^2} + k^2 E_y = 0, \tag{3.2}$$

Since the propogation is along x- axis, $E_y(x,z)$ can be written as

$$E_y(x,z) = E_y(z)e^{i\beta x} \quad . \tag{3.3}$$

Eq. (3.2) becomes

$$\frac{d^2 E_y}{dz^2} + k_0^2(\varepsilon_i \mu_i - N^2)E_y(z) = 0, \tag{3.4}$$

where $\beta = k_0$, $k^2 = k_0^2 \varepsilon_i \mu_i$ and N is the effective refractive index

The solution of Eq. (3.4) in the *l*-th cell can be written as [33]

$$E_{y1}(z) = a_l e^{iq_1(z-ld)} + b_l e^{-iq_1(z-ld)}, \quad (l-1)d + d_2 < z < ld \tag{3.5}$$

$$E_{y2}(z) = c_l e^{iq_2(z-ld)} + f_l e^{-iq_2(z-ld)}, \quad (l-1)d < z < (l-1)d + d_2 \tag{3.6}$$

where $q_1 = k_0\sqrt{\varepsilon_1 \mu_1 - N^2}$, $q_2 = k_0\sqrt{\varepsilon_2 \mu_2 - N^2}$

The nonzero components of the magnetic field (H_x and H_z) can be calculated using

$$H_x = \frac{-1}{i\mu\omega}\frac{\partial E_y}{\partial z}, \tag{3.7}$$

from which

$$H_{x1} = \frac{-q_1}{\mu_1 \omega}(a_l e^{iq_1(z-ld)} - b_l e^{-iq_1(z-ld)}), \tag{3.8}$$

$$H_{x2} = \frac{-q_2}{\mu_2 \omega}(c_l e^{iq_2(z-ld)} - f_l e^{-iq_2(z-ld)}), \tag{3.9}$$

and

$$H_z = \frac{i}{\omega\mu}\frac{\partial Ey}{\partial x}, \tag{3.10}$$

$$H_{z1} = -\frac{\beta}{\mu_1 \omega}(a_l e^{iq_1(z-ld)} + b_l e^{-iq_1(z-ld)}), \tag{3.11}$$

$$H_{z2} = -\frac{\beta}{\mu_2 \omega}(c_l e^{iq_2(z-ld)} + f_l e^{-iq_2(z-ld)}) \, . \tag{3.12}$$

The boundary conditions require that the tangential components of $\boldsymbol{E}$ and $\boldsymbol{H}$ to be continuous at $z = (l-1)d$ and $z = (l-1)d + d_2$, yielding a set of homogeneous linear equations for the coefficients a_i, b_i, c_i, and f_i.

The continunity of E_y and H_x at $z = (l-1)d$ gives

$$a_{l-1} + b_{l-1} = c_l e^{-iq_2 d} + f_l e^{iq_2 d}, \tag{3.13}$$

$$q_{TE}(a_{l-1} - b_{l-1}) = q_2\left(c_l e^{-iq_2 d} - f_l e^{iq_2 d}\right). \tag{3.14}$$

The two above equations can be written in a matrix form as

$$\begin{pmatrix} 1 & 1 \\ 1 & -1 \end{pmatrix}\begin{pmatrix} a_{l-1} \\ b_{l-1} \end{pmatrix} = \begin{pmatrix} e^{-iq_2 d} & e^{iq_2 d} \\ \frac{q_2}{q_{TE}} e^{-iq_2 d} & \frac{-q_2}{q_{TE}} e^{iq_2 d} \end{pmatrix}\begin{pmatrix} c_l \\ f_l \end{pmatrix}, \tag{3.15}$$

where $q_{TE} = \frac{\mu_2}{\mu_1} q_1$.

The continunity of E_y and H_x at $z = [(l-1)d] + d_2$ gives

$$c_l e^{-iq_2 d_1} + f_l e^{iq_2 d_1} = a_l e^{-iq_1 d_1} + b_l e^{iq_1 d_1}, \tag{3.16}$$

$$q_2\left(c_l e^{-iq_2 d_1} - f_l e^{iq_2 d_1}\right) = q_{TE}\left(a_l e^{-iq_1 d_1} - b_l e^{iq_1 d_1}\right). \tag{3.17}$$

Eqs. (3.16) and (3.17) can be written in matrix notation as

$$\begin{pmatrix} e^{-iq_2 d_1} & e^{iq_2 d_1} \\ e^{-iq_2 d_1} & -e^{iq_2 d_1} \end{pmatrix}\begin{pmatrix} c_l \\ f_l \end{pmatrix} = \begin{pmatrix} e^{-iq_1 d_1} & e^{iq_1 d_1} \\ \frac{q_{TE}}{q_2} e^{-iq_2 d} & \frac{-q_{TE}}{q_2} e^{iq_1 d_1} \end{pmatrix}\begin{pmatrix} a_l \\ b_l \end{pmatrix}. \tag{3.18}$$

Consider

$$X = \begin{pmatrix} e^{-iq_2 d_1} & e^{iq_2 d_1} \\ e^{-iq_2 d_1} & -e^{iq_2 d_1} \end{pmatrix}. \tag{3.19}$$

The inverse of matrix X is given by

$$X^{-1} = \frac{1}{2}\begin{pmatrix} e^{iq_2 d_1} & e^{iq_2 d_1} \\ e^{-iq_2 d_1} & -e^{-iq_2 d_1} \end{pmatrix}. \tag{3.20}$$

Multiplying Eq. (3.18) by X^{-1}, we get

$$\begin{pmatrix} c_l \\ f_l \end{pmatrix} = \frac{1}{2}\begin{pmatrix} e^{-iq_2 d_1} & e^{iq_2 d_1} \\ e^{-iq_2 d_1} & -e^{iq_2 d_1} \end{pmatrix}\begin{pmatrix} e^{-iq_1 d_1} & e^{iq_1 d_1} \\ \frac{q_{TE}}{q_2} e^{-iq_2 d} & \frac{-q_{TE}}{q_2} e^{iq_1 d_1} \end{pmatrix}\begin{pmatrix} a_l \\ b_l \end{pmatrix}. \tag{3.21}$$

Substituting from Eq. (3.21) into Eq. (3.15), we obtain

$$\begin{pmatrix} 1 & 1 \\ 1 & -1 \end{pmatrix}\begin{pmatrix} a_{l-1} \\ b_{l-1} \end{pmatrix} = \frac{1}{2}\begin{pmatrix} e^{-iq_2 d} & e^{iq_2 d} \\ \frac{q_2}{q_{TE}} e^{-iq_2 d} & \frac{-q_2}{q_{TE}} e^{iq_2 d} \end{pmatrix}\begin{pmatrix} e^{-iq_2 d_1} & e^{iq_2 d_1} \\ e^{-iq_2 d_1} & -e^{iq_2 d_1} \end{pmatrix}\begin{pmatrix} e^{-iq_1 d_1} & e^{iq_1 d_1} \\ \frac{q_{TE}}{q_2} e^{-iq_2 d} & \frac{-q_{TE}}{q_2} e^{iq_1 d_1} \end{pmatrix}\begin{pmatrix} a_l \\ b_l \end{pmatrix}. \tag{3.22}$$

Performing the product of matrices and multiplying both sides of the above equation by $\frac{1}{2}\begin{pmatrix} 1 & 1 \\ 1 & -1 \end{pmatrix}$, we get

$$\begin{pmatrix} a_{l-1} \\ b_{l-1} \end{pmatrix} = \frac{1}{2}\begin{pmatrix} 1 & 1 \\ 1 & -1 \end{pmatrix}\begin{pmatrix} \cos(q_2 d_2)e^{-iq_1 d_1} - \frac{iq_{TE}}{q_2}e^{-iq_1 d_1}sin(q_2 d_2) & \cos(q_2 d_2)e^{iq_1 d_1} + \frac{iq_{TE}}{q_2}sin(q_2 d_2)e^{iq_1 d_1} \\ -\frac{iq_2}{q_{TE}}sin(q_2 d_2)e^{-iq_1 d_1} + \cos(q_2 d_2)e^{-iq_1 d_1} & -\frac{iq_2}{q_{TE}}sin(q_2 d_2)e^{iq_1 d_1} - \cos(q_2 d_2)e^{iq_1 d_1} \end{pmatrix}\begin{pmatrix} a_l \\ b_l \end{pmatrix}, \tag{3.23}$$

which can be reduced to take the form

$$\begin{pmatrix} a_{l-1} \\ b_{l-1} \end{pmatrix} = \begin{pmatrix} A & B \\ C & D \end{pmatrix}\begin{pmatrix} a_l \\ b_l \end{pmatrix} = M\begin{pmatrix} a_l \\ b_l \end{pmatrix}, \tag{3.24}$$

where M is called the transfer matrix with the elements

$$A = e^{-iq_1 d_1}\left[\cos(q_2 d_2) - \frac{1}{2}i\left(\frac{q_2}{q_{TE}} + \frac{q_{TE}}{q_2}\right)sin(q_2 d_2)\right], \tag{3.25}$$

$$B = e^{iq_1 d_1}\left[-\frac{1}{2}i\left(\frac{q_2}{q_{TE}} - \frac{q_{TE}}{q_2}\right)sin(q_2 d_2)\right], \tag{3.26}$$

$$C = e^{-iq_1 d_1}\left[\frac{1}{2}i\left(\frac{q_2}{q_{TE}} - \frac{q_{TE}}{q_2}\right)sin(q_2 d_2)\right], \tag{3.27}$$

$$D = e^{iq_1 d_1}\left[\cos(q_2 d_2) + \frac{1}{2}i\left(\frac{q_2}{q_{TE}} + \frac{q_{TE}}{q_2}\right)sin(q_2 d_2)\right]. \tag{3.28}$$

The transfer matrix of the structure shown in Fig. 3.1 can be written as

$$\begin{pmatrix} a_0 \\ b_0 \end{pmatrix} = \begin{pmatrix} A & B \\ C & D \end{pmatrix}^l \begin{pmatrix} a_l \\ b_l \end{pmatrix}, \tag{3.29}$$

which may written as

$$\begin{pmatrix} a_l \\ b_l \end{pmatrix} = \begin{pmatrix} A & B \\ C & D \end{pmatrix}^{-l} \begin{pmatrix} a_0 \\ b_0 \end{pmatrix}. \tag{3.30}$$

The electric field vector in a periodic layered medium can be written using Bloch theorem as [45]

$$E_{K_B}(x, z) = E_{K_B}(z)e^{iK_B z}e^{-i(\omega t - \beta x)}, \tag{3.31}$$

where $E_{K_B}(z + d) = E_{K_B}(z)$, (3.32)

where K_B is the Bloch wave number

In terms of column-vector representation, and from Eq. (3.5) the periodic condition in Eq. (3.32) for Bloch wave is

$$\begin{pmatrix} a_l \\ b_l \end{pmatrix} = e^{ik_B d}\begin{pmatrix} a_{l-1} \\ b_{l-1} \end{pmatrix}. \tag{3.33}$$

Substituting for $\begin{pmatrix} a_{l-1} \\ b_{l-1} \end{pmatrix}$ from Eq. (3.24) into Eq. (3.33), we get

$$\begin{pmatrix} A & B \\ C & D \end{pmatrix}\begin{pmatrix} a_l \\ b_l \end{pmatrix} = e^{-ik_B d}\begin{pmatrix} a_l \\ b_l \end{pmatrix}, \tag{3.34}$$

$$\begin{pmatrix} A - e^{-ik_B d} & B \\ C & D - e^{-ik_B d} \end{pmatrix} \begin{pmatrix} a_l \\ b_l \end{pmatrix} = 0. \tag{3.35}$$

By taking the determinant

$$\begin{vmatrix} A - e^{-ik_B d} & B \\ C & D - e^{-ik_B d} \end{vmatrix} = 0,$$

Then

$$(A - e^{-ik_B d})(D - e^{-ik_B d}) - BC = 0. \tag{3.36}$$

But $AD - BC = 1$,

$$e^{-2ik_B d} - (A + D)e^{-ik_B d} + 1 = 0. \tag{3.37}$$

The solution of the above equation for $e^{-ik_B d}$ is given by

$$e^{-ik_B d} = \left(\frac{A+D}{2}\right) \mp \left(\left(\frac{A+D}{2}\right)^2 - 1\right)^{\frac{1}{2}}. \tag{3.38}$$

The eigenvectors corresponding to the eigenvalues are obtained from Eq. (3.34) as

$$\begin{pmatrix} a_0 \\ b_0 \end{pmatrix} = \begin{pmatrix} B \\ e^{-ik_B d} - A \end{pmatrix}, \tag{3.39}$$

Then the corresponding column vectors for the *l*-th unit cell are given by

$$\begin{pmatrix} a_l \\ b_l \end{pmatrix} = e^{lk_B d} \begin{pmatrix} B \\ e^{-ik_B d} - A \end{pmatrix}. \tag{3.40}$$

Multiplying Eq. (3.37) by $e^{-ik_B d}$, we get

$$e^{-ik_B d} + e^{ik_B d} = A + D. \tag{3.41}$$

Using the identity $\cos x = \frac{e^{ix} + e^{-ix}}{2}$, we get

$$2\cos(k_B d) = A + D. \tag{3.42}$$

Substituting for A and D from Eq. (3.25) and Eq. (3.28) into Eq. (3.42), we get

$$2\cos(k_B\, d) = \cos(q_2 d_2)(e^{iq_1 d_1} + e^{-iq_1 d_1}) + \frac{1}{2} i \left(\frac{q_2}{q_{TE}} + \frac{q_{TE}}{q_2}\right) \sin q_2 d_2 \left(e^{iq_1 d_1} - q^{-iq_1 d_1}\right),$$

$$\cos(k_B\, d) = \cos(q_2 d_2)\cos(q_1 d_1) - \frac{1}{2}\left(\frac{q_2}{q_{TE}} + \frac{q_{TE}}{q_2}\right) \sin(q_2 d_2)\sin(q_1 d_1). \tag{3.43}$$

Equation (3.43) represents the dispersion relation for TE wave.

3.2.2. Sensitivity

The sensitivity of the effective refractive index to any change in an analyte refractive index is calculated as the change of the effective index (N) with respect to the change in the analyte index (n_1); i.e.,

$$S = \frac{\partial N}{\partial n_1}. \tag{3.44}$$

Differentiating the dispersion relation given by Eq. (3.43) with respect to N, then calculating S as $S=\left(\frac{\partial n_1}{\partial N}\right)^{-1}$ (3.45)

$$-2\,d_2 cos(q_1 d_1)\, sin(q_2 d_2)\frac{k_0^2 N}{q_2} + 2d_1\, cos(\,q_2 d_2\,) sin(\,q_1 d_1)\frac{k_0^2(n_1\frac{\partial n_1}{\partial N}-N)}{q_1} + \frac{\mu_1}{\mu_2}\left(\frac{-K_0^2 N}{q_1 q_2} - \frac{q_2 k_0^2}{q_1^3}\left(n_1\frac{\partial n_1}{\partial N}-N\right)\right) sin(\,q_1 d_1\,) sin(\,q_2 d_2) + d_1\frac{\mu_1}{\mu_2}\frac{q_2}{q_1} cos(q_1 d_1)\, sin(q_2 d_2)\frac{k_0^2}{q_1}\left(n_1\frac{\partial n_1}{\partial N}-N\right) - d_2\frac{\mu_1}{\mu_2}\frac{q_2}{q_1} cos(q_2 d_2)\, sin(q_1 d_1)\frac{k_0^2 N}{q_2} + \frac{\mu_2}{\mu_1}\left(\frac{K_0^2\left(\left(n_1\frac{\partial n_1}{\partial N}-N\right)\right)}{q_1 d_2} + \frac{q_1}{q_2^3}k_0^2 N\right) sin(\,q_1 d_1\,) sin(\,q_2 d_2) + d_1\frac{\mu_2}{\mu_1}\frac{q_1}{q_2} cos(q_1 d_1)\, sin(q_2 d_2)\frac{k_0^2}{q_1}\left(n_1\frac{\partial n_1}{\partial N}-N\right) - d_2\frac{\mu_2}{\mu_1}\frac{q_1}{q_2} cos(q_2 d_2)\, sin(q_1 d_1)\frac{k_0^2 N}{q_2}=0. \tag{3.46}$$

After some arrangement, we obtain

$$-2d_2\cos(q_1 d_1)\sin(q_2 d_2)\frac{k_o^2 N}{q_2} - 2d_1\cos(q_1 d_1)\sin(q_2 d_2)\frac{k_0^2 N}{q_1} - \frac{\mu_1}{\mu_2}\frac{k_0^2 N}{q_1 q_2}\sin(q_1 d_2)\sin(q_2 d_2) + \frac{\mu_1}{\mu_2}\frac{q_2}{q_1^3}k_o^2 N\sin(q_1 d_1)\sin(q_2 d_2) - d_1\frac{\mu_1}{\mu_2}\frac{q_2}{q_1}\cos(q_1 d_1)\sin(q_2 d_2) - d_2\frac{\mu_1}{\mu_2}\frac{q_2}{q_1}\cos(q_2 d_2)\sin(q_1 d_1)\frac{k_0^2 N}{q_2} - \frac{\mu_2}{\mu_1}\frac{k_0^2 N}{q_1 q_2}\sin(q_1 d_1)\sin(q_2 d_2) + \frac{\mu_2}{\mu_1}\frac{q_1}{q_2^3}k_0^2 N\sin(q_1 d_1)\sin(q_2 d_2) - d_1\frac{\mu_2}{\mu_1}\frac{q_1}{q_2}\cos(q_1 d_1)\sin(q_2 d_2)\frac{k_0^2 N}{q_1} - d_2\frac{\mu_2}{\mu_1}\frac{q_1}{q_2}\cos(q_2 d_2)\sin(q_1 d_1)\frac{k_0^2 N}{q_2} =$$

$$-2d_1\cos(q_2 d_2)\sin(q_1 d_1)\frac{k_o^2}{q_1}n_1\frac{\partial n_1}{\partial N} + \frac{\mu_1}{\mu_2}\frac{q_2}{q_1^3}k_0^2 n_1\frac{\partial n_1}{\partial N}\sin(q_1 d_1)\sin(q_2 d_2) - d_1\frac{\mu_1}{\mu_2}\frac{q_2}{q_1}\frac{k_0^2}{q_1}n_1\frac{\partial n_1}{\partial N}\cos(q_1 d_1)\sin(q_2 d_2) - \frac{\mu_2}{\mu_1}\frac{k_o^2}{q_1 q_2}n_1\frac{\partial n_1}{\partial N}\sin(q_1 d_1)\sin(q_2 d_2) - d_1\frac{\mu_2}{\mu_1}\frac{q_2}{q_1}\frac{k_0^2}{q_1}n_1\frac{\partial n_1}{\partial N}\cos(q_1 d_1)\cos(q_2 d_2). \tag{3.47}$$

$$\mathrm{N}\Big[-2\left(\frac{d_1}{q_1}u+\frac{d_2}{q_2}v\right)+sin(\,q_1d_1\,)sin(\,q_2d_2)\left\{\left(\frac{\mu_1}{\mu_2}\frac{q_2}{q_1}\right)\left(\frac{1}{q_1^2}-\frac{1}{q_2^2}\right)+\frac{\mu_2}{\mu_1}\frac{q_1}{q_2}\left(\frac{1}{q_2^2}-\frac{1}{q_1^2}\right)\right\}-\frac{d_1}{q_1}v\left(\frac{\mu_1}{\mu_2}\frac{q_2}{q_1}+\frac{\mu_2}{\mu_1}\frac{q_1}{q_2}\right)-\frac{d_2}{q_2}u\left(\frac{\mu_1}{\mu_2}\frac{q_2}{q_1}+\frac{\mu_2}{\mu_1}\frac{q_1}{q_2}\right)\Big]=n_1\left[-2\frac{d_1}{q_1}u-\frac{d_1}{q_1}v\left(\frac{\mu_1}{\mu_2}\frac{q_2}{q_1}+\frac{\mu_2}{\mu_1}\frac{q_1}{q_2}\right)+\left(\frac{\mu_1}{\mu_2}\frac{q_2}{q_1}-\frac{\mu_2}{\mu_1}\frac{q_1}{q_2}\right)\frac{1}{q_1^2}sin(q_1d_1)\,sin(q_2d_2)\right]\frac{\partial n_1}{\partial N}. \quad (3.48)$$

$$\mathrm{N}\Big[-2\left(\frac{d_1}{q_1}u+\frac{d_2}{q_2}v\right)+w\left(\frac{\mu_1}{\mu_2}\frac{q_2}{q_1}-\frac{\mu_1}{\mu_2}\frac{q_2}{q_1}\right)\left(\frac{q_2^2-q_1^2}{q_1^2q_2^2}\right)-\left(\frac{d_1}{q_1}v+\frac{d_2}{q_2}u\right)\tau_{TE}\Big]=n_1\left[-2\frac{d_1}{q_1}u-\frac{d_1}{q_1}\tau_{TE}v+\frac{1}{q_1^2}\sigma_{TE}w\right]\frac{\partial n_1}{\partial N}. \quad (3.49)$$

$$S=\frac{n_1\left[-2\frac{d_1}{q_1}u-\frac{d_1}{q_1}\tau_{TE}v+\frac{1}{q_1^2}\sigma_{TE}w\right]}{N\left[-2\left(\frac{d_1}{q_1}u+\frac{d_2}{q_2}v\right)+\left(\frac{q_2^2-q_1^2}{q_1^2q_2^2}\right)\sigma_{TE}w-(\frac{d_1}{q_1}v+\frac{d_2}{q_2}u)\tau_{TE}\right]}\,, \quad (3.50)$$

where $u=\cos(\mathrm{q_2d_2})\sin(\mathrm{q_1d_1})$, $w=\sin(q_1d_1)\sin(q_2d_2)$, $\tau_{TE}=(\frac{\mu_1}{\mu_2}\frac{q_2}{q_1}+\frac{\mu_2}{\mu_1}\frac{q_1}{q_2})$, and $\sigma_{TE}=\left(\frac{\mu_1}{\mu_2}\frac{q_2}{q_1}-\frac{\mu_1}{\mu_2}\frac{q_2}{q_1}\right)$.

3.2.3. Power flowing within the photonic crystal layers

It is useful to find the total time-average power transported by the photonic crystal layers, since there is a close connection between the sensitivity of the proposed sensor and the power flowing in the analyte layer

$$P_{total}=\frac{\beta}{2\omega}\int_{-\infty}^{\infty}\frac{\left|E_y(z)\right|^2}{\mu_i(z)}dz\ . \quad (3.51)$$

For the first unit cell, $l=1$

In the first layer

$$p_1=\frac{\beta}{2\omega\mu_1}\int_0^{d_1}\left(a_1^2e^{2iq_1(z-d)}+b_1^2e^{-2iq_1(z-d)}+2a_1b_1\right)dz,$$

$$=\frac{\beta}{2\omega\mu_1}\left(a_1^2\frac{e^{2iq_1(z-d)}}{2iq_1}+b_1^2\frac{e^{2iq_1(z-d)}}{-2iq_1}+2a_1b_1z\right),$$

$$=\frac{\beta}{2\omega\mu_1}\left(\frac{a_1^2}{2iq_1}\left(e^{-2iq_1d_2}-e^{-2iq_1d}\right)-\frac{b_1^2}{2iq_1}\left(e^{2iq_1d_2}-e^{2iq_1d}\right)+2a_1b_1d_1\right). \quad (3.52)$$

In the second layer

$$p_1{}'=\frac{\beta}{2\omega\mu_1}\int_{d_1}^{d}\left(c_1^2e^{2iq_1(z-d)}+f_1^2e^{-2iq_1(z-d)}+2c_1f_1\right)dz,$$

$$=\frac{\beta}{2\omega\mu_1}\left(c_1^2\frac{e^{2iq_1(z-d)}}{2iq_1}+f_1^2\frac{e^{2iq_1(z-d)}}{-2iq_1}+2c_1f_1z\right),$$

$$= \frac{\beta}{2\mu\omega_1}\left(\frac{c_1^2}{2iq_2}\left(1-e^{-2iq_2d_2}\right) - f_1^2\frac{\left(1-e^{2iq_2d_2}\right)}{2iq_2} + 2c_1f_1d_2\right). \quad (3.53)$$

For the second unit cell, $l = 2$

In the first layer

$$p_2 = \frac{\beta}{2\omega\mu_2}\int_d^{d+d_1}\left(a_2^2e^{2iq_1(z-2d)} + b_2^2e^{-2iq_1(z-2d)} + 2a_1b_1\right)dz,$$

$$= \frac{\beta}{2\omega\mu_2}\left(a_2^2\frac{e^{2iq_1(z-2d)}}{2iq_1} + b_2^2\frac{e^{-2iq_1(z-2d)}}{-2iq_1} + 2a_2b_2z\right),$$

$$= \frac{\beta}{2\omega\mu_2}\left(\frac{a_2^2}{2iq_1}\left(e^{-2iq_1d_2} - e^{-2iq_1d}\right) - \frac{b_2^2}{2iq_1}\left(e^{2iq_1d_2} - e^{2iq_1d}\right) + 2a_2b_2d_1\right). \quad (3.54)$$

In the second layer

$$p_2{}' = \frac{\beta}{2\omega\mu_2}\int_{d+d_1}^{2d}\left(c_2^2e^{2iq_2(z-2d)} + f_2^2e^{-2iq_1(z-2d)} + 2c_2f_2\right)dz,$$

$$= \frac{\beta}{2\omega\mu_2}\left(c_2^2\frac{e^{2iq_2(z-2d)}}{2iq_2} + f_2^2\frac{e^{-2iq_2(z-d)}}{-2iq_2} + 2c_2f_2z\right),$$

$$= \frac{\beta}{2\omega\mu_2}\left(\frac{c_2^2}{2iq_2}\left(1-e^{-2iq_2d_2}\right) - f_2^2\frac{\left(1-e^{2iq_2d_2}\right)}{2iq_2} + 2c_1f_1d_2\right). \quad (3.55)$$

For the third unit cell, $l = 3$

In the first layer

$$p_3 = \frac{\beta}{2\omega\mu_3}\int_{2d}^{2d+d_1}\left(a_3^2e^{2iq_1(z-3d)} + b_3^2e^{-2iq_1(z-3d)} + 2a_3b_3\right)dz,$$

$$= \frac{\beta}{2\omega\mu_3}\left(a_3^2\frac{e^{2iq_1(z-3d)}}{2iq_1} + b_3^2\frac{e^{-2iq_1(z-3d)}}{-2iq_1} + 2a_3b_3z\right),$$

$$= \frac{\beta}{2\omega\mu_3}\left(\frac{a_3^2}{2iq_1}\left(e^{-2iq_1d_2} - e^{-2iq_1d}\right) - \frac{b_3^2}{2iq_1}\left(e^{2iq_1d_2} - e^{2iq_1d}\right) + 2a_3b_3d_1\right). \quad (3.56)$$

In the second layer

$$p_3{}' = \frac{\beta}{2\omega\mu_2}\int_{2d+d_1}^{3d}\left(c_3^2e^{2iq_2(z-3d)} + f_3^2e^{-2iq_1(z-3d)} + 2c_3f_3\right)dz,$$

$$= \frac{\beta}{2\omega\mu_3}\left(c_3^2\frac{e^{2iq_2(z-3d)}}{2iq_2} + f_3^2\frac{e^{-2iq_2(z-3d)}}{-2iq_2} + 2c_3f_3z\right),$$

$$= \frac{\beta}{2\omega\mu_2}\left(\frac{c_3^2}{2iq_2}\left(1-e^{-2iq_2d_2}\right) - f_3^2\frac{\left(1-e^{2iq_2d_2}\right)}{2iq_2} + 2c_3f_3d_2\right). \quad (3.57)$$

For l^{th} cell, the power for the first layer can be written as

$$p_l = \frac{\beta}{2\omega\mu_l}\left(\frac{a_l^2}{2iq_1}\left(e^{-2iq_1d_2} - e^{-2iq_1d}\right) - \frac{b_l^2}{2iq_1}\left(e^{2iq_1d_2} - e^{2iq_1d}\right) + 2a_lb_ld_1\right). \quad (3.58)$$

and for the second layer it can be written as

$$p_l' = \frac{\beta}{2\omega\mu_2}\left(\frac{c_l^2}{2iq_2}\left(1 - e^{-2iq_2d_2}\right) - f_l^2\frac{\left(1-e^{2iq_2d_2}\right)}{2iq_2} + 2c_lf_ld_2\right). \quad (3.59)$$

3.3. **Results and discussion**

The dispersion relation given by Eq. (3.43) was solved numerically and the sensitivity was calculated using Eq. (3.50). In the following computations, a two layer photonic crystal was assumed in which the first layer was considered to be the analyte layer and the second layer was considered to be LHM, dielectric or metal. This section was divided into three subsections. In the first subsection, the second layer was assumed to be LHM. In the second and third subsections, the second layer was assumed metal and dielectric, respectively. In all subsections, the sensitivity was plotted with different parameters of the structure such as layer thickness and wave frequency.

3.3.1. Left-handed material (LHM)

The LHM is characterized by ε_2 and μ_2 which are given by Eqs. (2.1) and (2.2) with $\omega_p=2\omega$, $\omega_0=0.4\omega_p$, F=0.56 and $\gamma=0.012\omega_p$. The frequency range was taken from 4.0 GHz to 6.0 GHz in which ε_2 and μ_2 are simultaneously negative according to Eqs. (2.1) and (2.2). The analyte layer was assumed to be water with $n_1=1.33$.

Figure 3.2 shows the sensitivity of the proposed sensor versus the thickness of the LHM layer for different values of the wave frequency. It is obvious from the figure that the sensitivity increases with increasing the LHM layer thickness and peaks at an optimum value of the thickness. For thicknesses beyond the optimum thickness, the sensitivity decreases towards extremely low values. Increasing the LHM layer thickness beyond the optimum value enhances the electric field in the LHM layer and the sensitivity decreases. The figure also illustrates the dependence of the sensitivity on the guided wave frequency. The sensitivity can be dramatically enhanced with decreasing the guided wave frequency. As the frequency increases, the wavelength decreases and the wave confinement in the LHM layer increases. Consequently the evanescent field in the analyte medium decreases and so does the sensitivity. It is also clear that as the wave frequency increases, the sensitivity peak is shifted toward higher value of optimum thickness of the LHM layer. For ω= 5.0 GHz, the maximum sensitivity is 1.28 obtained

at d_2=13.34mm whereas it is 1.05 at d_2=14.37mm for ω=5.1GHz. On the other hand, for ω=5.2 GHz, the sensitivity reaches a peak of 0.87 at an optimum thickness of 16.73 mm. Also the sensitivity takes the range of 0.31≤ S≤ 1.28 when ω= 5.0 GHz whereas it takes the range of 0.36 ≤ S≤ 1.05 when ω= 5.1 GHz. When ω= 5.2 GHz, the sensitivity takes the range of 0.31 ≤ S≤ 0.87. It is worth comparing our results for the sensitivity with the conventional slab waveguide sensor comprising lossless dielectric media proposed by Tiefenthaler [18] in which the maximum sensitivity achieved is 0.25. Our results show that it is possible for LHM phototnic crystal to achieve a sensitivity improvement of 412% compared to conventional slab waveguide.

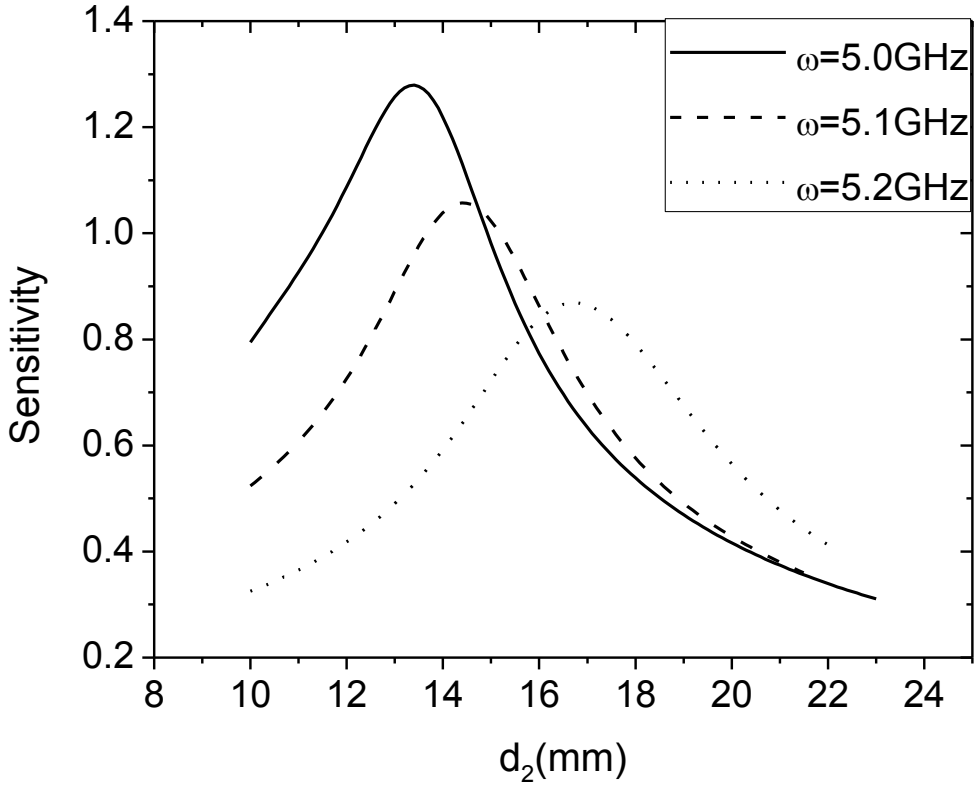

Fig. 3.2. Sensitivity of the proposed sensor versus the thickness of LHM layer for different values of frequency for ε_1=1.77, n_1=1.33, F=0.56, γ=0.012ω_p, d_1= 7.13mm, ω_p= 2ω, ω_0=0 .4 ω_p and k_B=π/(5d) .

Figure 3.3 shows the sensitivity versus the LHM layer thickness for some different values of the analyte thickness. It is clear that the sensitivity increases as the LHM layer thickness increases until it reaches a maximum value at an optimum thickness, then decreases with increasing the thickness of LHM layer. The maximum sensitivity can be enhanced with increasing the analyte layer thickness. As the analyte layer thickness increases, the evanescent field in the analyte medium is enhanced and so does the maximum sensitivity. It is also observed that as the analyte layer thickness increases, the maximum sensitivity is shifted toward higher value of optimum LHM thickness. The sensitivity reaches a maximum value of 1.28 at d_1=7.2mm and d_2=13.36 mm, whereas it has a value of 1.24 at d_2=12.3 mm for d_1=7.1mm. But at d_1=7.0mm, the sensitivity reaches 1.18 for an optimum LHM thickness of 12.12mm. It can be noted from Fig. 3.3 that when d_1 increases from 7.0 mm to 7.1 mm, the maximum sensitivity enhances by 3.2%. On the other hand, the maximum sensitivity increases by 5.1% as d_1 increases from 7.1mm to 7.2mm.

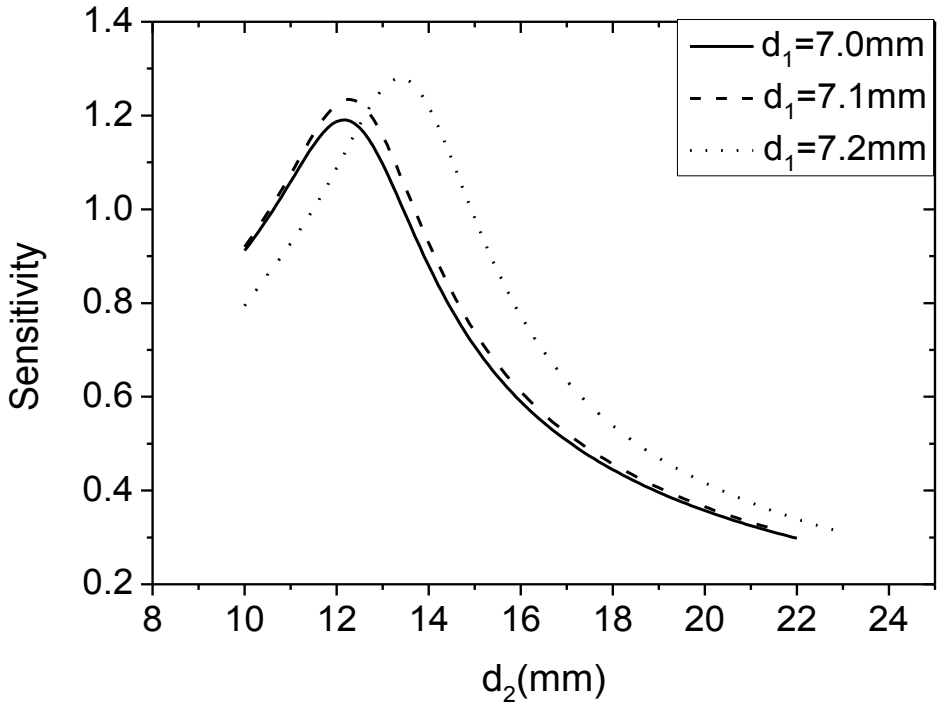

Fig. 3.3. Sensitivity of the proposed sensor versus the thickness of LHM layer for different values of the analyte thickness for ε_1=1.77, n_1=1.33, F=0.56, γ=0.012ω_p, ω=5.0 GHz, ω_p= 2ω, ω_0= 0.4 ω_p and k_B=π/(5d) .

The dependence of the sensitivity of the proposed sensor on the thickness of LHM layer for different values of electron scattering rate (γ) is plotted in Fig. 3.4. The sensitivity can be enhanced with decreasing the electron scattering rate (γ). As can be seen from the figure, as the electron scattering rate changes, the maximum sensitivity occurs at the same value of an optimum LHM thickness. The maximum sensitivity obtained has a value of 1.03 at $\gamma = 0.012\omega_p$. For $\gamma = 0.013\omega_p$, the sensitivity has a peak value of 0.99 whereas it is 0.95 at $\gamma = 0.014\omega_p$. As γ reduces from $0.014\omega_p$ to $0.013\omega_p$, the maximum sensitivity can be improved by 4.2%, while when γ reduces from $0.013\omega_p$ to $0.012\omega_p$, the maximum sensitivity can be improved by 4.0%.

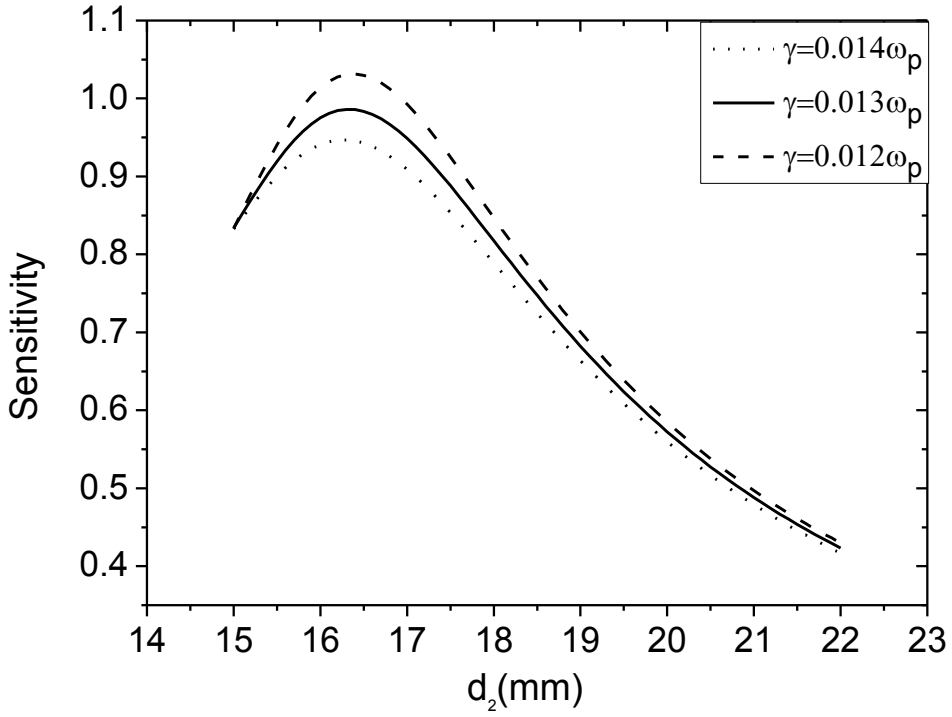

Fig. 3.4. Sensitivity of the proposed sensor versus the thickness of LHM layer for different values of electron scattering rate for $\varepsilon_1=1.77$, $n_1=1.33$, $F=0.56$, $k_B=\pi/(3d)$, $\omega=5.0$GHz, $\omega_p=2\omega$, $\omega_0=0.4\,\omega_p$ and $d_1=7.1$mm.

The variation of the sensitivity of the proposed sensor with the analyte thickness for different values of the thickness of LHM layer is illustrated in Fig. 3.5. As is clearly seen from the figure, the sensitivity increases slowly with d_1 until it reaches 0.87 at $d_1=6.7$mm, then it shows a sharp increase by furher of increasing d_1. One interesting

feature can be seen from the figure, the sensitivity can reach 2.17 for d_1= 8.82 mm and d_2= 14.1 mm which is extremely high value. The sensitivity exhibits a very slight dependence on d_2 as d_2 changes from 13.8mm to 14.1mm.

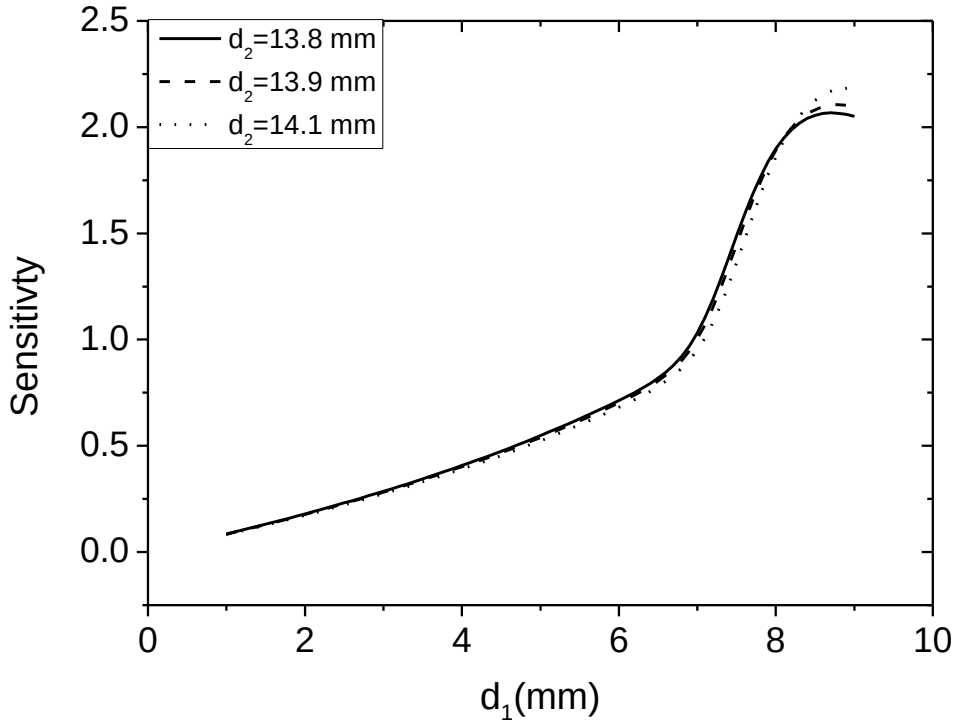

Fig. 3.5. Sensitivity of the proposed sensor versus analyte thickness for different values of the thickness of LHM layer for ε_1=1.77, n_1=1.33, F=0.56, γ =0.012ω_p, ω=5.0 GHz, ω_p= 2ω, ω_0=0 .4 ω_p and k_B=π/(5d).

3.3.2. Metal material

In this section, we assume the layer of thickness d_2 to be a metal. Two metals were considered : nickel and chromium.

Figures 3.6 and 3.7 show the sensitivity of the proposed sensor versus the thickness of metals (Ni) and (Cr) layer, respectively, for different values of the wavelength (λ). The sensitivity increases with increasing d_2 untill it reaches a maximum value at optimum d_2, then decreases very slightly with further increasing of d_2 untill it has a fixed value. Increasing the metal layer thickness beyond the optimum value does not show a

significant effect on the sensitivity. As can be seen from Fig. 3.6 and Fig. 3.7, increasing the wavelength decreases the sensitivity of the proposed sensor. It is also obvious that as the wavelength decreases, the sensitivity peak is shifted toward lower value of optimum thickness of the metal layer. For λ=632.8 nm, the sensitivity has a maximum value of 0.385 at nickel thickness of 148.7 nm whereas it has a maximum value of 1.27 at chromium thickness of 156.49 nm. For λ= 650 nm, the sensitivity has a peak of 0.375 at Ni thickness of 150.2 nm, whereas it has a peak of 1.15 at Cr thickness of 161.95 nm. On the other hand, the sensitivity of Ni metal structure has a peak of 0.348 at thickness of 161.9 nm for λ= 700 nm, but for Cr metal structure it has a peak of 0.86 at thickness of 187.01 nm for λ=700 nm. It can be seen from Fig. 3.6 that as λ decreases from 700nm to 650nm, the maximum sensitivity increases by 7.75% for Ni metal whereas it increases by 33.7% for Cr metal as shown in Fig. 3.7. As λ decreases from 650 nm to 632.8 nm, the maximum sensitivity increases by 2.7% for Ni metal as shown in Fig. 3.6 whereas it increases by 10.4% for Cr metal as shown in Fig. 3.7.

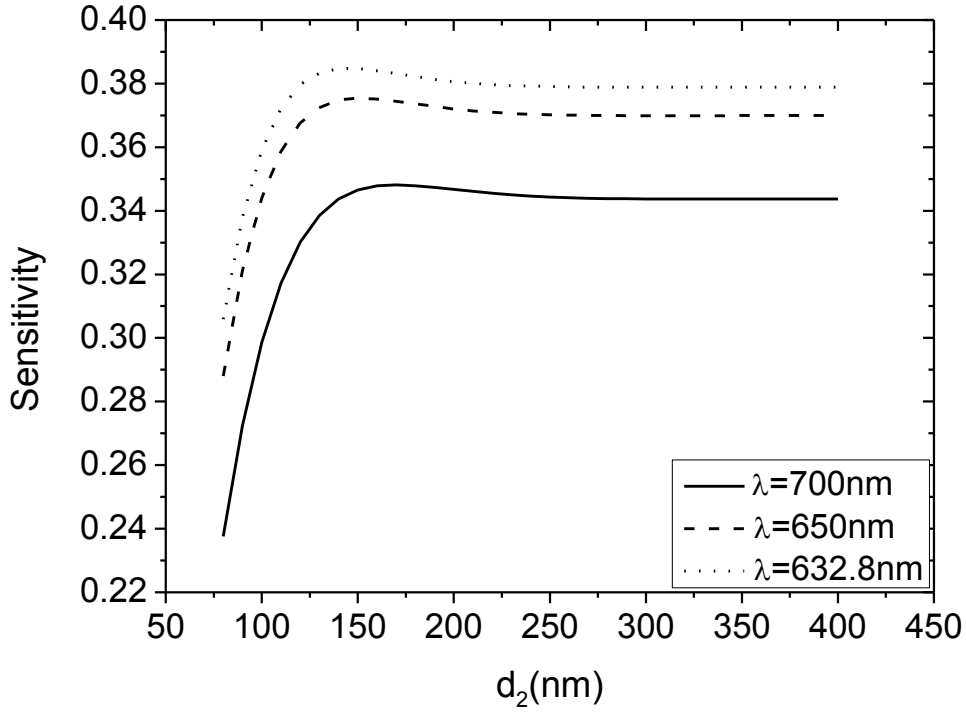

Fig. 3.6. Sensitivity of the proposed sensor versus the thickness of metal (Ni) layer for different values of wavelength (λ) for ε_1=1.77, μ_1=1,ε_2= - 9.96+14.66i, μ_2=1, k_B=π/(5d) and d_1=550nm.

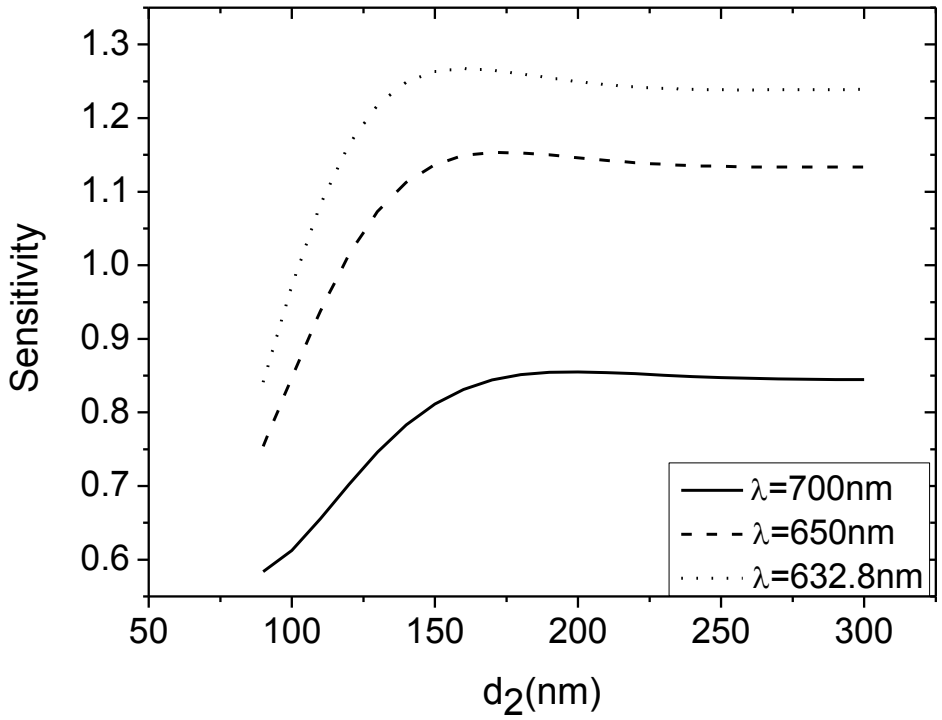

Fig. 3.7. Sensitivity of the proposed sensor versus the thickness of metal (Cr) layer for different values of wavelength (λ) for ε_1=1.77, μ_1=1, ε_2=-1.1+ 20.79i, μ_2=1, k_B=π/(5d) and d_1=670nm.

The sensitivity of the proposed sensor as a function of the metal layer thickness is plotted in Fig. 3.8 for (Ni) and in Fig. 3.9 for (Cr) for different values of the analyte thicknesses. Figures 3.8 and 3.9 show that the sensitivity can be increased by increasing the analyte thickness. It is observed from Fig. 3.8 that the sensitivity has maximum values of 0.370, 0.378 , and 0.385 at Ni thickness of 145.54nm for d_1= 530nm, 540 and 550nm, respectively, but Fig. 3.9 shows that it has maximum values of 1.14, 1.22 and 1.27 at Cr thickness of 163.37nm for d_1=650nm, 660nm and 670nm, respectively. As d_1 increases from 530nm to 540nm, the sensitivity increases by 2.16% whereas it enhances by 1.85% as d_1 increases from 540nm to 550nm for Ni metal structure. On the other hand, the

sensitivity enhances by 7.0% when d_1 increases from 650nm to 660nm, but it increases by 5.0% as d_1 increases from 660nm to 670nm for Cr metal structure.

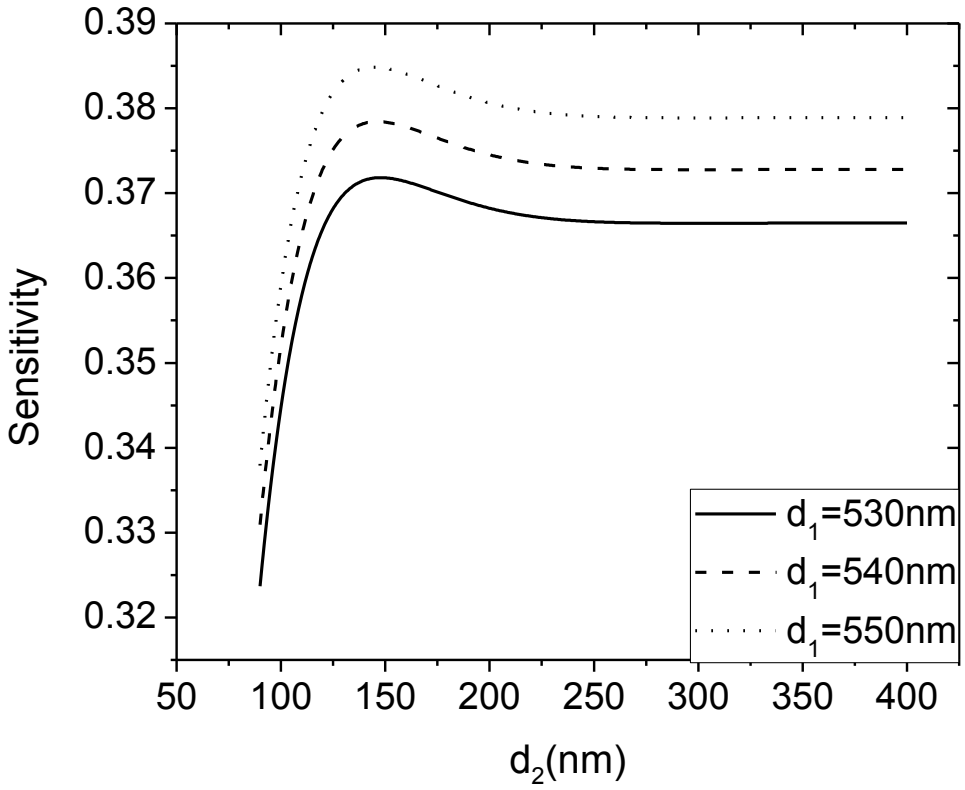

Fig. 3.8. Sensitivity of the proposed sensor versus the thickness of metal layer (Ni) for different values of the analyte thickness for λ=632.8nm, ε_1=1.77, μ_1=1, ε_2= -9.96+ 14.66i, μ_2=1 and $k_B=\pi/(5d)$.

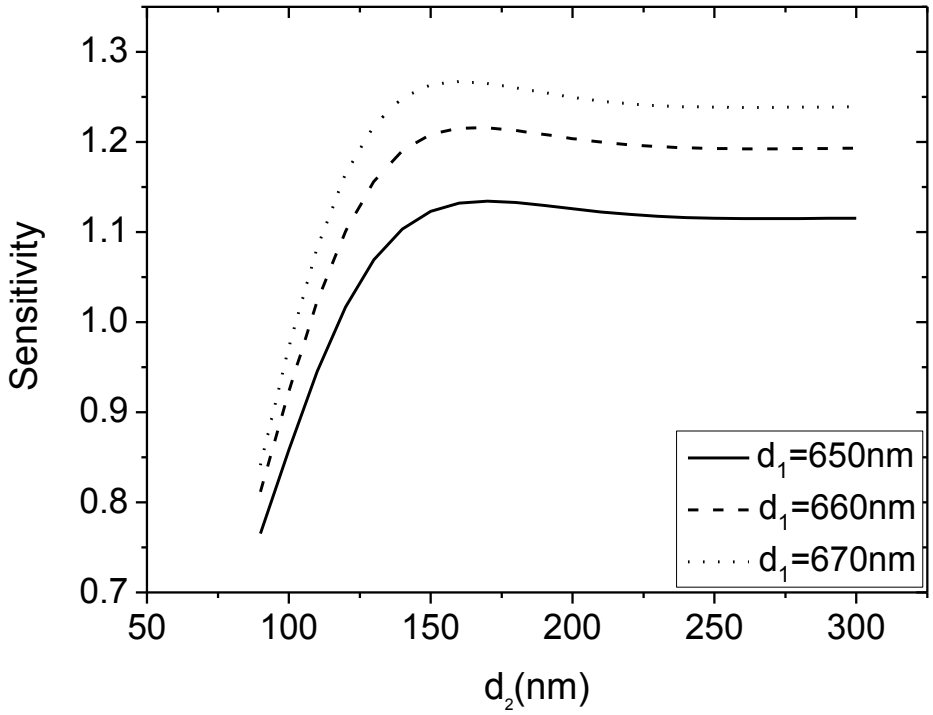

Fig. 3.9. Sensitivity of the proposed sensor versus the thickness of metal layer (Cr) for different values of the analyte thickness for λ=632.8nm, ε_1=1.77, μ_1=1, ε_2= -1.1+ 20.79i, μ_2 =1 and $k_B=\pi/(5d)$.

The sensitivity of the proposed sensor as a function of the analyte thickness is illustrated in Fig. 3.10 for (Ni) and in Fig. 3.11 for (Cr) for different values of the metal thicknesses. It can be shown from Fig. 3.10 that the sensitivity of the proposed sensor with (Ni) metal can be increased by increasing the thickness of analyte layer whereas Fig. 3.11 shows that the sensitivity of the proposed sensor with (Cr) metal can be increased by increasing the thickness of analyte layer untill it reaches a maximum value at an optimum d_1=670 nm, then decreases with further increasing of d_1. For 180 nm $\leq d_2 \leq$ 220 nm, changing the thickness of metal layer has an ignorable effect on the sensitivity of Ni metal structure as noted from Fig. 3.10. Also changing the thickness of Cr layer has a slight effect on the sensitivity in the range of 150 nm $\leq d_2 \leq$ 190 nm.

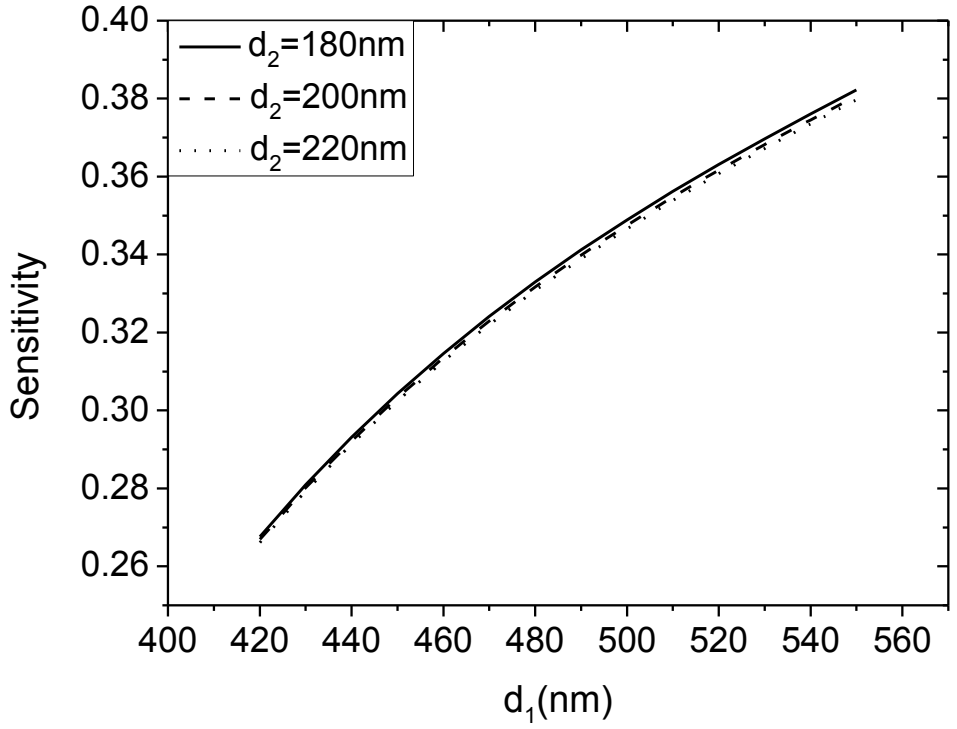

Fig. 3.10. Sensitivity of the proposed sensor versus the analyte thickness for different values of thickness of the metal layer (Ni) for λ=632.8nm, ε_1=1.77, μ_1=1, ε_2= -9.96+ 14.66i, μ_2=1 and $k_B=\pi/(5d)$.

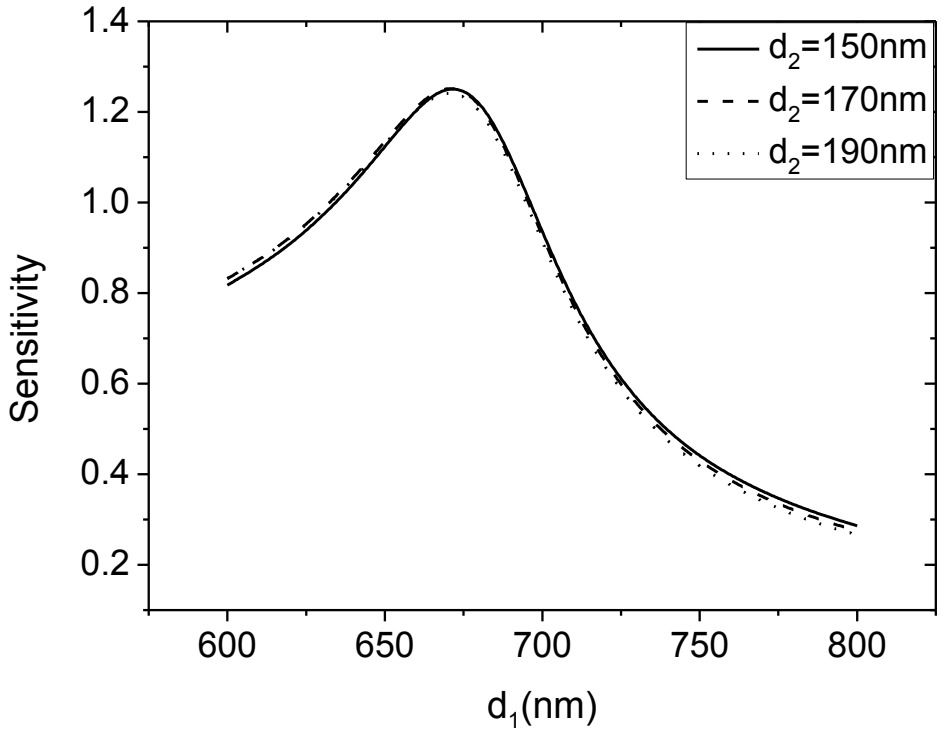

Fig. 3.11. Sensitivity of the proposed sensor versus the analyte thickness for different values of the thickness of metal layer (Cr) for λ=632.8nm, ε_1=1.77, μ_1=1, ε_2= -1.1+ 20.79i, μ_2=1 and k_B=π/(5d).

3.3.3. Dielectric material

In this subsection, we assume the layer of thickness d_2 to be a dielectric, silicon dioxide, of parameters ε_2=4.0 and μ_2=1.

The dependence of sensitivity on the thickness of the dielectric layer for various values of the analyte layer is shown in Fig. 3.12. It is found that the sensitivity increases very sharply with increasing the thickness of dielectric layer and reaches a maximum value at an optimum thickness of the dielectric layer, then decreases very slowly with increasing the thickness of the dielectric layer beyond the optimum thickness. The behaviour of the sensitivity with the analyte thickness is also illustrated in Fig. 3.12. It is obvious from the figure that as d_1 decreases, the maximum sensitivity is shiftd toward higher value of dielectric layer. For d_1= 100 nm, the sensitivity has a maximum value of 1.31 at d_2=

218.77 nm whereas it has a peak of 1.23 at d_2= 215.82 nm for d_1=105nm. The sensitivity has a peak of 1.16 at d_2= 212.72 nm for d_1= 110nm. An enhancement of 6.5% can be obtained when the analyte thickness is reduced from 105nm to 100nm whereas the sensitivity increases by 6.0% as the analyte thickness is reduced from 110nm to 105nm.

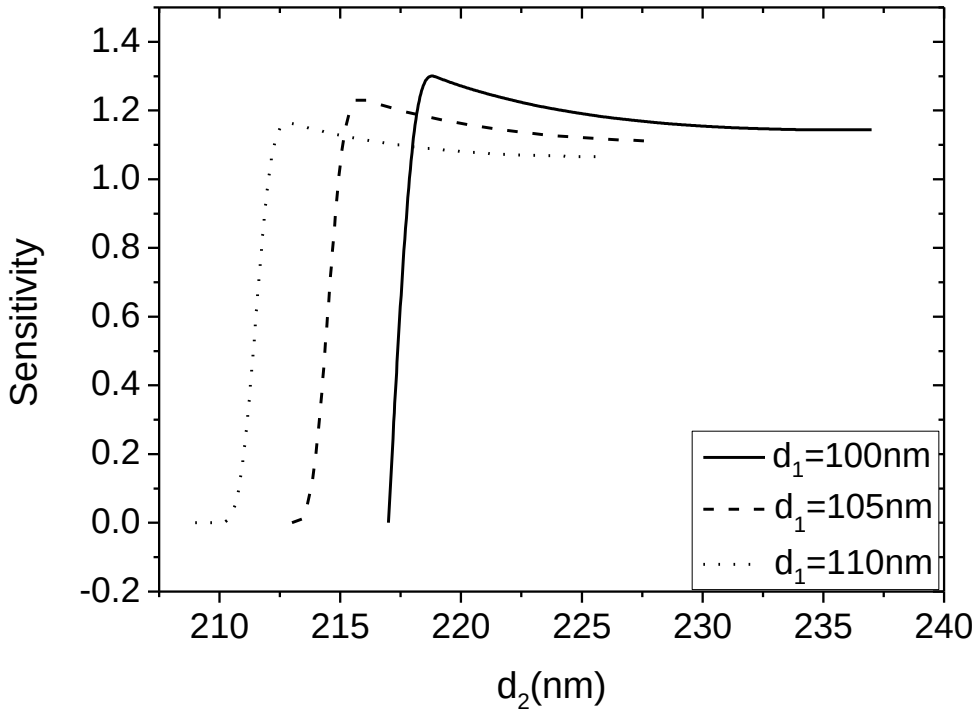

Fig. 3.12. Sensitivity of the proposed sensor versus the thickness of dielectric layer for different values of thickness of the analyte layer for λ=632.8nm, ε_1=1.77, μ_1=1, ε_2=4, μ_2=1 and k_B=π/(4d).

Figure 3.13 is plotted to study the variation of the sensitivity with the thickness of the dielectric layer for different value of wavelength. The Figure shows that the maximum sensitivity increases with increasing the wavelength. It is also clear that the maximum sensitivity at the optimal thickness of dielectric layer is shifted towards larger values of dielectric thickness as the wavelength increases. For λ = 632.8nm, the sensitivity has a maximum value of 1.16 at d_2= 212.81 nm and d_1=110nm whereas it has a maximum value of 1.30 at d_2=218.67 nm and d_1=100nm. On the other hand, for λ= 650nm, the sensitivity reaches a peak of 1.22 at an optimum dielectric thickness of 219.68 nm and d_1=110nm whereas it has a peak of 1.29 at an optimum thickness 227.74 nm and

d_1=100nm . As can be seen from Fig. 3.13 when λ increases from 632.8nm to 650nm, the sensitivity enhances by 0.8% for d_1=100nm whereas it enhances by 5.2% for d_2=110nm.

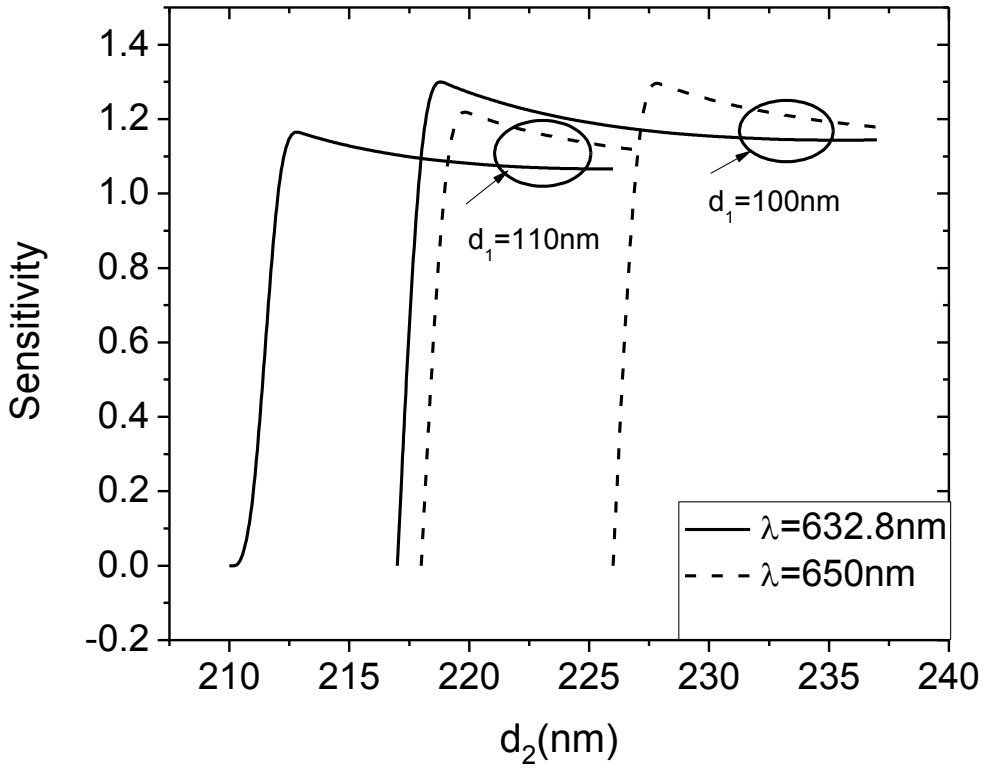

Fig. 3.13. Sensitivity of the proposed sensor versus the thickness of dielectric layer for different values of wavelength (λ), for d_1=(100 ,110)nm, ε_1=1.77, μ_1=1, ε_2=4, μ_2=1 and k_B=π/(4d).

Figure 3.14. is plotted to illustrate the effect of the thickness of the analyte layer on the sensitivity at some different values of the thickness of the dielectric layer. It is clear that the sensitivity of the proposed sensor increases with decreasing the thickness of the analyte. The sensitivity has the range of 1.06≤S≤1.33 at d_2=220 nm. For d_2=225 nm, the sensitivity has the range of 1.05≤S≤1.22 whereas it has the range of 1.06≤S≤1.39 for d_2=218nm. It is also obvious that the maximum sensitivity enhances by 4.5% as d_2

decreases from 225 nm to 220 nm, but it increases by 9.0% as d_2 decreases from 220 nm to 218 nm.

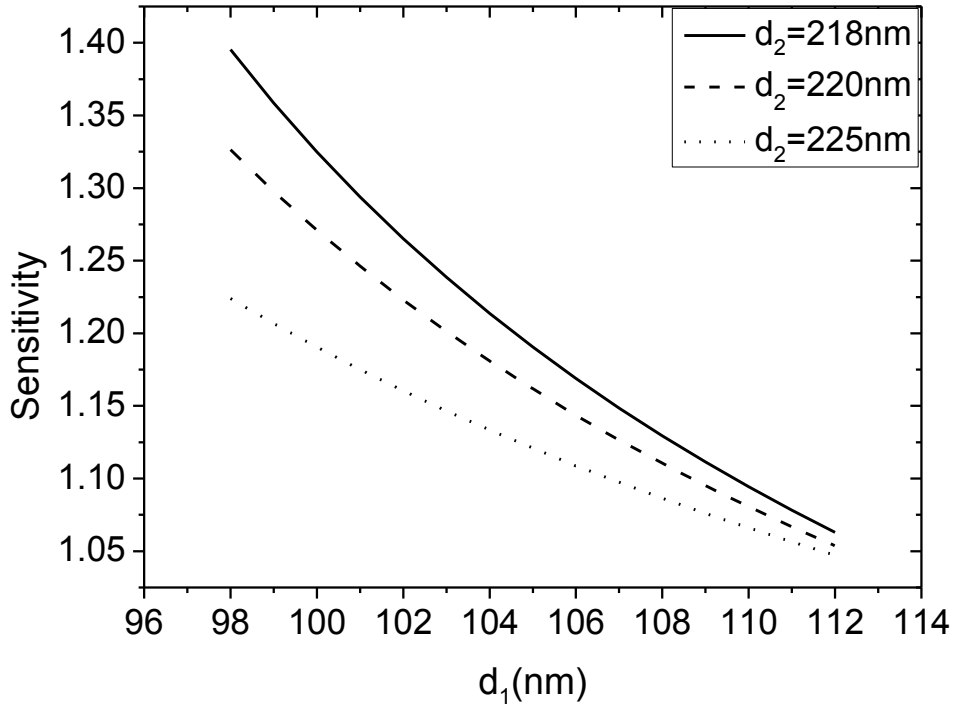

Fig. 3.14. Sensitivity of the proposed sensor versus the thickness of analyte layer for different values of thickness of the dielectric layer for λ=632.8 nm, ε_1=1.77, μ_1=1, ε_2=4, μ_2=1 and $k_B=\pi/(4d)$.

Chapter four

Photonic crystal sensor: TM-mode

In this chapter, two-layer slab photonic crystal consisting of two different layers is studied for sensing applications. The dispersion relation, sensitivity, and power flow relations are presented in details for TM-mode.

4.1. Dispersion relation

Consider TM polarized light in which the waves are travelling along the x-axis. The magnetic field is polarized along the y- axis. There's a non-zero y-component of the magnetic field, whereas the electric field has a non-zero x and z −components.

Helmholtz equation for TM modes can be written as

$$\frac{\partial^2 H_y}{\partial x^2} + \frac{\partial^2 H_y}{\partial z^2} + k^2 H_y = 0, \tag{4.1}$$

The dependence of $H_y(x,z)$ on x is given by $exp(i\beta x)$, then

$$H_y(x,z) = H_y(z)e^{i\beta x}, \tag{4.2}$$

Eq. (4.1) can be written as

$$\frac{d^2 H_y}{dz^2} + k_0^2(\epsilon_i \mu_i - N^2)H_y(z) = 0, \tag{4.3}$$

where $\beta = k_0 N \; and \;\; k^2 = k_0^2 \epsilon_i \mu_i.$ (4.4)

The solution of Eq. (4.3) in the *l*-th cell can be written as

$$H_{y1}(z) = a_l e^{iq_1(z-ld)} + b_l e^{-iq_1(z-ld)}, \;\; (l-1)d + d_2 < z < ld \tag{4.5}$$

$$H_{y2}(z) = c_l e^{iq_2(z-ld)} + f_l e^{-iq_2(z-ld)}, \;\; (l-1)d < z < (l-1)d + d_2 \tag{4.6}$$

The nonzero components of the electric field can be calculated as

$$E_x = \frac{-i}{\varepsilon\omega}\frac{\partial H_y}{\partial z}, \tag{4.7}$$

From which

$$E_{x1} = \frac{q_1}{\varepsilon_1 \omega}(a_l e^{iq_1(z-ld)} - b_l e^{-iq_1(z-ld)}), \tag{4.8}$$

$$E_{x2} = \frac{q_2}{\varepsilon_2 \omega}(c_l e^{iq_2(z-ld)} - f_l e^{-iq_2(z-ld)}), \tag{4.9}$$

and

$$E_z = \frac{-\beta}{\omega\varepsilon} H_y, \tag{4.10}$$

which leads to

$$E_{z1} = \frac{-\beta}{\varepsilon_1 \omega}(a_l e^{iq_1(z-ld)} + b_l e^{-iq_1(z-ld)}), \tag{4.11}$$

$$E_{z2} = \frac{-\beta}{\varepsilon_2 \omega}(c_l e^{iq_2(z-Ld)} + f_l e^{-iq_2(z-ld)}). \tag{4.12}$$

Applying the boundary conditions

The continuity of H_y and E_x at $z = (l-1)d$ leads to

$$a_{l-1} + b_{l-1} = c_l e^{-iq_2 d} + f_l e^{iq_2 d}\,, \tag{4.13}$$

$$q_{TM}(a_{l-1} - b_{l-1}) = q_2\left(c_l e^{-iq_2 d} - f_l e^{iq_2 d}\right), \tag{4.14}$$

where $q_{TM} = \frac{\varepsilon_2}{\varepsilon_1} q_1$.

The two above equations can be written in matrix form as

$$\begin{pmatrix} 1 & 1 \\ 1 & -1 \end{pmatrix}\begin{pmatrix} a_{l-1} \\ b_{l-1} \end{pmatrix} = \begin{pmatrix} e^{-iq_2 d} & e^{iq_2 d} \\ \frac{q_2}{q_{TM}} e^{-iq_2 d} & \frac{-q_2}{q_{TM}} e^{iq_2 d} \end{pmatrix}\begin{pmatrix} c_l \\ f_l \end{pmatrix}. \tag{4.15}$$

The continunity of H_y and E_x at $z = [(l-1)d] + d_2$ gives

$$c_l e^{-iq_2 d_1} + f_l e^{iq_2 d_1} = a_l e^{-iq_1 d_1} + b_l e^{iq_1 d_1}, \tag{4.16}$$

$$q_2\left(c_l e^{-iq_2 d_1} - f_l e^{iq_2 d_1}\right) = q_{TM}\left(a_l e^{-iq_1 d_1} - b_l e^{iq_1 d_1}\right). \tag{4.17}$$

Eqs. (4.16) and (4.17) can be written in matrix notation as

$$\begin{pmatrix} e^{-iq_2 d_1} & e^{iq_2 d_1} \\ e^{-iq_2 d_1} & -e^{iq_2 d_1} \end{pmatrix}\begin{pmatrix} c_l \\ f_l \end{pmatrix} = \begin{pmatrix} e^{-iq_1 d_1} & e^{iq_1 d_1} \\ \frac{q_{TM}}{q_2} e^{-iq_2 d} & \frac{-q_{TM}}{q_2} e^{iq_1 d_1} \end{pmatrix}\begin{pmatrix} a_l \\ b_l \end{pmatrix}. \tag{4.18}$$

Multiplying Eq.(4.18) by X^{-1} ,where matrix X is given by Eq. 3.20.

$$\begin{pmatrix} c_l \\ f_l \end{pmatrix} = \frac{1}{2}\begin{pmatrix} e^{iq_2 d_1} & e^{iq_2 d_1} \\ e^{-iq_2 d_1} & -e^{-iq_2 d_1} \end{pmatrix}\begin{pmatrix} e^{-iq_1 d_1} & e^{iq_1 d_1} \\ \frac{q_{TM}}{q_2} e^{-iq_2 d} & \frac{-q_{TM}}{q_2} e^{iq_1 d_1} \end{pmatrix}\begin{pmatrix} a_l \\ b_l \end{pmatrix}. \tag{4.19}$$

Substituting from Eq. (4.19) into Eq. (4.15), we obtain

$$\begin{pmatrix} 1 & 1 \\ 1 & -1 \end{pmatrix}\begin{pmatrix} a_{l-1} \\ b_{l-1} \end{pmatrix} = \frac{1}{2}\begin{pmatrix} e^{-iq_2 d} & e^{iq_2 d} \\ \frac{q_2}{q_{TM}} e^{-iq_2 d} & \frac{-q_2}{q_{TM}} e^{iq_2 d} \end{pmatrix}\begin{pmatrix} e^{-iq_2 d_1} & e^{iq_2 d_1} \\ e^{-iq_2 d_1} & -e^{iq_2 d_1} \end{pmatrix}\begin{pmatrix} e^{-iq_1 d_1} & e^{iq_1 d_1} \\ \frac{q_{TM}}{q_2} e^{-iq_2 d} & \frac{-q_{TM}}{q_2} e^{iq_1 d_1} \end{pmatrix}\begin{pmatrix} a_l \\ b_l \end{pmatrix}. \tag{4.20}$$

By taking the result of the product of the above matrices and multiplying both sides of the above equation by $\frac{1}{2}\begin{pmatrix} 1 & 1 \\ 1 & -1 \end{pmatrix}$, we get

$$\begin{pmatrix} a_{l-1} \\ b_{l-1} \end{pmatrix} = \frac{1}{2}\begin{pmatrix} 1 & 1 \\ 1 & -1 \end{pmatrix}\begin{pmatrix} \cos(q_2 d_2)e^{-iq_1 d_1} - \frac{iq_{TM}}{q_2} e^{-iq_1 d_1} sin(q_2 d_2) & \cos(q_2 d_2)e^{iq_1 d_1} + \frac{iq_{TM}}{q_2} sin(q_2 d_2) e^{iq_1 d_1} \\ -\frac{iq_2}{q_{TM}} sin(q_2 d_2)e^{-iq_1 d_1} + \cos(q_2 d_2)e^{-iq_1 d_1} & -\frac{iq_2}{q_{TM}} sin(q_2 d_2)e^{iq_1 d_1} - \cos(q_2 d_2)e^{iq_1 d_1} \end{pmatrix}, \tag{4.21}$$

which can be reduced to take the form

$$\begin{pmatrix} a_{l-1} \\ b_{l-1} \end{pmatrix} = \begin{pmatrix} A' & B' \\ C' & D' \end{pmatrix} \begin{pmatrix} a_l \\ b_l \end{pmatrix} = M' \begin{pmatrix} a_l \\ b_l \end{pmatrix}. \tag{4.22}$$

where M′ is called the transfer matrix with the elements

$$A' = e^{-iq_1 d_1} \left[\cos(q_2 d_2) - \frac{1}{2} i \left(\frac{q_2}{q_{TM}} + \frac{q_{TM}}{q_2} \right) sin(q_2 d_2) \right], \tag{4.23}$$

$$B' = e^{iq_1 d_1} \left[-\frac{1}{2} i \left(\frac{q_2}{q_{TM}} - \frac{q_{TM}}{q_2} \right) sin(q_2 d_2) \right], \tag{4.24}$$

$$C' = e^{-iq_1 d_1} \left[\frac{1}{2} i \left(\frac{q_2}{q_{TM}} - \frac{q_{TM}}{q_2} \right) sin(q_2 d_2) \right], \tag{4.25}$$

$$D' = e^{iq_1 d_1} \left[\cos(q_2 d_2) + \frac{1}{2} i \left(\frac{q_2}{q_{TM}} + \frac{q_{TM}}{q_2} \right) sin(q_2 d_2) \right]. \tag{4.26}$$

The total transfer matrix of the structure shown in Fig. 3.1 can be written as

$$\begin{pmatrix} a_0 \\ b_0 \end{pmatrix} = \begin{pmatrix} A' & B' \\ C' & D' \end{pmatrix}^l \begin{pmatrix} a_l \\ b_l \end{pmatrix}, \tag{4.27}$$

which may be written as

$$\begin{pmatrix} a_l \\ b_l \end{pmatrix} = \begin{pmatrix} A' & B' \\ C' & D' \end{pmatrix}^{-l} \begin{pmatrix} a_0 \\ b_0 \end{pmatrix}, \tag{4.28}$$

$$\begin{pmatrix} A' & B' \\ C' & D' \end{pmatrix} \begin{pmatrix} a_l \\ b_l \end{pmatrix} = e^{-ik_B d} \begin{pmatrix} a_l \\ b_l \end{pmatrix}, \tag{4.29}$$

$$\begin{pmatrix} A' - e^{-ik_B d} & B' \\ C' & D' - e^{-ik_B d} \end{pmatrix} \begin{pmatrix} a_l \\ b_l \end{pmatrix} = 0. \tag{4.30}$$

By taking the determinant

$$\begin{vmatrix} A' - e^{-ik_B d} & B' \\ C' & D' - e^{-ik_B d} \end{vmatrix} = 0, \tag{4.31}$$

Then $(A' - e^{-ik_B d})(D' - e^{-ik_B d}) - B'C' = 0$. (4.32)

But $A'D' - B'C' = 1$,

$$e^{-2ik_B d} - (A' + D')e^{-ik_B d} + 1 = 0. \tag{4.33}$$

The solution of the above equation for $e^{-ik_B d}$ is given by

$$e^{-ik_B d} = \left(\frac{A' + D'}{2} \right) \mp \left(\left(\frac{A' + D'}{2} \right)^2 - 1 \right)^{\frac{1}{2}}. \tag{4.34}$$

The eigenvectors corresponding to the eigenvalues are obtained from Eq. (4.34) as

$$\begin{pmatrix} a_0 \\ b_0 \end{pmatrix} = \begin{pmatrix} B' \\ e^{-ik_B d} - A' \end{pmatrix}. \tag{4.35}$$

Then the corresponding column vectors for the *l*-th unit cell are given by

$$\begin{pmatrix} a_l \\ b_l \end{pmatrix} = e^{lk_B d} \begin{pmatrix} B' \\ e^{-ik_B d} - A' \end{pmatrix}. \quad (4.36)$$

Multiplying Eq. (4.33) by $e^{lk_B d}$, we get

$$e^{lk_B d} + e^{-ik_B d} = A' + D'. \quad (4.37)$$

using the identity $\cos x = \frac{e^{ix}+e^{-ix}}{2}$,

$$2\,cos(k_B d) = A' + D'. \quad (4.38)$$

Substituting for A' and D' from Eq. (4.23) and Eq.(4.26) into Eq. (4.37), we get

$$2\cos(k_B\, d) = e^{-iq_1 d_1}(cos(q_2 d_2) - \frac{1}{2} i(\frac{q_2}{q_{TM}} + \frac{q_{TM}}{q_2})\, sin(q_2 d_2)) + e^{iq_1 d_1}(cos(\, q_2 d_2) +$$

$$\frac{1}{2} i(\frac{q_2}{q_{TM}} + \frac{q_{TM}}{q_2})\, sin(q_2 d_2)),$$

$$2\cos(k_B\, d) = 2\cos(q_2 d_2)\cos(q_1 d_1) - \frac{1}{2} i \left(\frac{q_2}{q_{TM}} + \frac{q_{TM}}{q_2}\right) \sin(q_2 d_2) \left(e^{iq_1 d_1} - q^{-iq_1 d_1}\right),$$

$$\cos(k_B\, d) = \cos(q_2 d_2)\cos(q_1 d_1) - \frac{1}{2}\left(\frac{q_2 \varepsilon_1}{q_1 \varepsilon_2} + \frac{q_1 \varepsilon_2}{q_2 \varepsilon_1}\right) \sin(q_2 d_2)\sin(q_1 d_1). \quad (4.39)$$

Equation (4.39) represents the dispersion relation for TM wave.

4.2. **Sensitivity**

The differentiation of the LHS of the dispersion relation is zero and that of the RHS is given by

$$-2\, d_2 cos(q_1 d_1)\, sin(q_2 d_2) \frac{k_0^2 N}{q_2} + 2 d_1\, cos(\, q_2 d_2\,) sin(\, q_1 d_1) \frac{k_0^2 (n_1 \frac{\partial n_1}{\partial N} - N)}{q_1} + \frac{\varepsilon_1}{\varepsilon_2}\left(\frac{-K_0^2 N}{q_1 q_2} -\right.$$

$$\left.\frac{q_2 k_0^2}{q_1^3}\left(n_1 \frac{\partial n_1}{\partial N} - N\right)\right) sin(\, q_1 d_1\,) sin(\, q_2 d_2) + d_1 \frac{\varepsilon_1}{\varepsilon_2}\frac{q_2}{q_1} cos(q_1 d_1)\, sin(q_2 d_2) \frac{k_0^2}{q_1}\left(n_1 \frac{\partial n_1}{\partial N} -\right.$$

$$\left. N\right) - d_2 \frac{\varepsilon_1}{\varepsilon_2}\frac{q_2}{q_1} cos(q_2 d_2)\, sin(q_1 d_1) \frac{k_0^2 N}{q_2} +$$

$$\frac{\varepsilon_2}{\varepsilon_1}\left(\frac{K_0^2\left(\left(n_1 \frac{\partial n_1}{\partial N} - N\right)\right)}{q_1 d_2} + \frac{q_1}{q_2^3} k_0^2 N\right) sin(\, q_1 d_1\,) sin(\, q_2 d_2) +$$

$$d_1 \frac{\varepsilon_2}{\varepsilon_1}\frac{q_1}{q_2} cos(q_1 d_1)\, sin(q_2 d_2) \frac{k_0^2}{q_1}\left(n_1 \frac{\partial n_1}{\partial N} - N\right) - d_2 \frac{\varepsilon_2}{\varepsilon_1}\frac{q_1}{q_2} cos(q_2 d_2)\, sin(q_1 d_1) \frac{k_0^2 N}{q_2}. \quad (4.40)$$

After some arrangements, we obtain

$$-2d_2\cos(q_1d_1)\sin(q_2d_2)\frac{k_0^2N}{q_2}-2d_1\cos(q_2d_2)\sin(q_1d_1)\frac{k_0^2N}{q_1}$$

$$-\frac{\varepsilon_1}{\varepsilon_2}\frac{k_0^2N}{q_1q_2}\sin(q_2d_2)\sin(q_1d_1)+\frac{\varepsilon_1}{\varepsilon_2}\frac{q_2}{q_1^3}k_0^2N\sin(q_2d_2)\sin(q_1d_1)$$

$$-d_1\frac{\varepsilon_1}{\varepsilon_2}\frac{q_2}{q_1}\cos(q_1d_1)\sin(q_2d_2)\frac{k_0^2N}{q_1}-d_2\frac{\varepsilon_1}{\varepsilon_2}\frac{q_2}{q_1}\cos(q_2d_2)\sin(q_1d_1)$$

$$-\frac{\varepsilon_2}{\varepsilon_1}\frac{k_0^2N}{q_1q_2}\sin(q_2d_2)\sin(q_1d_1)+\frac{\varepsilon_2}{\varepsilon_1}\frac{q_1}{q_2^3}k_0^2N\sin(q_2d_2)\sin(q_1d_1)$$

$$-d_1\frac{\varepsilon_2}{\varepsilon_1}\frac{q_1}{q_2}\cos(q_1d_1)\sin(q_2d_2)\frac{k_0^2N}{q_1}-d_2\frac{\varepsilon_2}{\varepsilon_1}\frac{q_1}{q_2}\cos(q_2d_2)\sin(q_1d_1)\frac{k_0^2N}{q_2}$$

$$=-2d_1\cos(q_2d_2)\sin(q_1d_1)\frac{k_0^2}{q_1}n_1\frac{\partial n_1}{\partial N}+\frac{\varepsilon_1}{\varepsilon_2}\frac{q_2}{q_1^3}k_0^2n_1\frac{\partial n_1}{\partial N}\sin(q_2d_2)\sin(q_1d_1)-$$

$$d_1\frac{\varepsilon_1}{\varepsilon_2}\frac{q_2}{q_1}\frac{k_0^2}{q_1}n_1\frac{\partial n_1}{\partial N}\cos(q_1d_1)\sin(q_2d_2)-\frac{\varepsilon_2}{\varepsilon_1}\frac{k_0^2}{q_1q_2}n_1\frac{\partial n_1}{\partial N}\sin(q_2d_2)\sin(q_1d_1)-$$

$$d_1\frac{\varepsilon_2}{\varepsilon_1}\frac{q_2}{q_1}\frac{k_0^2}{q_1}n_1\frac{\partial n_1}{\partial N}\cos(q_1d_1)\sin(q_2d_2). \tag{4.41}$$

Rearranging the above equation gives

$$\mathrm{N}\left[-2\left(\frac{d_1}{q_1}u+\frac{d_2}{q_2}v\right)+\sin(q_1d_1)\sin(q_2d_2)\left\{\left(\frac{\varepsilon_1}{\varepsilon_2}\frac{q_2}{q_1}\right)\left(\frac{1}{q_1^2}-\frac{1}{q_2^2}\right)+\frac{\varepsilon_2}{\varepsilon_1}\frac{q_1}{q_2}\left(\frac{1}{q_2^2}-\frac{1}{q_1^2}\right)\right\}-\right.$$
$$\left.\frac{d_1}{q_1}v\left(\frac{\varepsilon_1}{\varepsilon_2}\frac{q_2}{q_1}+\frac{\varepsilon_2}{\varepsilon_1}\frac{q_1}{q_2}\right)-\frac{d_2}{q_2}u\left(\frac{\varepsilon_1}{\varepsilon_2}\frac{q_2}{q_1}+\frac{\varepsilon_2}{\varepsilon_1}\frac{q_1}{q_2}\right)\right]=n_1\left[-2\frac{d_1}{q_1}u-\frac{d_1}{q_1}v\left(\frac{\varepsilon_1}{\varepsilon_2}\frac{q_2}{q_1}+\frac{\varepsilon_2}{\varepsilon_1}\frac{q_1}{q_2}\right)+\right.$$
$$\left.\left(\frac{\varepsilon_1}{\varepsilon_2}\frac{q_2}{q_1}-\frac{\varepsilon_2}{\varepsilon_1}\frac{q_1}{q_2}\right)\frac{1}{q_1^2}\sin(q_1d_1)\sin(q_2d_2)\right]\frac{\partial n_1}{\partial N}. \tag{4.42}$$

$$\mathrm{N}\left[-2\left(\frac{d_1}{q_1}u+\frac{d_2}{q_2}v\right)+w\left(\frac{\varepsilon_1}{\varepsilon_2}\frac{q_2}{q_1}-\frac{\varepsilon_1}{\varepsilon_2}\frac{q_2}{q_1}\right)\left(\frac{q_2^2-q_1^2}{q_1^2q_2^2}\right)-\left(\frac{d_1}{q_1}v+\frac{d_2}{q_2}u\right)\tau_{TM}\right]\frac{\partial n_1}{\partial N}=n_1\left[-2\frac{d_1}{q_1}u-\right.$$
$$\left.\frac{d_1}{q_1}\tau_{TM}v+\frac{1}{q_1^2}\sigma_{TM}w\right]\frac{\partial n_1}{\partial N}. \tag{4.43}$$

$$S=\frac{n_1\left[-2\frac{d_1}{q_1}u-\frac{d_1}{q_1}\tau_{TM}v+\frac{1}{q_1^2}\sigma_{TM}w\right]}{N\left[-2\left(\frac{d_1}{q_1}u+\frac{d_2}{q_2}v\right)+\left(\frac{q_2^2-q_1^2}{q_1^2q_2^2}\right)\sigma_{TM}w-\left(\frac{d_1}{q_1}v+\frac{d_2}{q_2}u\right)\tau_{TM}\right]}, \tag{4.44}$$

where $\tau_{TM}=\left(\frac{\varepsilon_1}{\varepsilon_2}\frac{q_2}{q_1}+\frac{\varepsilon_2}{\varepsilon_1}\frac{q_1}{q_2}\right)$ and $\sigma_{TM}=\left(\frac{\varepsilon_1}{\varepsilon_2}\frac{q_2}{q_1}-\frac{\varepsilon_1}{\varepsilon_2}\frac{q_2}{q_1}\right)$.

4.3. **Power flowing within the photonic crystal layers**

The total time- average power transported by the proposed sensor for TM mode is given by

$$P_{total} = \frac{\beta}{2\omega}\int_{-\infty}^{\infty}\frac{\left|E_y(z)\right|^2}{\varepsilon_i(z)}dz\,. \tag{4.45}$$

For the first unit cell, $l = 1$

In the first layer

$$p_1 = \frac{\beta}{2\omega\mu_1}\int_0^{d_1}\left(a_1^2 e^{2iq_1(z-d)} + b_1^2 e^{-2iq_1(z-d)} + 2a_1b_1\right)dz,$$

$$= \frac{\beta}{2\omega\mu_1}\left(a_1^2\frac{e^{2iq_1(z-d)}}{2iq_1} + b_1^2\frac{e^{2iq_1(z-d)}}{-2iq_1} + 2a_1b_1z\right),$$

$$= \frac{\beta}{2\omega\mu_1}\left(\frac{a_1^2}{2iq_1}\left(e^{-2iq_1d_2} - e^{-2iq_1d}\right) - \frac{b_1^2}{2iq_1}\left(e^{2iq_1d_2} - e^{2iq_1d}\right) + 2a_1b_1d_1\right). \tag{4.46}$$

In the second layer

$$p_1{}' = \frac{\beta}{2\omega\varepsilon_0\varepsilon_1}\int_{d_1}^{d}\left(c_1^2 e^{2iq_1(z-d)} + f_1^2 e^{-2iq_1(z-d)} + 2c_1f_1\right)dz,$$

$$= \frac{\beta}{2\omega\varepsilon_0\varepsilon_1}\left(c_1^2\frac{e^{2iq_1(z-d)}}{2iq_1} + f_1^2\frac{e^{2iq_1(z-d)}}{-2iq_1} + 2c_1f_1z\right),$$

$$= \frac{\beta}{2\omega\varepsilon_0\varepsilon_1}\left(\frac{c_1^2}{2iq_2}\left(1 - e^{-2iq_2d_2}\right) - f_1^2\frac{(1-e^{2iq_2d_2})}{2iq_2} + 2c_1f_1d_2\right). \tag{4.47}$$

For the second unit cell, $l = 2$

In the first layer

$$p_2 = \frac{\beta}{2\omega\varepsilon_0\varepsilon_2}\int_d^{d+d_1}\left(a_2^2 e^{2iq_1(z-2d)} + b_2^2 e^{-2iq_1(z-2d)} + 2a_1b_1\right)dz,$$

$$= \frac{\beta}{2\omega\varepsilon_0\varepsilon_2}\left(a_2^2\frac{e^{2iq_1(z-2d)}}{2iq_1} + b_2^2\frac{e^{-2iq_1(z-2d)}}{-2iq_1} + 2a_2b_2z\right),$$

$$= \frac{\beta}{2\omega\varepsilon_0\varepsilon_2}\left(\frac{a_2^2}{2iq_1}\left(e^{-2iq_1d} - e^{-2iq_1d_2}\right) - \frac{b_2^2}{2iq_1}\left(e^{2iq_1d_2} - e^{2iq_1d}\right) + 2a_2b_2d_1\right). \tag{4.48}$$

In the second layer

$$p_2{}' = \frac{\beta}{2\omega\varepsilon_0\varepsilon_2}\int_{d+d_1}^{2d}\left(c_2^2 e^{2iq_2(z-2d)} + f_2^2 e^{-2iq_1(z-2d)} + 2c_2f_2\right)dz,$$

$$= \frac{\beta}{2\omega\varepsilon_0\varepsilon_2}\left(c_2^2\frac{e^{2iq_2(z-2d)}}{2iq_2} + f_2^2\frac{e^{-2iq_2(z-d)}}{-2iq_2} + 2c_2f_2z\right),$$

$$= \frac{\beta}{2\omega\varepsilon_0\varepsilon_2}\left(\frac{c_2^2}{2iq_2}\left(1-e^{-2iq_2d_2}\right) - f_2^2\frac{\left(1-e^{2iq_2d_2}\right)}{2iq_2} + 2c_1f_1d_2\right). \quad (4.49)$$

For the third unit cell, $l = 3$

In the first layer

$$p_3 = \frac{\beta}{2\omega\varepsilon_0\varepsilon_3}\int_{2d}^{2d+d_1}\left(a_3^2e^{2iq_1(z-3d)} + b_3^2e^{-2iq_1(z-3d)} + 2a_3b_3\right)dz,$$

$$= \frac{\beta}{2\omega\varepsilon_0\varepsilon_3}\left(a_3^2\frac{e^{2iq_1(z-3d)}}{2iq_1} + b_3^2\frac{e^{-2iq_1(z-3d)}}{-2iq_1} + 2a_3b_3z\right),$$

$$= \frac{\beta}{2\omega\varepsilon_0\varepsilon_3}\left(\frac{a_3^2}{2iq_1}\left(e^{-2iq_1d_2} - e^{-2iq_1d}\right) - \frac{b_3^2}{2iq_1}\left(e^{2iq_1d_2} - e^{2iq_1d}\right) + 2a_3b_3d_1\right). \quad (4.50)$$

In the second layer

$$p_3' = \frac{\beta}{2\omega\varepsilon_0\varepsilon_2}\int_{2d+d_1}^{3d}\left(c_3^2e^{2iq_2(z-3d)} + f_3^2e^{-2iq_1(z-3d)} + 2c_3f_3\right)dz,$$

$$= \frac{\beta}{2\omega\varepsilon_0\varepsilon_3}\left(c_3^2\frac{e^{2iq_2(z-3d)}}{2iq_2} + f_3^2\frac{e^{-2iq_2(z-3d)}}{-2iq_2} + 2c_3f_3z\right),$$

$$= \frac{\beta}{2\omega\varepsilon_0\varepsilon_3}\left(\frac{c_3^2}{2iq_2}\left(1-e^{-2iq_2d_2}\right) - f_3^2\frac{\left(1-e^{2iq_2d_2}\right)}{2iq_2} + 2c_3f_3d_2\right). \quad (4.51)$$

For l^{th} cell, the power for the first layer can be written as

$$p_l = \frac{\beta}{2\omega\mu_l}\left(\frac{a_l^2}{2iq_1}\left(e^{-2iq_1d_2} - e^{-2iq_1d}\right) - \frac{b_l^2}{2iq_1}\left(e^{2iq_1d_2} - e^{2iq_1d}\right) + 2a_lb_ld_1\right). \quad (4.52)$$

and that for the second layer it can be written as

$$p_l' = \frac{\beta}{2\omega\mu_2}\left(\frac{c_l^2}{2iq_2}\left(1-e^{-2iq_2d_2}\right) - f_l^2\frac{\left(1-e^{2iq_2d_2}\right)}{2iq_2} + 2c_lf_ld_2\right). \quad (4.53)$$

4.4. Results and Discussion

4.4.1. Left-handed material (LHM)

Figure 4.1. shows the sensitivity of the proposed sensor versus the thickness of LHM layer for different values of the wave frequency. It is apparent from the figure that the sensitivity increases with increasing the LHM layer thickness until it reaches a maximum value at an optimum thickness. For thicknesses greater than optimum thickness, the

sensitivity decreases towards extremely low values. Increasing the LHM layer thickness beyond optimum value of thickness increases the electric field in the LHM layer and the sensitivity decreases. The figure also illustrates the dependence of the sensitivity on the guided wave frequency which shows that the sensitivity can be enhanced with increasing the guided wave frequency. It is also clear that as the wave frequency increases, the sensitivity peak is shifted toward higher value of optimum thickness of the LHM layer. The sensitivity has the range of $0.39 \leq S \leq 2.89$ when $\omega = 5.0$ GHz whereas it has the range of $0.27 \leq S \leq 2.35$ when $\omega = 4.9$ GHz. When $\omega = 4.8$ GHz, the sensitivity has the range of $0.18 \leq S \leq 1.89$. An enhancement of 24.3% in the sensitivity peak can be obtained when the wave frequency is increased from 4.8 GHz to 4.9 GHz whereas it improves by 52.9% as the wave frequency is increased from 4.9 GHz to 5.0 GHz.

When the results of the sensitivity of the proposed sensor are compared with those of the conventional slab waveguide sensor with positive index guiding layer proposed by Tiefenthaler [18] in which the maximum sensitivity achieved was 0.25, it is clear that the proposed sensor has an improvement in sensitivity of 1056% compared to conventional slab waveguide sensor.

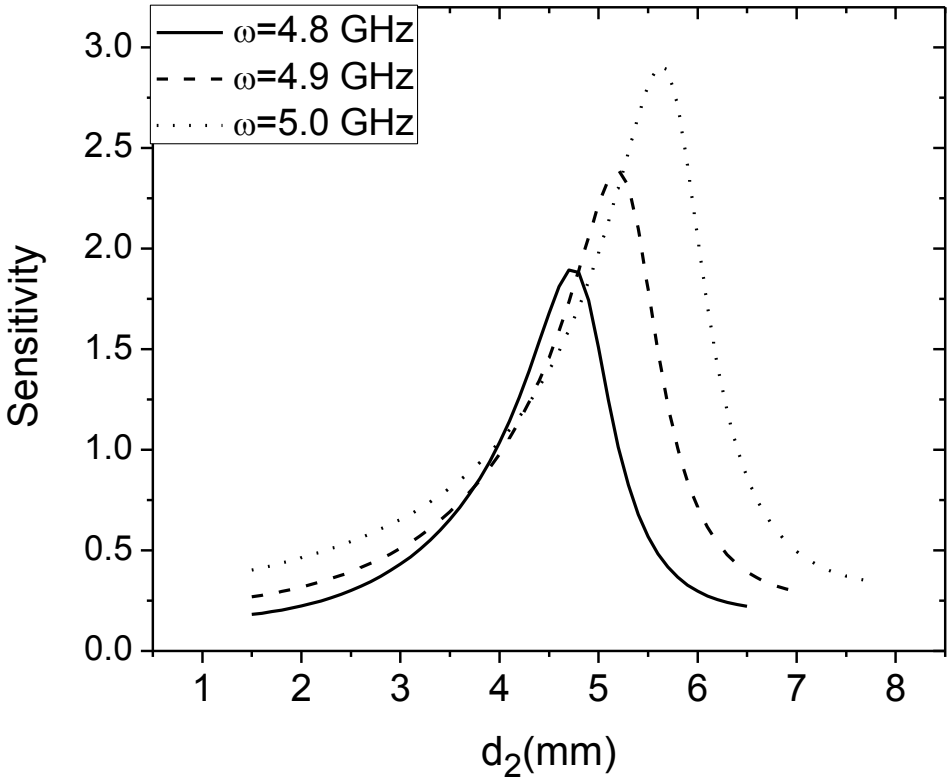

Fig. 4.1. Sensitivity of the proposed sensor versus the thickness of LHM layer for different values of frequency for ε_1=1.77, n_1=1.33, F= 0.56, γ=0.012ω_p, ω_p= 2ω, ω_0=0 .4 ω_p, d_1= 14.0 mm and k_B=π/(3d) .

The impact of the analyte thickness on the sensitivity is shown in Fig. 4.2 which shows that the maximum sensitivity can be slightly enhanced with increasing the analyte layer. This is due to increasing the evanescent field in the analyte medium and so does the maximum sensitivity. It is obvious from the figure that the sensitivity increases with increasing the LHM layer thickness and peaks at an optimum value of the thickness . For thicknesses beyond the optimum thickness, the sensitivity decreases with increasing the thickness of LHM layer. It is also observed that as the analyte layer thickness increases, the maximum sensitivity is slightly shifted toward higher value of optimum thickness of the LHM layer. The sensitivity reaches a maximum value of 2.97 at d_1=14.2mm and d_2=5.79mm whereas it has a value of 2.94 at d_2=5.7 mm for d_1=14.1mm. But at

d_1=14.0mm, the sensitivity reaches 2.89 at an optimum LHM thickness of 5.65mm. It can be noted from Fig. 4.2 that when d_1 increases from 14.0 mm to 14.2 mm, the maximum sensitivity enhances by 2.77%.

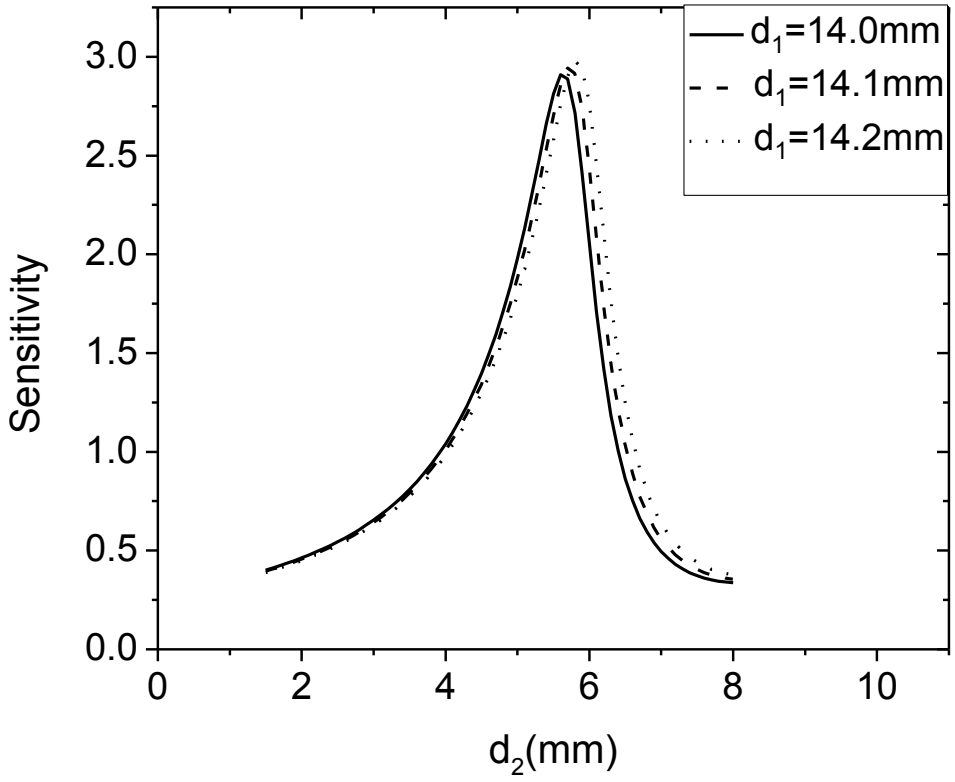

Fig. 4.2. Sensitivity of the proposed sensor versus the thickness of LHM layer for different values of analyte thickness for ε_1=1.77, n_1=1.33, F=0.56, γ=0.012ω_p, ω=5.0 GHz , ωp= 2ω, $\omega 0$= 0.4 ωp and k_B=π/(3d) .

Figure 4.3 illustrates the dependence of the sensitivity of the proposed sensor on the thickness of LHM layer for different values of electron scattering rate (γ). It is seen that, the sensitivity can be enhanced with decreasing the electron scattering rate. The optimum thickness of LHM at which the peak occurs does not depend on the electron scattering rate. The maximum sensitivity obtained has a value of 2.99 at γ= 0.012ω_p. For γ= 0.013ω_p, the sensitivity has a peak value of 2.75 whereas it is 2.63 at γ= 0.014ω_p. The

sensitivity can be enhanced by 4.5% when γ is reduced from $0.014\omega_p$ to $0.013\omega_p$, but when γ is reduced from $0.013\omega_p$ to $0.012\omega_p$, the sensitivity can be enhanced by 5.5%.

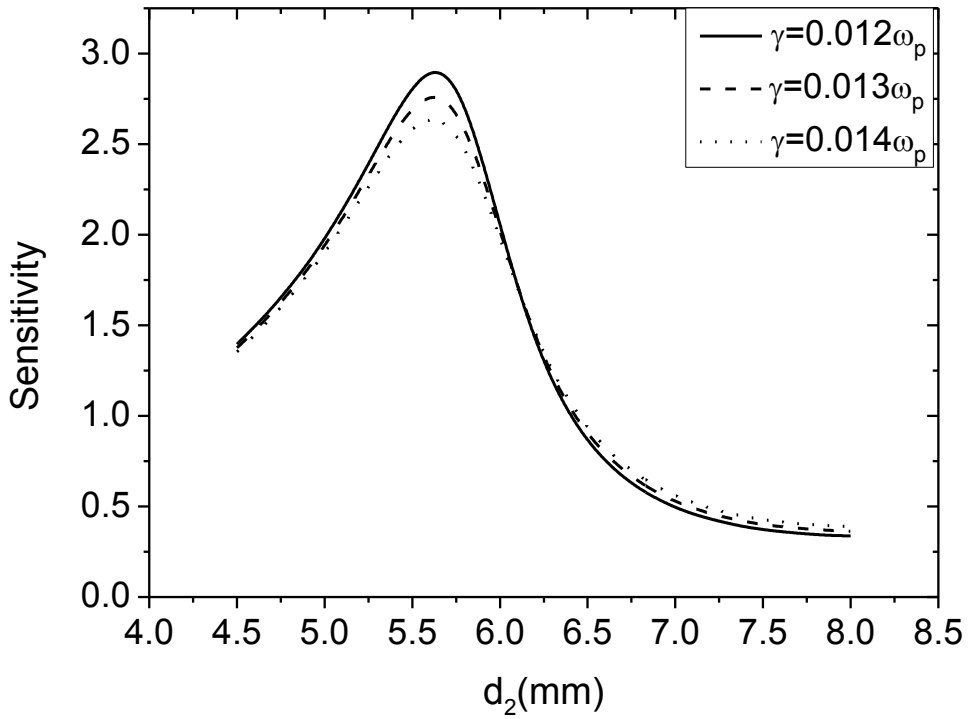

Fig. 4.3. Sensitivity of the proposed sensor versus the thickness of LHM layer for different values of electron scattering rate for ε_1=1.77, n_1=1.33, F=0.56, $k_B=\pi/(3d)$, ω=5.0GHz, ω_p= 2ω, ω_0=0 .4 ω_p, and d_1= 14.0mm.

Figure 4.4 shows the variation of the sensitivity of the proposed sensor with the analyte thickness for different values of the thickness of LHM layer. As is clearly seen from the figure the sensitivity is increasing with d_1 until reaches 2.97, 3.0 and 3.03 at d_1=14.2mm, 14.3mm and 14.4mm, respectively, then the sensitivity has a sharp decrease by further increasing of the analyte layer thickness. The maximum sensitivity can be enhanced slightly with increasing the thickness of LHM layer in the considered range of values. It can be noted from Fig. 4.4 that the sensitivity takes the range of $0.35 \leq S \leq 3.02$ when d_2=6.0mm whereas it takes the range of $0.37 \leq S \leq 2.99$ when d_2=5.9mm. For d_2=5.8mm

the sensitivity takes the range of 0.41 ≤ S≤ 2.96. An enhancement in sensitivity by 1% as d_2 increases by 0.1mm.

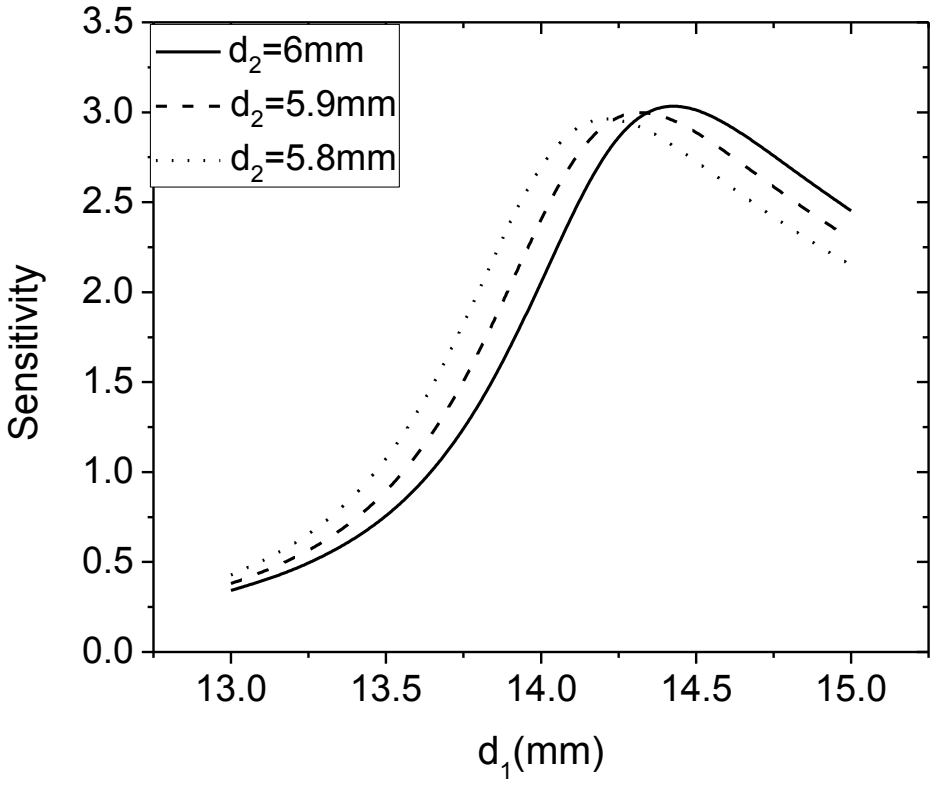

Fig. 4.4. Sensitivity of the proposed sensor versus analyte thickness for different values of the thickness of LHM layer for ε_1=1.77, n_1=1.33, F=0.56, γ=0.012ω_p,ω=5.0 GHz, ω_p= 2ω, ω_0= 0.4 ω_p and k_B=π/(3d).

4.4.2. Metal material

In Figs. 4.5 and 4.6, the sensitivity of the proposed sensor is plotted versus the thickness of metals (Ni) and (Cr) layer, respectively, for different values of the light wavelength (λ). The sensitivity increases with increasing the metal layer untill it reaches a maximum value at an optimum d_2, then decreases slightly with increasing d_2 untill it has a fixed value. Increasing the metal layer thickness beyond the optimum value does not show a significant effect on the sensitivity. As can be seen from Fig. 4.5 and Fig. 4.6, increasing the wavelength decreases the sensitivity of the proposed sensor. As the wavelength

decreases, the sensitivity peak is shifted toward lower values of optimum thickness of the metal layer.

In Fig. 4.5, the sensitivity has the range of $0.7 \leq S \leq 1.64$ for λ=632.8nm whereas it has the range of $0.1 \leq S \leq 1.01$ for λ=650nm. For λ= 700nm, the sensitivity has the range of $0.14 \leq S \leq 0.53$ as shown in Fig. 4.5. On the other hand, the sensitivity takes the range of $0.19 \leq S \leq 0.76$ for λ=632.8nm whereas it takes the range of $0.19 \leq S \leq 0.69$ for λ=650nm as shown in Fig. 4.6. Also Fig. 4.6 shows that the sensitivity has the range of $0.1\ 0 \leq S \leq 0.42$ for λ=700nm. The effect of decreasing the wavelength on the sensitivity can be noted from Figs. 4.5 and 4.6. As λ decreases from 700nm to 650nm, the maximum sensitivity increases by 90% for Ni metal whereas it increases by 64.4% for Cr metal. But as λ decreases from 650nm to 632.8nm, the maximum sensitivity increases by 62% for Ni metal whereas it increases by 10.1% for Cr metal.

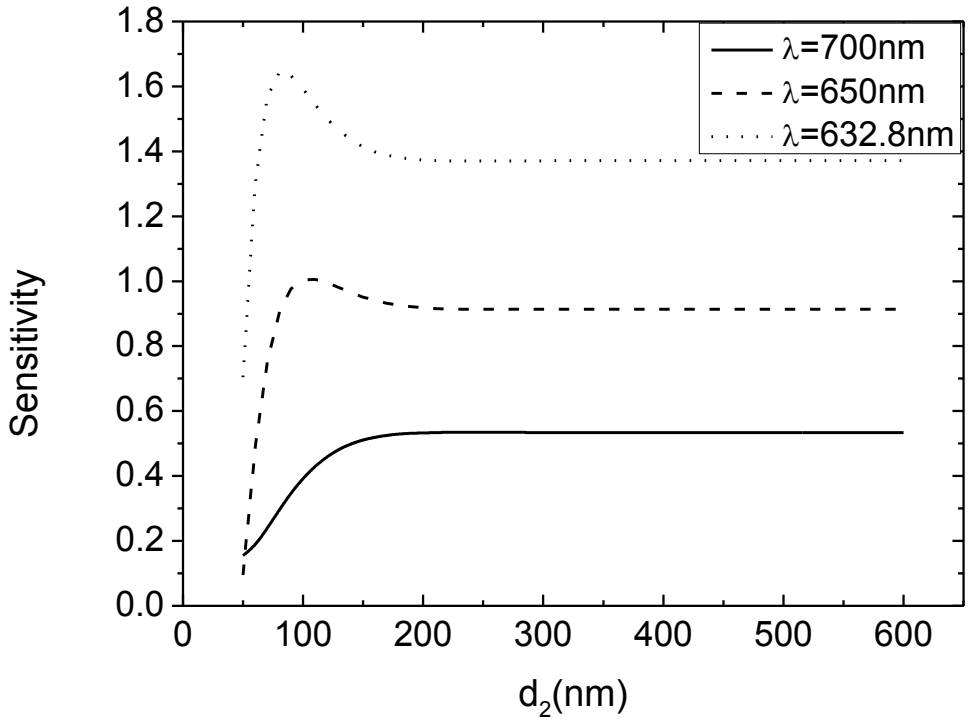

Fig. 4.5. Sensitivity of the proposed sensor versus the thickness of metal (Ni) layer for different values of wavelength (λ) for ε_1=1.77, μ_1=1,ε_2= -9.96+ 4.66i, μ_2=1, $k_B=\pi/(5d)$ and d_1=900 nm.

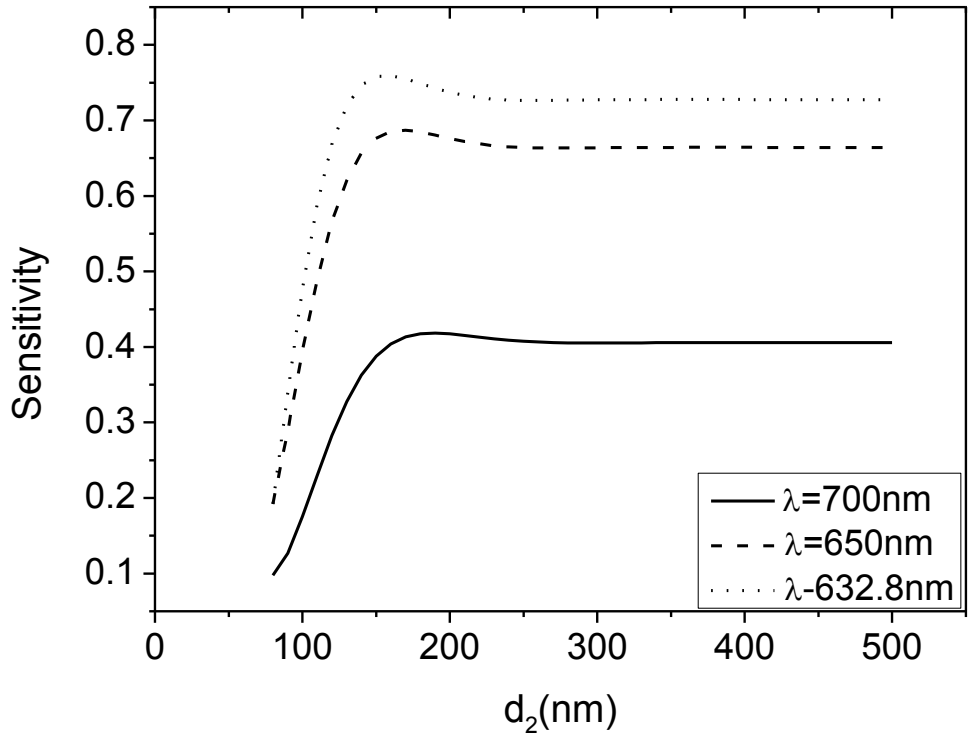

Fig. 4.6. Sensitivity of the proposed sensor versus the thickness of metal (Cr) layer for different values of wavelength for ε_1=1.77, μ_1=1,ε_2= -1.1+i20.79, μ_2 =1, k_B=π/(5d) and d_1=670nm.

The sensitivity is investigated in Fig. 4.7 for (Ni) and in Fig. 4.8 for (Cr) with the analyte thickness. As can be seen, the sensitivity can be increased by increasing the analyte thickness. It is also obvious that the sensitivity increases with increasing d_2 untill reaches a maximum value at an optimum d_2, then decreases slowly with increasing d_2 to 200nm for (Ni) and 233nm for (Cr). Then no dependence of the sensitivity on the thickness of metal layer can be noted. It is clear from Fig. 4.7 that the sensitivity has a maximum value of 1.08 at Ni thickness of 99.76nm for d_1= 880nm whereas it has a peak of 0.67 at Cr thickness of 164.79 nm for d_1=650nm as shown in Fig. 4.8. For Ni structure, the sensitivity has a peak of 1.31 at d_2= 96.01nm and d_1=890nm and for Cr structure, it has a maximum value of 0.73 at d_2=160.54nm and d_1=660nm. The maximum sensitivity obtained for Ni is 1.62 at d_2=85nm and d_1=900nm whereas it is 0.76 at d_2=159.04nm and d_1=670nm for Cr structure. An improvement in sensitivity by 21.3% was obtained when

d_1 increases from 880nm to 890nm whereas an enhancement by 23.67% was obtained as d_1 increases from 890nm to 900nm for Ni metal structure. On the other hand, the improvement in the sensitivity reaches 8.95% when d_1 increases from 650nm to 660nm, but it reaches 4.1% as d_1 increases from 660nm to 670nm for Cr metal structure.

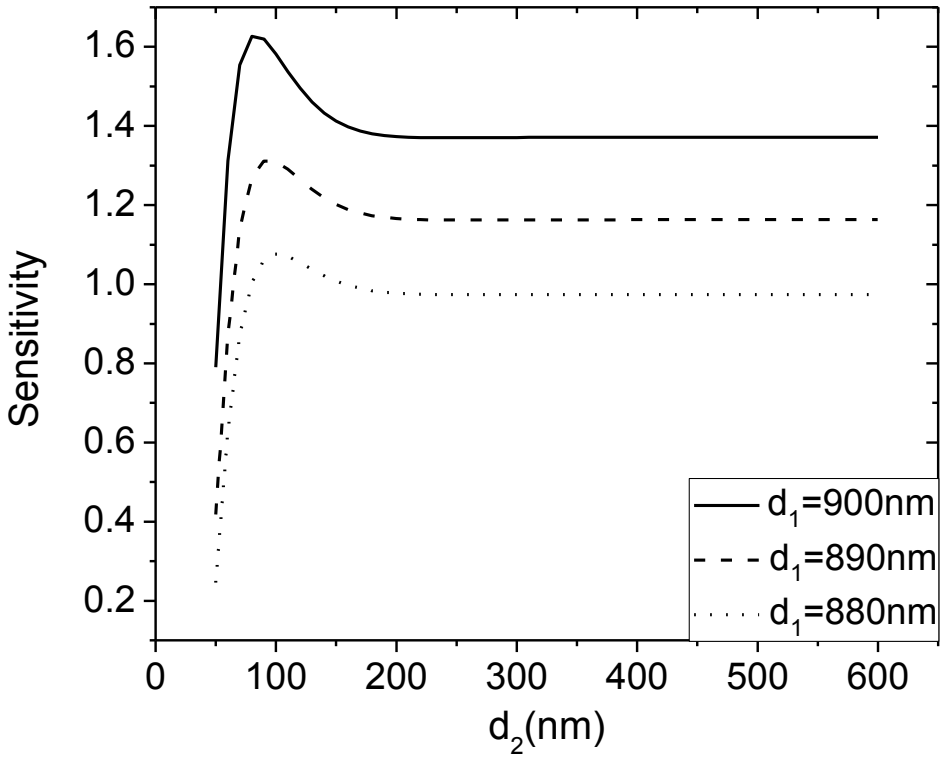

Fig. 4.7. Sensitivity of the proposed sensor versus the thickness of metal layer (Ni) for different values of thickness of the analyte layer for λ=632.8nm, ε_1=1.77, μ_1=1, ε_2=-9.96+ 14.66i, μ_2=1 and $k_B=\pi/(4d)$.

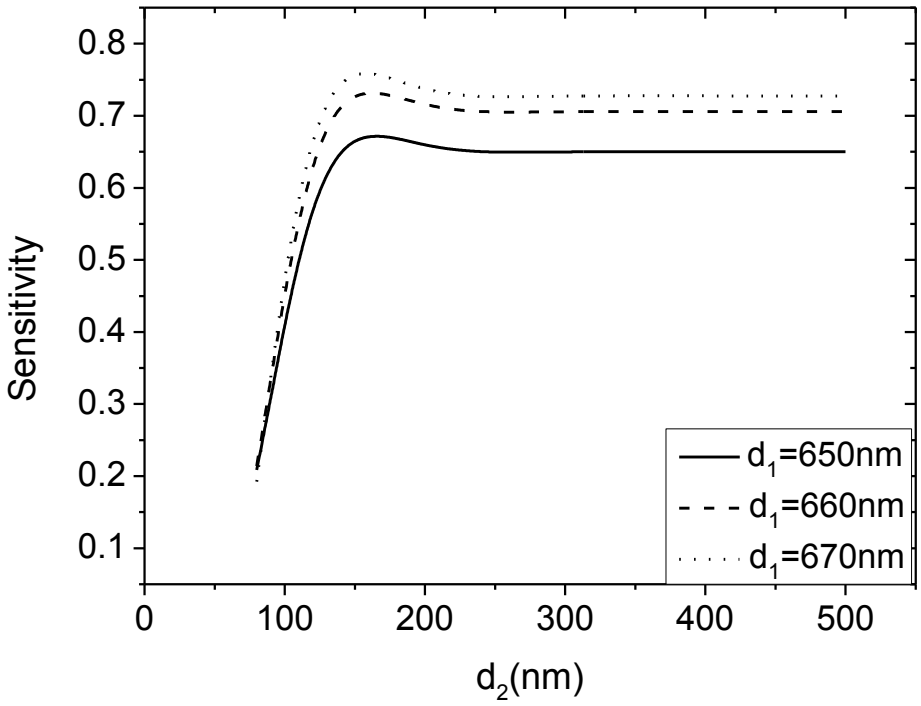

Fig. 4.8. Sensitivity of the proposed sensor versus the thickness of metal layer (Cr) for different values of thickness of the analyte layer for λ=632.8nm, ε_1 =1.77, μ_1=1, ε_2= -1.1+ 20.79i, μ_2=1 and $k_B=\pi/(4d)$.

Figure 4.9 and Fig. 4.10 show the sensitivity of the proposed sensor versus the thickness of analyte layer for different values of thickness of the metal (Ni) and (Cr) layer. The sensitivity increases with increasing d_1 untill reaches a maximum value at an optimum d_1 which is 910 nm for Ni and 670nm for Cr, then decreases with further increasing of d_1. From Fig. 4.9, the maximum sensitivity decreases with increasing Ni layer thickness. For Ni metal, the sensitivity can be enhanced by 3.4% when d_2 decreases from 200 nm to 160 nm whereas it enhances by 2.1% as d_2 decreases from 160 nm to 130 nm. For 180nm $\leq d_2 \leq$ 200nm, changing the thickness of metal layer has an ignorable effect on the sensitivity of Cr metal structure as noted from Fig. 4.10.

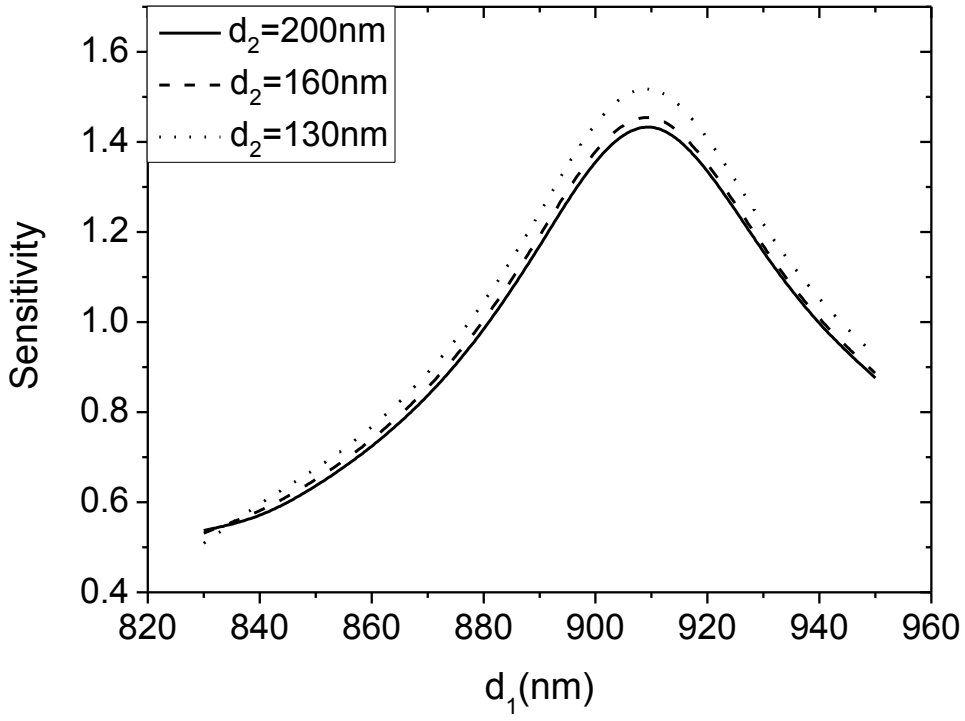

Fig. 4.9. Sensitivity of the proposed sensor versus the thickness of analyte layer for different values of thickness of the metal layer (Ni) for λ=632.8nm, ε_1=1.77, μ_1=1, ε_2=-9.96+14.66i, μ_2=1 and $k_B=\pi/(4d)$.

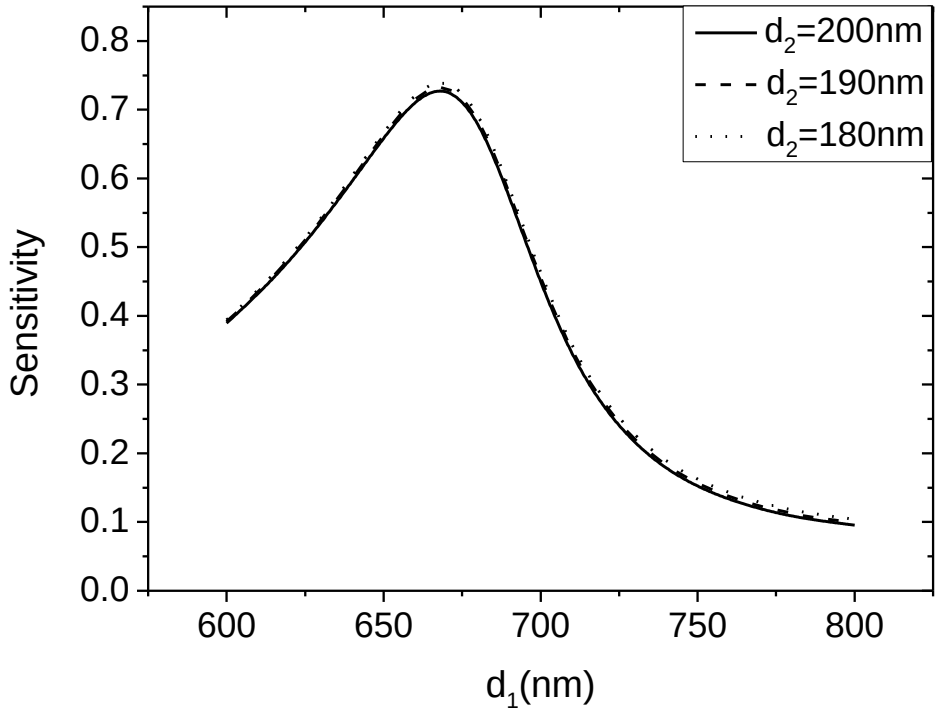

Fig. 4.10. Sensitivity of the proposed sensor versus the thickness of analyte layer for different values of thickness of the metal layer (Cr) for λ=632.8nm, ε_1=1.77, μ_1=1, ε_2=-1.1+ 20.79i, μ_2=1 and $k_B=\pi/(4d)$.

4.4.3. Dielectric material

In this subsection, the layer of thickness d_2 is considered to be a dielectric , silicon dioxide, of parameters ε_2=4.0 and μ_2=1.

The dependence of the sensitivity on the thickness of the dielectric layer for various values of the analyte layer is shown in Fig. 4.11. It is found that the sensitivity exhibits a sharp increase with increasing the dielectric thickness and reaches a maximum value at an optimum dielectric thickness. Increasing the dielectric thickness beyond the optimum thickness does not have a significant effect on the sensitivity. The behaviour of the sensitivity with the analyte thickness is also illustrated in Fig. 4.11, which shows that the maximum sensitivity increases very slightly by decreasing the analyte thickness.

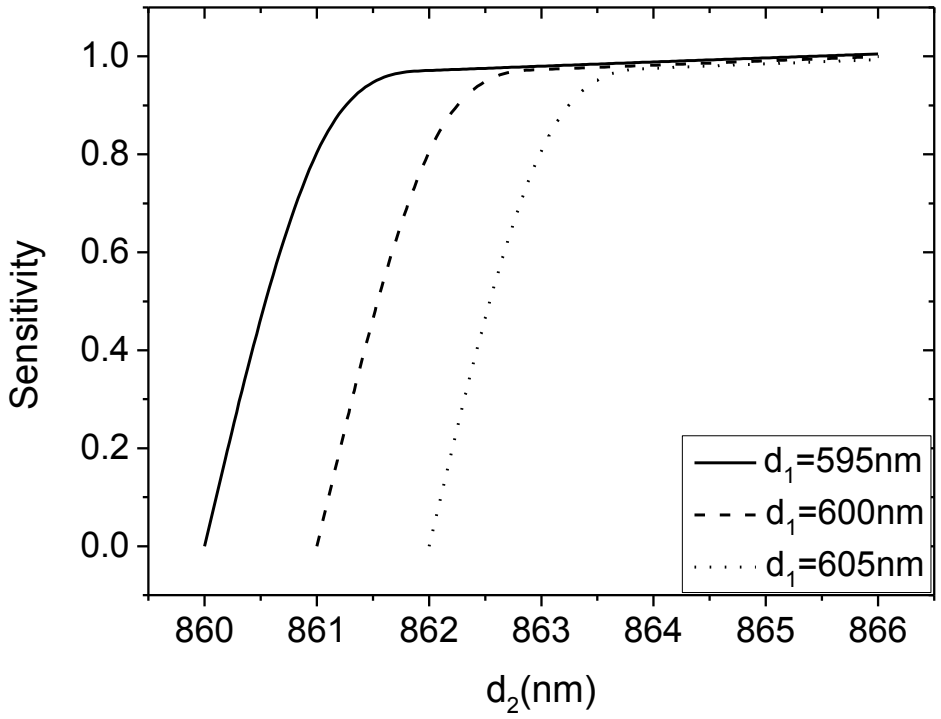

Fig. 4.11. Sensitivity of the proposed sensor versus the thickness of dielectric layer for different values of thickness of the analyte layer for λ=632.8nm, ε_1=1.77, μ_1=1, ε_2=4, μ_2=1 and $k_B=\pi/(4d)$.

Figure 4.12 shows the variation of the sensitivity with the dielectric layer thickness for different values of the light wavelength. Figure 4.12 shows that the sensitivity increases with decreasing the wavelength. For λ=650nm, the sensitivity reaches a maximum value of 0.09 whereas it reaches a maximum value of 1.0 for λ=632.8nm. An enhancement in sensitivity by 1011.1% is obtained as λ decreases from 650nm to 632.8nm.

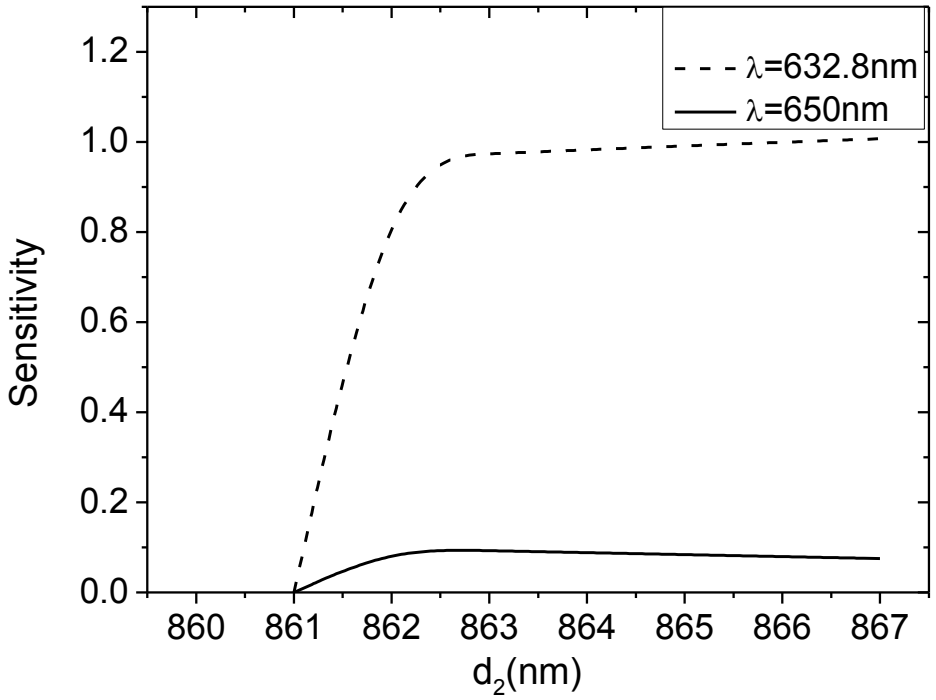

Fig. 4.12. Sensitivity of the proposed sensor versus the thickness of dielectric layer for different values of wavelength (λ), for d_1=600nm, ε_1=1.77, μ_1=1, ε_2=4, μ_2=1 and $k_B=\pi/(4d)$.

Figure 4.13 shows the effect of the thickness of the analyte layer on the sensitivity at some different values of the thickness of the dielectric layer. As can be seen from Fig. 4.13, the sensitivity of the proposed sensor increases with decreasing the thickness of the analyte layer. The maximum sensitivity enhances by 2.0% as d_2 decreases from 865 nm to 863 nm, but it increases by 2.1% as d_2 decreases from 863 nm to 860 nm.

For at d_2=860 nm, the sensitivity has the range of $0.96 \leq S \leq 0.98$. On the other hand, it has the ranges of $0.99 \leq S \leq 1.0$ at d_2=863 nm and $1.0 \leq S \leq 1.02$ at d_2=865nm.

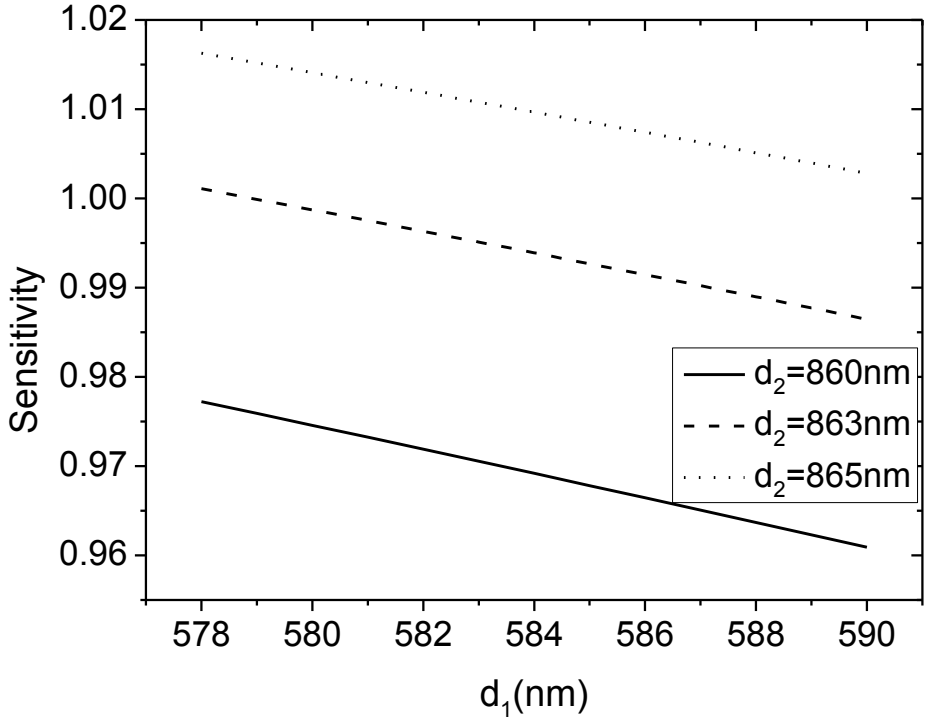

Fig. 4.13. Sensitivity of the proposed sensor versus the thickness of analyte layer for different values of thickness of the dielectric layer for λ=632.8nm, ε_1=1.77, μ_1=1, ε_2=4, μ_2=1 and $k_B=\pi/(4d)$.

Chapter five

Photonic crystal as a refractometric sensor

In this chapter, one dimensional ternary photonic crystal is investigated as refractometric sensor. Using Fresnel reflection coefficients, the transmission of an incident wave are studied in details. The transmission coefficient is plotted with the angle of incidence and wavelength of incident light for air and water as analyte materials.

5.1. Introduction

As mentioned before, photonic band gap structures are multilayer structures formed by using two or more materials, where the multilayered structures lead to formation of photonic band gaps or stop bands in which propagation of electromagnetic waves of certain wavelengths are prohibited. However, these bands or ranges depend upon a number of parameters such as refractive indices of materials and angle of incidence. If all other parameters are kept constant, then any change in refractive index of a material will change the photonic band gaps and ranges of transmission. By monitoring transmission or reflection profile, a slight change in the refractive index of a structural material can be detected. This is the principle of operation of photonic crystal as a refractometric sensor.

5.2. Theory of reflection and transmission

Figure 5.1 shows a photonic crystal having three layers of refractive indices n_1, n_2 and n_3 with thicknesses d_1, d_2 and d_3. Here, the material layer of index of refraction n_3 is considered the analyte material.

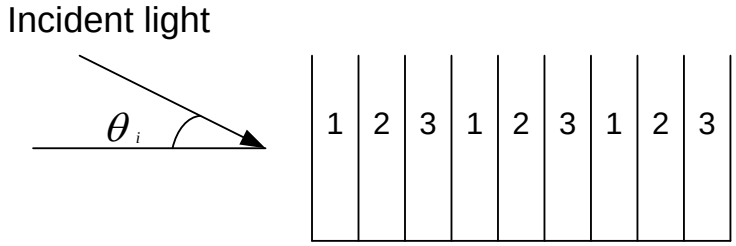

Fig. 5.1. Structure of one- dimensional ternary photonic crystal sensing element.

Let the plane of incidence be $y-z$ plane, then for TE mode, $E_{\mathrm{y}} = E_{\mathrm{z}} = 0$

The solution of Maxwell's equation is given by [46]

$$E_x = U(z)e^{i(k_0 ay - \omega t)}\,, \tag{5.1}$$

$$H_y = V(z)e^{i(k_0 ay - \omega t)}, \tag{5.2}$$

$$H_z = W(z)e^{i(k_0 ay - \omega t)}\,, \tag{5.3}$$

where

k_0 is the wavenumber in the vacuum.

$a = nsin\theta,$ where θ denotes the angle which the normal axis makes with the z-axis.

After substitutions in Maxwell's equation, U, V and W are related to each other by the following equations [46]

$$U` = ik_0 \mu V, \tag{5.4}$$

$$V` = ik_0(\varepsilon - \frac{a^2}{\mu})U, \tag{5.5}$$

$$aU + \mu W = 0\,. \tag{5.6}$$

U, V can be expressed as combinations of two particular solutions as

$$U`_1 = ik_0\mu V_1, \tag{5.7}$$

$$U`_2 = ik_0\mu V_2, \tag{5.8}$$

$$V`_1 = ik_0\left(\varepsilon - \frac{a^2}{\mu}\right)U_1, \tag{5.9}$$

$$V`_2 = ik_0\left(\varepsilon - \frac{a^2}{\mu}\right)U_2. \tag{5.10}$$

The relations (5.7 - 5.10) follow that

$$U_1V_2` - V_1`U_2 = 0 \tag{5.11}$$

$$V_1U_2` - U_1`V_2 = 0 \tag{5.12}$$

$$\frac{d(U_1V_2 - U_2V_1)}{dZ} = 0 \tag{5.13}$$

For our purpose, the most convenient choice of the particular solution is

$$U_1 = f(z), \quad U_2 = F(z), V_1 = g(z), \quad V_2 = G(z) \tag{5.14}$$

Such that

$$f(0) = G(0) = 0 \text{ and } F(0) = g(0) = 1. \tag{5.15}$$

Then the solutions with $U(0) = U_0, V(0) = V_0$ may be expressed in the form

$$U = FU_0 + fV_0. \tag{5.16}$$

$$V = GU_0 + gV_0. \tag{5.17}$$

or in matrix notation

$$Q = NQ_0\,, \tag{5.18}$$

where

$$Q = \begin{bmatrix} U(z) \\ V(z) \end{bmatrix}, \; Q_0 = \begin{bmatrix} U_0 \\ V_0 \end{bmatrix}, N = \begin{bmatrix} F(z) & f(z) \\ G(z) & g(z) \end{bmatrix}, \tag{5.19}$$

then

$$Q_0 = MQ\,, \tag{5.20}$$

where

$$M = \begin{bmatrix} g(z) & -f(z) \\ -G(z) & F(z) \end{bmatrix}, \tag{5.21}$$

Now differentiating Eq. (5.4) with respect to z and substituting from Eq. (5.5), we get

$$\frac{d^2U}{dz^2} + {k_0}^2(n^2 - a^2)U = 0. \tag{5.22}$$

Differentiating Eq. (5.5) with respect to z and substituting from Eq. (5.4), we get

$$\frac{d^2V}{dz^2} + {k_0}^2(n^2 - a^2)V = 0. \tag{5.23}$$

Substituting for $a = nsin\theta$

$$\frac{d^2U}{dz^2} + ({k_0}^2 n^2 cos^2\theta)U = 0. \tag{5.24}$$

$$\frac{d^2V}{dz^2} + +({k_0}^2 n^2 cos^2\theta)V = 0. \tag{5.25}$$

The solution of the above equations is given by

$$U(z) = A\cos(k_0 nz\cos\theta) + B\sin(k_0 nz\cos\theta)\,, \tag{5.26}$$

$$V(z) = \frac{1}{i}\sqrt{\frac{\varepsilon}{\mu}}\cos\theta\,[B\cos(k_o nz\cos\theta) - A\sin(k_0 nz\cos\theta)]. \tag{5.27}$$

Applying the boundary condition in Eq. (5.15) and using Eqs. (5.14), we obtain

$$U_1 = f(z) = \frac{i}{\cos\theta}\sqrt{\frac{\mu}{\varepsilon}}\sin(k_0 nz\cos\theta), \tag{5.28}$$

$$U_2 = F(z) = \cos(k_0 nz\cos\theta), \tag{5.29}$$

$$V_1 = g(z) = \cos(k_0 nz\cos\theta), \tag{5.30}$$

$$V_2 = G(z) = i\sqrt{\frac{\varepsilon}{\mu}}\sin(k_0 nz\cos\theta), \tag{5.31}$$

$$\begin{pmatrix} U_0 \\ V_0 \end{pmatrix} = \begin{pmatrix} \cos(k_0 nz\cos\theta) & -\frac{i}{p}\sin(k_0 nz\cos\theta) \\ -ip\sin(k_0 nz\cos\theta) & \cos(k_o nz\cos\theta) \end{pmatrix}\begin{pmatrix} U \\ V \end{pmatrix}. \tag{5.32}$$

Then the solutions may be expressed in the form

$$\text{M[d]}= \prod_{i=1}^{l}\begin{bmatrix} \cos\beta_i & \frac{-i\sin\beta_i}{p_i} \\ -ip_i\sin\beta_i & \cos\beta_i \end{bmatrix} = \begin{bmatrix} M_{11} & M_{12} \\ M_{21} & M_{22} \end{bmatrix}, \tag{5.33}$$

where

l=3, $\beta_1 = \frac{2\pi n_1 d_1\cos\theta_1}{\lambda_0}$, $\beta_2 = \frac{2\pi n_2 d_2\cos\theta_2}{\lambda_0}$, $\beta_3 = \frac{2\pi(n_3+\Delta n)d_3\cos\theta_3}{\lambda_0}$, λ_0 is the free space wavelength, $p_1 = \sqrt{\frac{\varepsilon_1}{\mu_1}}cos\theta_1$, $p_2 = \sqrt{\frac{\varepsilon_2}{\mu_2}}cos\theta_2$ and $p_3 = \sqrt{\frac{\varepsilon_3}{\mu_3}}cos\theta_3$.

where Δn is the change in refractive index of the third material layer due to introduction or adsorption of any material and θ_1, θ_2 and θ_3 are the ray angles inside the layers 1, 2 and 3, respectively which related to the angle of incidence θ_0 by

$$\cos\theta_1 = \left[1-\frac{n_0^2 sin^2\theta_0}{n_1^2}\right]^{\frac{1}{2}}, \cos\theta_2 = \left[1-\frac{n_0^2 sin^2\theta_0}{n_2^2}\right]^{\frac{1}{2}}, \cos\theta_3 = \left[1-\frac{n_0^2 sin^2\theta_0}{(n_3+\Delta n)^2}\right]^{\frac{1}{2}}. \tag{5.34}$$

The matrix M [d] in Eq. (1) is unimodular as $|M[d]| = 1$.

For an N period structure, the characteristic matrix of the matrix is given by [47]

$$[M(d)]^N = \begin{bmatrix} M_{11}U_{N-1}(a) - U_{N-2}(a) & M_{12}U_{N-1}(a) \\ M_{21}U_{N-1}(a) & M_{22}U_{N-1}(a) - U_{N-2}(a) \end{bmatrix} = \begin{bmatrix} m_{11} & m_{12} \\ m_{21} & m_{22} \end{bmatrix}, \tag{5.35}$$

where

$$M_{11} = \left(\cos\beta_1\cos\beta_2\cos\beta_3 - \frac{p_2\sin\beta_1\sin\beta_2\cos\beta_3}{p_1} - \frac{p_3\cos\beta_1\sin\beta_2\sin\beta_3}{p_2} - \frac{p_3\sin\beta_1\cos\beta_2\sin\beta_3}{p_1}\right), \quad (5.36)$$

$$M_{12} = -i\left(\frac{\sin\beta_1\cos\beta_2\cos\beta_3}{p_1} + \frac{\cos\beta_1\sin\beta_2\cos\beta_3}{p_2} + \frac{\cos\beta_1\cos\beta_2\sin\beta_3}{p_3} - \frac{p_2\sin\beta_1\sin\beta_2\sin\beta_3}{p_1p_2}\right), \quad (5.37)$$

$$M_{21} = -i\left(p_1\sin\beta_1\cos\beta_2\cos\beta_3 + p_2\cos\beta_1\sin\beta_2\cos\beta_3 + p_3\cos\beta_1\cos\beta_2\sin\beta_3 - \frac{p_1p_3\sin\beta_1\sin\beta_2\sin\beta_3}{p_2}\right), \quad (5.38)$$

$$M_{22} = \left(\cos\beta_1\cos\beta_2\cos\beta_3 - \frac{p_1\sin\beta_1\sin\beta_2\cos\beta_3}{p_2} - \frac{p_2\cos\beta_1\sin\beta_2\sin\beta_3}{p_3} - \frac{p_1\sin\beta_1\cos\beta_2\sin\beta_3}{p_3}\right). \quad (5.39)$$

U_N are the Chebyshev polynomials of the second kind

$$U_N(a) = \frac{\sin\left[(N+1)cos^{-1}a\right]}{[1-a^2]^{\frac{1}{2}}}, \quad (5.40)$$

where

$$a = \frac{1}{2}[M_{11} + M_{22}]. \quad (5.41)$$

The transmission coefficient of the multilayer is given by

$$t = \frac{2p_0}{(m_{11}+m_{12}p_0)p_0+(m_{21}+m_{22}p_0)}. \quad (5.42)$$

and the transmissitivity for this structure can be written in terms of the transmission coefficient as

$$T = |t|^2, \quad (5.43)$$

where

$$p_o = n_0\cos\theta_0 = \cos\theta_0. \quad (5.44)$$

where $n_0 = 1$

5.3. **Results and discussions**

In Fig. 5.1, a schematic diagram of the photonic crystal structure under consideration is presented. The photonic crystal basically comprises three layers with the parameters n_1=1.37, n_2=4.35, d_1= 70 nm, d_2= 70 nm, d_3= 90 nm and N= 6 with two values of n_3 of 1.0 (air) and 1.33 (water).

Figures 5.2 and 5.3 show the variation of the calculated transmission for one-dimensional ternary photonic crystal with the angle of incidence with air and water as analyte layers, respectively. The figures reveal many interesting features. The most important feature is the appearance of bands in which the transmission is close to unity. These bands are separated by very narrow valleys where the transmission approaches zero. When the index of refraction of the analyte layer (air in Fig. 5.2 and water in Fig. 5.3) changes, the transmission profile undergoes an angular shift. In Fig. 5.2 the air refractive index is assumed to change by $\Delta n = 0.02$, the angular shift is found to be $\Delta\theta = 0.02$ as can be seen from the inset. In Fig. 5.3, when $\Delta n = 0.01$, the angular shift is $\Delta\theta = 0.01$. Assuming a measurable angle of order 0.001, the resolution of the proposed one-dimensional ternary photonic crystal sensor is considerably high.

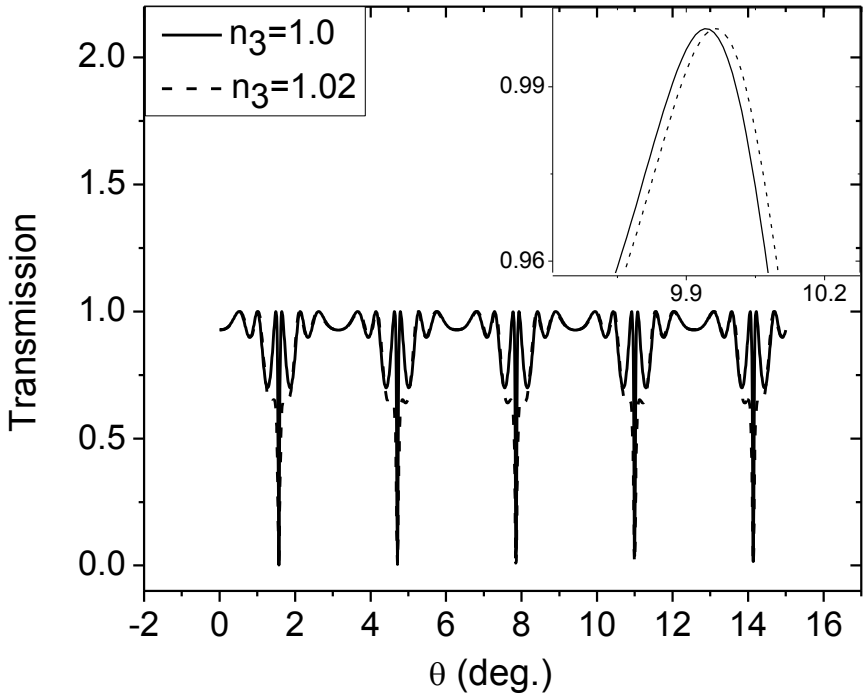

Fig. 5.2. Transmission versus the angle of incidence for one dimensional ternary photonic crystal with different values of n_3 for air as an analyte material.

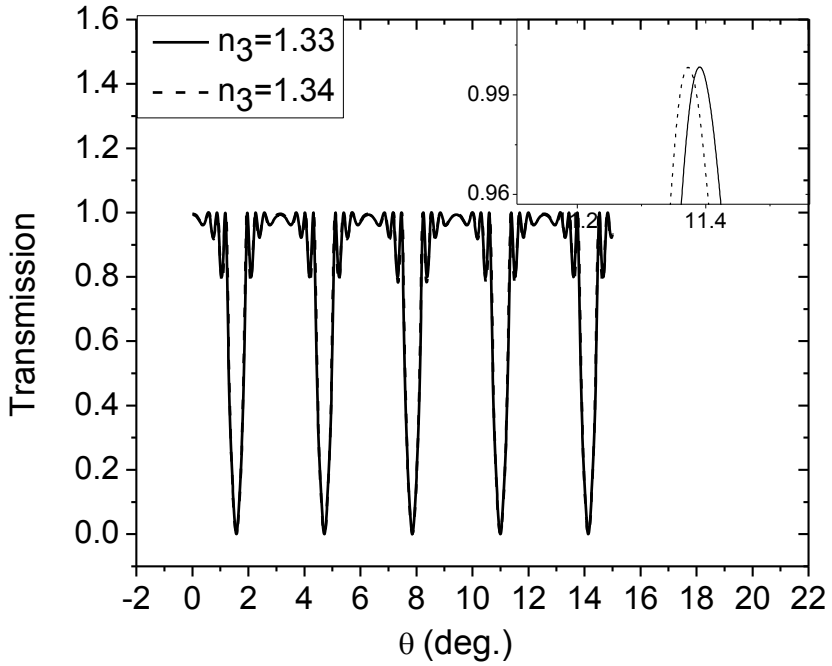

Fig. 5.3. Transmission versus the angle of incidence for one dimensional ternary photonic crystal with different values of n_3 for water as an analyte material.

It is important to study the effect of number of periods of one dimensional ternary photonic crystal on the transmission profile. The variation of the transmissivity with the angle of incidence for different values of number of periods with air as an analyte layer is depicted in Fig. 5.4. The calculations were conducted for periods of N=6, 8, 10 and 12. As can be seen from the figure, the number of valleys in the considered θ_i ranges is independent of the number of the repetitive periodic layers. Moreover, the number of bands is also independent of the number of periods but the number of ripple contained in each band increases with increasing the number of periods.

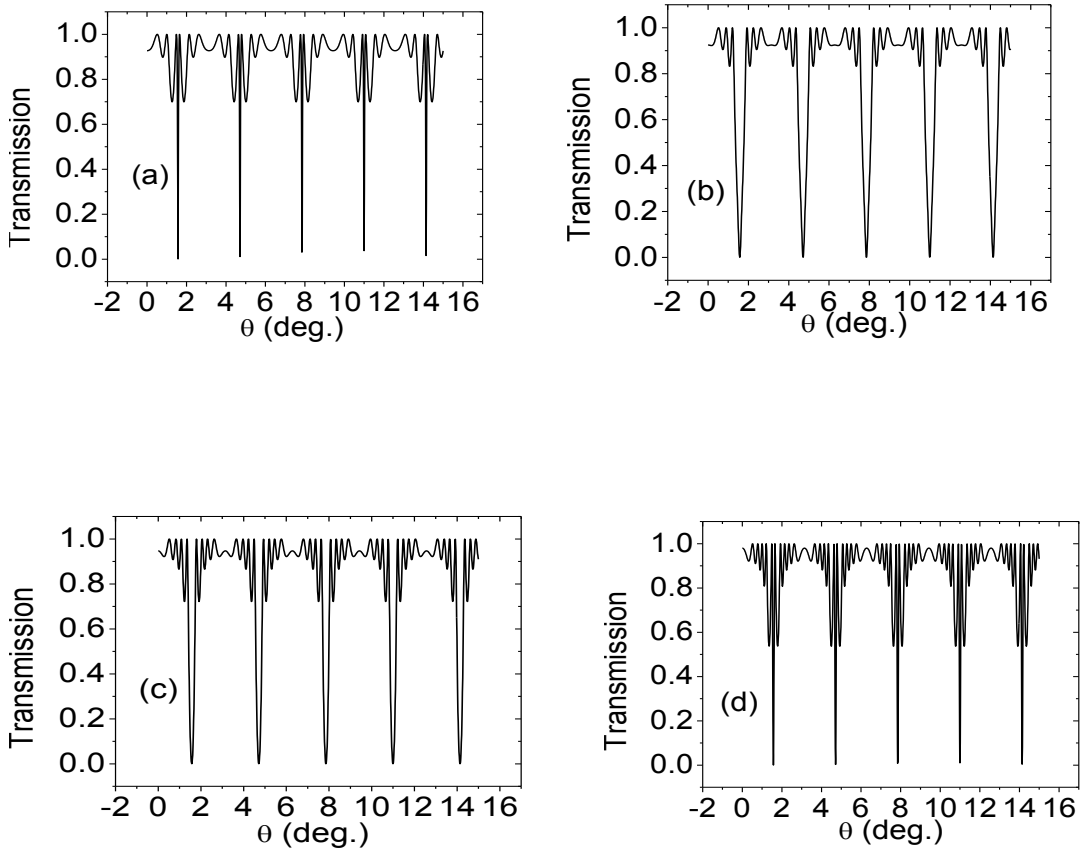

Fig. 5.4. Transmission from one dimensional ternary photonic crystal with the angle of incidence with N=6 (a), N=8 (b), N=10 (c), and N=12 (d).

The transmission profile is explored further in Figs. 5.5 and 5.6 which show the transmission spectrum versus wavelength for different values of n_3 with air and water as analyte layers, respectively, at normal incidence of light. As is clearly seen there is a peak shift towards larger wavelength as the refractive index of the analyte layer changes where these transmission peak shifts are very easily detectable with existing optoelectronic devices. Figures 5.5 and 5.6 show the transmission peaks at refractive index difference of 0.01. The solid transmission peak (centered at 1738.63 nm for air and at 1763.6 nm for water) is for $\Delta n = 0.00$. The dash transmission peak (centered at 1739.31nm for air and at 1764.6 nm for water) is for $\Delta n = 0.01$. The dot transmission peak (centered at 1739.99 nm for air and at 1765.6 nm for water) is for $\Delta n = 0.02$. The dash dot transmission peak (centered at 1740.67nm for air and at 1766.6 nm for water) is for

$\Delta n = 0.03$. It is found that this one-dimensional ternary photonic crystal exhibits narrow transmission peak near photonic band edge, which shifts by 0.68 nm for air and 1.0 nm for water for each refractive index change of 0.01.

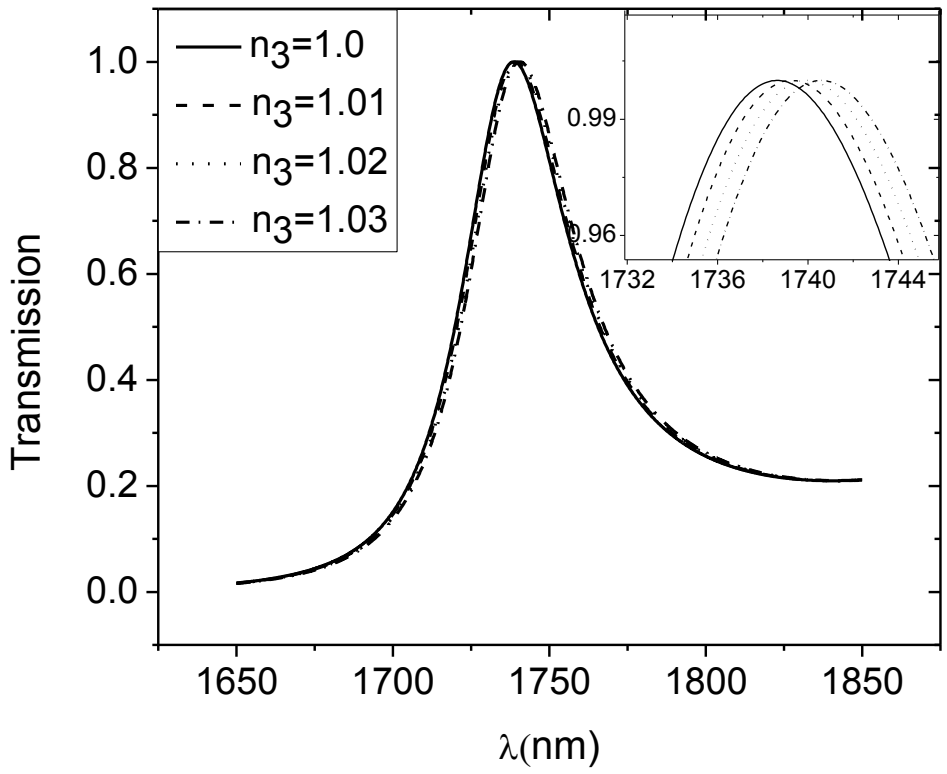

Fig. 5.5. Transmission peaks for one dimensional ternary photonic crystal with different values of n_3 for air as analyte material.

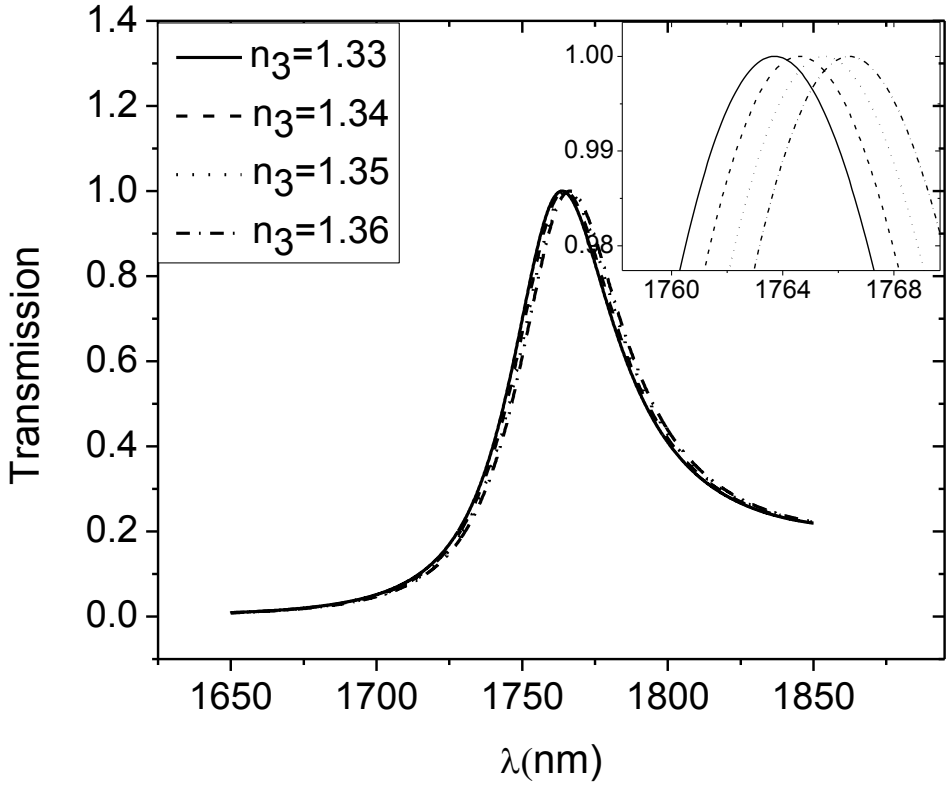

Fig. 5.6. Transmission peaks for one dimensional ternary photonic crystal with different values of n_3 for water as analyte material.

CONCLUSION

In this thesis, a comprehensive analytical studies have been presented on two layer one dimensional photonic crystal in which the first layer was considered to be the analyte layer and the second layer was considered to be LHM, dielectric or metal for transverse electric (TE) and transverse magnetic (TM) waves. The dispersion relations were derived for both polarizations. Expressions for the sensitivity were derived and plotted.

The main results can be summarized as follows:

1- The second layer was considered LHM

- The sensitivity increases with increasing the LHM layer thickness and peaks at an optimum value of the thickness. For thicknesses beyond the optimum thickness, the sensitivity decreases towards extremely low values for TE and TM modes.
- For TE and TM modes, increasing the analyte thickness, the evanescent field in the analyte medium is enhanced and so does the maximum sensitivity.
- The sensitivity can be enhanced with decreasing the electron scattering rate (γ) for TE and TM modes.
- It is possible for LHM photonic structure to achieve a sensitivity improvement of 412% for TE mode and 1056% for TM mode when compared to conventional slab waveguide sensor.

2- When the second layer was considered metal (Nickel and Chromium)

- The sensitivity of the photonic crystal which contains Ni and Cr metals can be enhanced by decreasing the wavelength for TE and TM modes.
- The sensitivity of the proposed sensor with (Ni) metal can be increased by increasing the thickness of analyte layer but the sensitivity of the proposed sensor with (Cr) metal can be increased by increasing the thickness of analyte layer untill it reaches a maximum value at an optimum thickness, then decreases with further increasing of d_1 for TE mode. The latter behavior was also observed for TM polarization for Ni and Cr metals.

3- When the second layer was considered a dielectric

- The sensitivity of the photonic crystal which contains dielectric layer increases very sharply with increasing the thickness of dielectric layer and reaches a maximum value at an optimum thickness of the dielectric layer, then decreases very slowly with increasing the thickness of the dielectric layer beyond the optimum thickness for TE.
- For TM mode, The sensitivity of the photonic crystal which contains dielectric increases very sharply with increasing the thickness of dielectric layer and reaches a maximum value at an optimum thickness of the dielectric layer.
- When the results of the structures comprising LHM, metals, and dielectric are compared, it can be concluded that the highest sensitivity was achieved with LHM structures.

Moreover, in this thesis, one dimensional ternary photonic crystals were investigated as refractometric sensors for sensing very small refractive index change of an analyte material. The transmission of an incident wave were studied in details using Fresnel reflection coefficients. The transmission coefficient was plotted with the angle of incidence and wavelength of incident light for air and water as analyte materials.

It was observed that a slight refractive index change in an analyte layer of the ternary structure causes a sufficiently large transmission peak shift.

REFERENCES

[1] D. Sengupta and T. Sarkar, "Maxwell, Hertz, the Maxwellians and the early history of electromagnetic waves", Antennas and propogation magazine, Vol. 45, No. 2, pp. 13-19 (2013).

[2] K. Kawano and T. Kitoh, "Introduction to optical waveguide analysis", John Wiley & sons, New York (2001).

[3] D. Griffith's, "Introduction to electrodynamics", Prentice Hall, New Jersy (1999).

[4] F. Pedrotti and L. Pedrotti, "Introduction to optics", Prentice- Hall, New Jersy (1993).

[5] D. Meister and J. E. Sheedy, " Introduction to Ophthalmic Optics", Carl Zeiss Vision, San Diego (2008).

[6] B. Crowell, " Optics " , Fullerton, California (2004).

[7] M. E. Browne, "Engineering and Science", Mc Graw-Hill companies, United States of America (1999).

[8] P. Hofmann, "Solid state physics: An introduction", Wiley-VCH, Weinheim (2008).

[9] A. Beiser, "Concepts of Modern Physics", McGrow-Hill companies, United States of America (2003).

[10] Y. Singh, "Electromagnetic Field Theory", Pearson Eduction, India (2011).

[11] R. Martin, "Electromagnetic field theory for physicists and engineers: Fundamentals and application", Gurso, Granda (2006).

[12] S. Orfanids, "Electromagnetic waves and Antennas", Sophocles Orfanidis, Ewa (2014).

[13] J. Lou, L. Tong and Z. Ye, "Modeling of silica nanowires for optical sensing", Optics Express, Vol. 13, No. 6, pp. 2135-2140 (2005).

[14] O. Parriaux and G. J. Veldhuis, "Normalized Analysis for the sensitivity optimization of integrated optical Evanescent –wave sensors", Journal of light wave technology, Vol. 16, No. 4, pp. 573-582 (1998).

[15] O. Parriaux and P. Dierauer, "Normalized expressions for the optical sensitivity of evanescent wave sensors", Optics Letters, Vol. 19, No. 20, pp.1665-1665 (1994).

[16] N. skivesen, R. Horvath and H. C. Pedersen, "Peak- type and dip- type metal-clad waveguide sensing", Optics Letters, Vol. 30, No. 13, pp. 1659-1661 (2005).

[17] G. Harsanyi, "Sensors in Biomedical Applications", CRC Press, Washington (2000).

[18] K. Tiefenthaler and W. Lukosz, "Sensitivity of Grating Couplers as Integrated-Optical Chemical Sensors ", Optical Society of America B, Vol. 6, No. 2, p.p. 209-220 (1989).

[19] N. Skiveseen, Metal-Clad Waveguide Sensors, PhD Thesis, University of Copenhagen (Denmark), 2005.

[20] N. Skivesen, R. Horvath, H.C. Pedersen, "Optimization of metal-clad waveguide sensors", Sensors and Actuators B, Vol. 106, No. 2, pp. 668–676 (2005).

[21] H. Mukundan, A. Anderson , W. Grace, K. Grace, N. Hartman, J. Martinez and B. Swanson, "Waveguide-Based Biosensors for Pathogen Detection", Sensors, Vol. 9, No. 7, pp. 5783-5809 (2009).

[22] X. Fan, I. M. White, S. Shopova, H. Zhu, J. Suter, and Y. Sun, "Sensitive optical biosensors for unlabeled targets: A review", Analytica Chimica Acta, Vol. 620, No. 1-2, pp. 8-26 (2008).

[23] S. Taya, M. Shabat, and H. Khalil, "Nonlinear Planar Asymmetrical Optical Waveguides for Sensing Applications", Optik, Vol. 121, No. 9, pp. 860-865 (2010).

[24] H. Khalil, M. Shabat, S. Taya, and M. Abadla, "Nonlinear Optical Waveguide Structure for Sensor Application: TM case", Int. J. Modern Phys. B, Vol. 21, No. 30, pp. 5075-5089 (2007).

[25] S. Taya, and T. El-Agez, "Theoretical spectroscopic scan of the sensitivity of asymmetric slab waveguide sensors", Optica Applicata, Vol. 41, No. 1, pp. 89-95 (2011).

[26] S. Taya, M. Shabat, and H. Khalil, "Enhancement of Sensitivity in optical sensors using left-handed materials", Optik, Vol. 120, No. 10, pp. 504-508 (2009).

[27] T. El-Agez, S. Taya, M. Shabat, and H. Kullab, "Planar Waveguide with Left-Handed Material Guiding Film for Refractometry Applications", Turkish Journal of Physics, Vol. 37, No. 2, pp. 250-258 (2013).

[28] M.Abadlla, S. Taya, M. Shabat, "Four- layer slab waveguide sensors supported with left handed materials", sensor letters, Vol. 9, No. 5 , pp. 1823-1829 (2011).

[29] S. Taya, H. El-khozondar, M. Shabat and E. Mehjez,"Transverse magnetic mode nonlinear waveguide slab optical sensor utilizing left handed materials", Functional Materials , Vol. 18, No. 4 , pp. 512-516 (2011).

[30] S. Taya ,T. El-Agez, H. Kullab, M. Abadla and M. Shabat, "Theoretical study of slab waveguide optical sensor with left- handed material as a core layer", Optica Applicata, Vol. 42, No. 1, pp. 194-205 (2012).

[31] H. Kullab and S. Taya, " Transverse magnetic peak type metal-clud optical waveguide sensors ", Optik, Vol. 125, No. 1, pp. 97-100 (2014).

[32] R. Nair, R. Vijaya, "photonic crystal sensors: An overview", Progress in Quantum Electronics, Vol. 34, No. 3, pp. 89-184 (2010).

[33] D. El-Amassi, left- handed photonic crystal sensors, analytical approach, M.Sc Thesis, the Islamic university (Gaza), 2013.

[34] V. G. Veselago, "The electrodynamics of substance with simultaneously negative values of ε and μ", Sov Phy Uspekh., Vol. 10, No. 4, PP. 509-514 (1968).

[35] S. Takeda and T. Yoshinaga, "left- handed Materials Technologies Significant for information and communication Devices", Science and Technology Trends, Vol. 3 , No. 34, pp. 36-48 (2009).

[36] S. Antipov, W. Liu, J. Poewr and L. k.Spentzouris, "left-handed metamaterial studies and their application to accelerator physics" , Particle Accelerator Conference, pp. 458-460 (2005).

[37] D. R. Smith and N. kroll, "Negative refractive index in left- handed materials", Physical review letters, Vol. 85, No.14, pp. 2933-2936 (2000).

[38] S. E. Mendhe and Y. P. Kosta ,"Metamaterials properities and application", International Journal of Information Technology and Knowledge Management, Vol. 4, No.1, pp. 85-89(2011).

[39] A. Bass, S. Tretyakov, p. Barois, T. Scharf, V. Kruglayk and I. Bergmair, "Nanostructured Metamaterials ", European Commission, Brussels (2010).

[40] S. Romanov and C. Stomayor Torres, "Three dimensional photonic crystals in the visible region", Progress in electromagnetic research, Vol. 41, No. 94 , pp. 307-335 (2003).

[41] G. Guida, A. de Lustrac and A. Priou, "An Introduction To Photonic Band Gap Materials", Progress in electromagnetic research, Vol.41, No. 1 , pp. 1-20 (2003).

[42] R. M. De La Rue and C. Seassal, " Photonic crystal devices: some basics and selected topics ", Laser and photonic reviews, Vol. 6, No. 4, pp. 564-587 (2012).

[43] T. F Krauss," Photonic crystal and light localization in the 21st century", Springer Netherlands (2001).

[44] A. Brzezinski, "Engineering and characterizing light-matter interaction in photonic crystals", Phd. Thesis , Illinois University (Urbana-Champaign), 2010.

[45] J. Jounnopoulos, S. Jahnson, J. Winn and R.t D. Medde, "Photonic crystal Modeling", Princeton University Press, New Jersey (2008).

[46] M. Born and E. Wolf, ," Principles of Optics", Cambridge University Press, United Kingdom (2003).

[47] A. Banerjee, "Enhanced Refractometric Optical Sensing By Using One-Dimensional Ternary Photonic Crystals", Progress in electromagnetic research, Vol. 89, No. 5 , pp. 11-22 (2009).